

Université de Lille  
Ecole Doctorale Science Pour l'ingénieur  
Laboratoire de Génie Civil et géo-Environnement (LCGgE)

# *THÈSE*

Pour l'obtention du grade de

**DOCTEUR DE UNIVERSITÉ DE LILLE**

Dicipline : *Génie civil*

Par

**Insan KAMIL**

## **Macro-Element Modeling For Single Pile And Pile Group**

**(Développement Numérique d'un Macro-Elément Pour Le Calcul des Pieux Sous Sollicitation Axiales,  
Transversales et Groupe de Pieux)**

Soutenue le 10 Juillet 2019

Devant de jury composé de:

Isam SHAHROUR	Professeur, Université de Lille	Président
Ahmed ARAB	Professeur, Université Hassiba Benbouali De Chlef	Rapporteurs
Daniel DIAS	Professeur, Université Grenoble-Alpes	Rapporteurs
Sébastien BURLON	Ingénieur de Recherche, Terrasol-Setec	Examineurs
Alia HATEM	Ingénieur de Recherche, ARCADIS	Examineurs
Hussein MROUEH	Professeur, Université de Lille	Directeur

## ABSTRACT

The proposed method presents a simple analysis of Soil-Structure Interaction (SSI) for deep foundation under static load that is applied for single pile and pile group. A model based on macro-element concept is developed to study the SSI taking into account the different nonlinearities. Its formulation is based on the theory of elastoplasticity and is inspired by European standards (Eurocodes 7 and 8). Wherein, the different parameters are defined from laboratory or in situ tests, or from numerical simulations under static conditions. This model reduces computational costs because the nonlinearities related to the SSI are concentrated in particular points of the computation model. The advantage of macroelement lies in its formulation in forces and displacements, which facilitates its use for the justification of the foundations (bearing capacity, sliding, detachment, settlements, translations, distortions and rotations). Furthermore, this macroelement is implemented in a Finite Element Method framework as a fish function in Flac3D. This tool is capable of simulating the SSI in the monotonic loaded pile. The proposed model has been validated with pile load test results, load transfer method (based on *Frank and Zhao* method) and computer programming (conventional Flac3D and Pilate). The approach succeeds with a good performance. Additionally, the efficiency and practical application of this method in the computation finite-element analysis are feasible for Single Pile and Pile Group .

Keywords: Macro-element, Elastoplasticity, Single Pile, Pile Group, Monotonic Load, Flac3D

# Développement Numérique d'un Macro-Elément Pour Le Calcul des Pieux Sous Sollicitation Axiales, Transversales et Groupe de Pieux

## RÉSUMÉ

La méthode proposée présente une analyse simple de l'interaction sol-structure (SSI) pour le calcul des pieux sous sollicitation axiales, transversales et groupe de pieux. Un modèle basé sur le concept de macroéléments est développé pour étudier la réponse du pieu en prenant en compte les différentes non-linéarités. Sa formulation est basée sur la théorie de l'élastoplasticité et s'inspire des normes européennes (Eurocodes 7 et 8). Les différents paramètres du modèle sont définis à partir d'essais en laboratoire ou in situ, ou à partir de simulations numériques dans des conditions statiques. Ce développement réduit les coûts de calcul car les non-linéarités liées à l'interaction Sol-Structure sont concentrées dans des points particuliers du modèle de calcul. L'avantage du macroélément réside dans sa formulation en forces et déplacements, ce qui facilite son utilisation pour la justification des fondations (capacité portante, glissement, détachement, tassement, translation, distorsions et rotation). De plus, ce macroélément est implémenté dans le cadre de la méthode des différences finis en tant que *fish function* dans Flac3D. Cet outil est capable de simuler le comportement d'un pieu sous charge monotone verticale et transversale. Le modèle proposé a été validé par les résultats des tests de chargement de pieu, des résultats numériques tels que la méthode des courbes de transfert (basée sur la méthode de Frank et Zhao) et les approches conventionnelles (Flac3D). De plus, l'efficacité et l'application pratique de cette méthode dans le calcul de groupe de pieux est aussi démontrée.

mots clés: Macro-élément, élastoplasticité, pieu isolé, groupe de pieux, Charge monotone, Flac3D

## ACKNOWLEDGMENT

I wish to deliver my special credit to my supervisor, Prof Hussein MROUEH, who gave me an opportunity working in Macro-element. My great appreciation also extends to DR Sébastien BURLON who first introduced me to the concept of macro-element and had been guiding me much in understanding and analyzing the numerical computational system. I feel lucky getting the opportunity of working under their supervision.

I would like to extend my appreciation to the Director of Laboratoire de Génie Civil et géo-Environnement, Prof Isam SAHROUR, for the help and warm welcome to me.

I also extend my appreciation to the reviewers, Prof. Ahmed ARAB and Prof. Daniel DIAS, for the review and suggestion in my defence.

I am indebted to my late parent (may the peace upon them), my wife and my daughters who continuously support and encourage my study abroad. Also to The Ministry of Research, Technology and Higher Education of Indonesia as the founding of my research.

## TABLE OF CONTENT

<b>ABSTRACT</b> .....	<b>ii</b>
<b>RÉSUMÉ</b> .....	<b>iii</b>
<b>ACKNOWLEDGMENT</b> .....	<b>iv</b>
<b>TABLE OF CONTENT</b> .....	<b>v</b>
<b>TABLE OF FIGURE</b> .....	<b>vii</b>
<b>LIST OF TABLE</b> .....	<b>xi</b>
<b>NOMENCLATURE</b> .....	<b>xiii</b>
<b>GENERAL INTRODUCTION</b> .....	<b>1</b>
<b>CHAPTER I: STATE OF ART</b> .....	<b>5</b>
I.1 REVIEW OF PILE DESIGN .....	6
I.2 BEHAVIOUR OF PILE UNDER MONOTONIC LOAD.....	7
I.2.1 Experimental Observation of the Soil-Structure Interaction .....	7
I.2.2 Load Distribution On Pile Group.....	10
I.3 CONVENTIONAL PREDICTION METHODS .....	12
I.3.1 Parameters Influence.....	12
I.3.1.1 Installation Effect .....	12
I.3.1.2 Time effect .....	13
I.3.1.3 Compressibility of Pile.....	14
I.3.2 Loads Transfer T-z Method .....	16
I.3.3 Loads Transfer P-y Method .....	26
I.3.4 Hyperbolic Method .....	30
I.4 FINITE ELEMENT METHOD.....	34
I.5 MACRO-ELEMENT MODELING .....	36
I.5.1 Macro-element Method for Shallow foundation .....	37
I.5.2 Macro-element Method for deep foundation .....	41
I.6 RESULT .....	41
<b>CHAPTER II: DEVELOPMENT OF MACRO-ELEMENT</b> .....	<b>46</b>
II.1 CONCEPT OF MACRO-ELEMENT .....	48
II.2 THE ELASTOPLASTIC LOAD-DISPLACEMENT LAW .....	49

II.2.1	Relative Displacements in Elastic Response.....	51
II.2.2	Relative Displacements in Elastic Perfectly-Plastic.....	55
II.2.3	Elastoplasticity With Hardening Law .....	57
II.2.4	Relative Displacement in Plastic Potential and Flow Rule .....	58
II.3	SYNTHESIS OF ELASTOPLASTIC MACRO-ELEMENT PARAMETERS.....	59
II.3.1	Vertical load .....	60
II.3.2	Transversal load.....	60
II.4	COMPARISON TO CONVENTIONAL LOAD TRANSFER METHOD .....	61
II.4.1	Case Studies For Vertical Load Response .....	61
II.4.2	Case Studies For Transversal Load Response.....	67
II.5	RESULT.....	71
<b>CHAPTER III: APPLICATION AND VALIDATION OF MACRO-ELEMENT .....</b>		<b>72</b>
III.1	SINGLE PILE.....	73
III.1.1	Vertically Loaded Pile .....	73
III.1.2	Transversally Loaded Pile.....	76
III.2	PILE GROUP .....	78
<b>CONCLUSION AND PERSPECTIVE .....</b>		<b>86</b>
<b>BIBLIOGRAPHY.....</b>		<b>88</b>

## TABLE OF FIGURE

Figure I.1. Piles capacity mechanism (a) axial loads (b) lateral load.....	7
Figure I.2. Bi-directional loading test.....	8
Figure I.3. Loads-Displacement curve, pile is loaded until Ultimate state .....	8
Figure I.4. Loads transfer curve (shaft and tip) .....	9
Figure I.5. Lateral load test layout.....	10
Figure I.6. Lateral load test layout.....	10
Figure I.7. Load settlement response of the piles at different location of nine-pile group connected to rigid pile-cap ( <i>Zhang et al, 2013</i> ) .....	11
Figure I.8. (a)Soil layer deformation on Displacement pile on driving pile (b) Non- Displacement on bore pile.....	12
Figure I.9. Variation of pile-capacity with time ( <i>Fleming et al, 2009</i> ).....	14
Figure I.10. The progressive failure of along pile .....	15
Figure I.11. Variation of reduction factor with pile stiffness ratio.....	16
Figure I.12. The mechanism on axially monotonic load (a) transfer mechanism and (b) spring-mass model .....	16
Figure I.13. End bearing resistance considering (a) plugged condition and (b) unplugged condition.....	17
Figure I.14. Free body diagram of pile segment.....	18
Figure I.15. Example of Pressure-meter Test result .....	19
Figure I.16. (a) Load-Transfer mechanism (b) the T-z curve (c) the q-z curve (after <i>Frank and Zhao,1982</i> ) .....	20
Figure I.17. Model of the full pile (a) model of the base of pile (b) .....	21
Figure I.18. Value of $kp$ and $D_{ef}/B$ .....	22
Figure I.19. Friction curve $f_{soil}(p_l^*)$ .....	23
Figure I.20. Area A and perimeter P to be used for open-end steel piles & sheet piles.....	25
Figure I.21. Unit stress distribution in lateral load.....	26
Figure I.22. Behavior of P-y curve ( <i>Coduto,1994</i> ).....	26
Figure I.23. Pile segment discretization pile element and soil element. ....	27
Figure I.24. The P-y curve at pile segment adjusts with depth .....	28
Figure I.25. Soil reaction against lateral displacement (after <i>Frank, 1999</i> ).....	30
Figure I.26. Hyperbolic representation of stress-strain, <i>Kondner (1963)</i> (a) real curve (b) transformed curve.....	31
Figure I.27. Observed and theoretical relationship between shaft resistance and displacement ( <i>Zhang et al. 2013</i> ).....	31

Figure I.28. Observed and theoretical relationship between end-bearing resistance and displacement ( <i>Zhang et al. 2013</i> ).....	32
Figure I.29. Schematic shape of the P-Y curve ( <i>Bouafia A, 2013</i> ) .....	32
Figure I.30. Pile segment discretization into pile element and soil element. ....	34
Figure I.31. The pattern of Plasticity Flow indicator on Flac3D.....	36
Figure I.32. General structure of macro-element a. Structure of macro-element b. System analogy .....	37
Figure I.33. Evolution of the charge surface within the rupture criterion of the Crémer model ( <i>Grange, 2008</i> ).....	38
Figure I.34. General structure of macro-element of <i>Chatzigogos,2007</i> . ....	38
Figure I.35. Ultimate and yield surface by <i>Chatzigogos,2007</i> . ....	39
Figure I.36. Lay out of variable global studied a. efforts b. displacement ( <i>Grange, 2008</i> ) ....	39
Figure I.37. Single Macro-element model ( <i>Abboud et all, 2017</i> ).....	40
Figure I.38. Distributed Macro-element model ( <i>Abboud et all, 2017</i> ).....	40
Figure I.39. Hybrid Macro-element model ( <i>Abboud et al, 2017</i> ).....	40
Figure I.40. (a) Macro-element on lateral load, (b) components of macro-element ( <i>Taciroglu, 2006</i> ) .....	42
Figure I.41. (a) Macro-element on multi axial load (b) basic element on multi axial model ( <i>Rha and Taciroglu, 2007</i> ).....	43
Figure I.42. Determining The initial stiffness parameter of the hypolplastic macro-element ( <i>Zheng li, 2015</i> ).....	44
Figure I.43. Failure envelope in the H:M/D loading plane: fitting curve based on model tests data and numerical simulation ( <i>Zhuang Ji, 2019</i> ).....	45
Figure I.44. Failure surface in 3D H-M-V space ( <i>Zhuang Ji, 2019</i> ).....	45
Figure II.1. The concept of Macro-element that work on single macro element. ....	48
Figure II.2. The concept of Macro-element that is attached on Flac3D for the single pile.....	49
Figure II.3. The concept of Macro-element that is attached on Flac3D for the Group pile .....	49
Figure II.4. Elastic and plastic zone in the stress-strain curve .....	50
Figure II.5. Elastic and plastic zone in the stress-strain curve .....	51
Figure II.6. Model of macro-element at a mass.....	52
Figure II.7. (a) Sketch of mesh and boundary condition, (b) Model in Flac3D.....	54
Figure II.9. Elastic-perfectly plastic zone in the stress-strain curve.....	55
Figure II.10. The stress-displacement curve on Elastic-perfectly plastic state. ....	56
Figure II.11. Real Hyperbolic graphic.....	57
Figure II.12. Influence of coefficient <i>b</i> to the curve.....	58



Figure II.13. The iterative development procedure of the mathematical tool plastic-hardening zone in the stress-strain curve .....	58
Figure II.14. (a) The single Macro-element for single pile and (b) Macro-element on Flac3D for pile group on vertically load .....	61
Figure II.15. (a) Sketch of mesh and boundary condition on the single Macro-element for single pile and (b) Model for Macro-element on Flac3D .....	62
Figure II.16. The load-settlement curve at the pile head of single pile from soil type 1 from 10m depth ( D= 30 cm to D= 60cm).....	64
Figure II.17. The load-settlement curve at the pile head of single pile from soil type 1 from 10m depth ( D= 70 cm to D= 100cm).....	64
Figure II.18. The load-settlement curve at the pile head of single pile from soil type 2 from 20m depth ( D= 30 cm to D= 60cm).....	65
Figure II.19. The load-settlement curve at the pile head of single pile from soil type 2 and 20m depth ( D= 70 cm to D= 100cm).....	65
Figure II.20. The comparison curve between T-z method and the macro-element method due to the variation of slope coefficient on macro-element $C_s$ (20m depth and diameter 70 cm ).....	66
Figure II.22. (a) Mesh and boundary condition (b) The plasticity flow on Flac3D in macro-element method (c) The plasticity flow on Conventional Flac3D.....	67
Figure II.23. (a) The single Macro-element for single pile and (b) Macro-element on Flac3D for pile group on Lateral load.....	67
Figure II.24. The load-settlement curve for at the pile head of single pile from Homogenous soil with 10m depth ( D= 30 cm to D= 100cm).....	69
Figure II.25. The load-settlement curve for at the pile head of single pile from bi-layered soil with 10m depth ( D= 30 cm to D= 100cm).....	70
Figure III.1. Sketch of Flac3D mesh and boundary condition, (a) Conventional method (b) Macro-element method .....	74
Figure III.2. (a) Model of the pile on flac3D (b) Displacement magnitude (c) Plasticity flow of soil .....	74
Figure III.3. (a) The simple model of the pile on flac3D for macro-element (b) Displacement magnitude .....	75
Figure III.4 Plasticity flow of soil on Flac3D for Macro-element method in Mohr-Coulomb criterion. ....	76
Figure III.5 Measured and calculated load-settlement curve at the pile head of single pile ...	76
Figure III.6. (a) Sketch of mesh and boundary condition on the single Macro-element for single pile and (b) Model for Macro-element on Flac3d .....	77
Figure III.7. Comparison of predicted and measured deflection.....	78

Figure III.8 Calculation Value of limiting unit skin friction of soil at each segment ( <i>Zhang et al. (2013)</i> ) and the assumption value of <i>Em</i> (Menard modulus).....	79
Figure III.9. The configuration of Four-pile group .....	80
Figure III.10 Measured and calculated load-settlement curve at the pile head of Four- pile group .....	80
Figure III.11 The configuration of nine-pile .....	81
Figure III.12 Sketch of Flac3D mesh and boundary condition (a) with pile-cap and (b) without pile-cap.....	81
Figure III.13. (a) model (b) plasticity flow.....	82
Figure III.14. Load-settlement response of pile at different location of Macro-element result and <i>Zhang et al</i> result. ....	83
Figure III.15. Measured and calculated load-settlement curve at the rigid pile head of nine-pile group .....	84
Figure III.16. Load distribution vs -settlement response of pile group .....	84

## LIST OF TABLE

Table I.1. Theoretical and measured load distribution tests of <i>Koizumi and Ito (1967)</i> .....	11
Table I.2. Spring values simulating pile under vertical loading ( <i>Comoros et al.,2009</i> ).....	11
Table I.3. Classification of piles ( <i>AFNOR,2012</i> ) .....	13
Table I.4. Value for the tip bearing resistance factor $k_{p,max}$ for $D_{ef} \geq 5$ ( <i>Burlon et al, 2014</i> )....	22
Table I.5. Selecting the $Q_i$ line to obtain the limit unit skin friction value $q_s$ ( <i>Burlon et al,2014</i> ) .....	23
Table I.6. Value of installation factor $\alpha_{soil-pile}$ ( <i>Burlon et al,2014</i> ) .....	24
Table I.7. The maximum Value ultimate skin friction $q_{s-max}$ .....	25
Table I.8. Value of the coefficient a,b,c,n and m for PMT ( <i>Bouafia A. 2013</i> ).....	33
Table I.9. Value of the coefficient a,b,n and m for Cone penetration test ( <i>Bouafia A. 2017</i> )..	33
Table I.10. Parameter of Macro-element ( <i>Abboud, 2017</i> ).....	41
Table II.1. The analytic calculation of internal forces on elastic state .....	53
Table II.3. Calculation on Flac3D with embedded Macro-element on elastic state.....	54
Table II.4. Parameters of elastoplastic macro-element model.....	60
Table II.4. (a) Menard Pressure-meter test for type soil 1 (layered soil) and (b) type soil 2 (Homogeneous soil) .....	62
Table II.5. The ultimate capacity of the pile head in each dimension of the pile in 10 m depth and soil type 1.a.....	63
Table II.6. The ultimate capacity of the pile head in each dimension of the pile in 20 m depth and soil type 1.b. ....	63
Table II.7. Calculation results of the macro-element parameters at each dimension of the pile in 10 m depth and soil type 1.a. ....	63
Table II.8. Calculation results of the macro-element parameters at each dimension of the pile in 10 m depth and soil type 1.b. ....	63
Table II.9. Menard Pressure-meter test for Homogenous soil.....	68
Table II.10. Calculation results of the macro-element parameters for laterally load at each dimension of the pile in 10 m depth in homogeneous soil.....	68
Table II.11. Menard Pressure-meter test for Bi-layered soil .....	69
Table II.12. Calculation results of the macro-element parameters for laterally load at each dimension of the pile in 10 m depth in bi-layered soil.....	70
Table III.1 Soil parameter value from Pressuremeter test.....	73
Table III. 2 Material properties .....	74
Table. III. 3 Macro-element parameters .....	75

Table III.4. The macro-element parameters .....	77
Table III.5 Macro-element Parameters.....	79
Table III.6 Predicted pile head load for four pile-group connected by rigid pile-cap.....	80
Table III.7. Predicted pile head load at different location connected by rigid pile-cap .....	82
Table III.8. Predicted pile head load at different location connected by Rigid pile-cap (Zhang <i>et al</i> , 2013).....	83
Table III.9. Predicted pile head load by Macro-element at different location connected by flexible pile-cap.....	85

## NOMENCLATURE

### File Properties

$A$	(m <sup>2</sup> )	Cross-section area of pile
$B$	(m)	Diameter of pile
$C$	(m)	circumference of pile at depth $z$
$E_p$	(GPa)	Modulus young of pile
$h_i$	(GPa)	Length at segment $i$
$K$		ratio of flexibility
$L$	(m)	length of pile
$P_i$	(m)	Perimeter of pile at segment $i$
$Rc$	(kN)	Pile capacity
$Rs$	(kN)	Shaft resistance
$Rb$	(kN)	Bearing capacity
$Q_z$	(kN)	internal pile force at depth $z$
$\Delta w_{res}$	(m)	Relative movement from peak to residual
$u_z$	(mm)	Displacement of pile segment at depth $z$

### Soil Properties

$E_m$	(MPa)	Menard Pressuremeter modulus
$P_{lm}$	(MPa)	Limit pressure in Pressuremeter
$Ple^*$	(MPa)	Net Equivalent Menard Limit pressure
$E_s$	(MPa)	Modulus young of soil
$\varphi$	(°)	Friction angle
$c_u$	(kPa)	Cohesion Undrained
$\sigma$	(kPa)	Stress
$\tau$	(kPa)	Shear stress
$\nu$		Poisson's ratio

### Interface properties

$q_b$	(kPa)	Unit end-bearing resistance
$q_{si}$	(kPa)	Unit skin resistance at section $i$
$\sigma$	(MPa)	Stress
$\varepsilon$	%	Strain
$u$	mm	Displacement

### Involved parameters of pile

$k_s$	(kPa/mm)	functions of the pressuremeter modulus $E_m$ for skin resistance
$k_b$	(kPa/mm)	functions of the pressuremeter modulus $E_m$ for base resistance
$qb$	(kPa)	bearing capacity
$qs$	(kPa)	shaft resistances

### Macroelement Properties

$a$	(kN)	Empirical coefficient on macroelement
$b$	(mm)	Empirical coefficient on macroelement
$D_{em}$	(m)	Effective depth on macro-element
$k_v$	(kN/mm)	Slope in elastic state on macro-element for vertically loaded
$k_h$	(kN/mm)	Slope in elastic state on macro-element for laterally loaded
$f_y$	(kN)	Yield
$du$	(mm)	Relative displacement on macro-element
$\lambda$		Multiplier
$\alpha$		Coefficient of curvature on macro-element
$C_s$		Slope coefficient on macro-element

## GENERAL INTRODUCTION

In recent decades, a growing number of civil engineering structures have emerged in increasingly complex configurations. The complexities arise either from (i) the geometrical configuration of the structure, or (ii) the nature of the soils in which they are built, or (iii) the types of external loading, or any combination thereof.

The analysis and the design of these structures is not an easy task, because it requires a good knowledge of the materials under consideration, of their reaction induced by complex loadings, but also and especially a good knowledge of the boundary conditions of the structure, in particular, the interface between the place where these solicitations originate and the structure itself. This requires a specific study which is commonly called Soil-Structures Analysis. Indeed, the term “interaction” has an important meaning, since it highlights the fact that not only does the nature of the soil have an influence on the behavior of the structure, but also the structure has an influence on the behavior of the soil.

There are several theories used to analyse soil-structure interaction problems. Among them, the numerical modelling, using finite element method and load transfer method (hyperstatic reaction methods), is the most suitable method because of its capability to solve the problem by taking into account the above several complexities. In practical engineering, **the load transfer method** is commonly used in design purpose. There is much particular interpretation to define the parameter used in this method such as pile material, type of soil, installation method and compressibility of the pile where it is provided in many codes such as API (American Petroleum Institut), Eurocode 7 and 8, AFNOR, etc. The **Finite Element Method** is used in the soil-structure interaction (SSI) analysis where it is possible to define more complex interactions at the local level in detail for all elements (soil, foundation, structure, etc.). However, it requires high cost in

calculation time, complexity in mesh construction and also difficulty in post-processing result due to the complexity of the soil-structure interaction (SSI) problems involved with. Although, many computation programmings have been introduced as an effort to minimise the calculation time such as Fast Lagrange Analysis of Continua (Flac3D). However, the conventional computer programming, in rendering process of plasticity flow indicator, takes extra time in every calculation step. The plasticity flow indicator indicates that the programme did analysis and calculation to all of the constructed models to define the result. In other words, the development of a new model which gives increased efficiency, accuracy and rapid prediction is still necessary.

To fill these lacks, the development of a tool that allows producing a simplified method to find out the behaviour of deep foundation embedded in the semi-infinite soil mass. The operation law will be constructed in an intermediate scale between global and local. This tool has been known as **Macro-element** that was initialized by *Nova and Montrasio, 1991* in geotechnical engineering. The concept of this method has been introduced in the context of the shallow foundation. The evolution of macro-element into several SSI problem solving was continued by *Pelluci, 1997, Cremer, 2001, Chatzigogos et al. 2007, Grange et al., 2008, Abboud et al. 2017*. Afterwards, the solution for deep foundation has been presented by *Tachiroglu 2006, Rha 2007, Li 2015 and Zheng Ji, 20019*. However, the developed macro-element concepts for deep foundation have been proposed only for a single pile.

This thesis presents the development of macro-element model for group pile. A model based on the macroelement concept is developed to study the soil-structure interaction (SSI) taking into account the different nonlinearities. Its formulation is based on the theory of elastoplasticity and is inspired by European standards (Eurocodes 7 and 8). The parameters are defined from laboratory or in situ tests, or from numerical simulations

under static and dynamic conditions. The computational costs are reduced because the nonlinearities related to the soil-structure interaction are concentrated in particular points of the computation model. The advantage of the macroelement lies in its formulation in forces and displacements, which facilitates its use for the justification of the foundations (bearing capacity, sliding, detachment, settlements, translations, distortions and rotations).

As a result, the efficiency of the calculation will effect to both the user and the machine.

The advantages at the user side are simplifying of preparation time in mesh construction, data input, and analysis result where will effect to the machine in computation time.

In order to achieve the objective of this research, this study is divided into two main part.

The first part is about constructing a mathematical model. And the second part deal with the running program by embedded macro-element model on Flac3d. The comparison and validation result with other approaches and field tests will be investigated to verify the accuracy and efficiency of the proposed macroelement method.

This report is composed into three chapters started with bibliography synthesis.

**The first chapter** is dealing with the synthesis of bibliography to present state of the art relating to the behaviour of the pile under monotonic axial and transversal load. Also, the parameters which influence the soil structure interaction such as installation methods, materials of the pile, and type of soil in conventional prediction method. Furthermore, It presents the constitutive law on soil structure interaction from elastic model to plastic model addressing to develop the macro-element method. The calculation method dealing with the mobilisation law of *Frank and Zhao* method. The previous studies about macro-element, shallow and deep foundation, are also synthesized in this chapter.

**The second chapter** is dealing with the development of macro-element. Base on the constitutive law of soil structure interaction the governing equation for the macro-element is constructed. It is started from the elastic model to plastic model. The first step is in the elastic model, where macro-element is developed in the elastic-perfectly plastic model to



the Mohr-Coulomb plastic model dealing with the calculation result of the macro-element model. Then, It is embedded to flac3d in the elastic model, elastic-perfectly plastic and the plasticity model on the axial and transversal monotonic load on macro-element. Also, the comparison and validation result with load transfer method base on *Frank and Zhao* method and also using the Pilate computer programme.

**The third** chapter is the implementation and validation. It is implemented in framework of Finite Element Method (Flac3D). Then, the result is validated with load transfer method (base on *Frank and Zhao* method) and computer programming (conventional Flac3D and Pilate). Next, it is compared to the other methods results, and pile load test results. Group of pile

## CHAPTER I: STATE OF ART

---

This chapter presents the behaviour of pile under monotonic axial and transversal load followed by the parameters which influence the soil-structure interactions. Then, It continues to the concept of the load transfer method (dealing with the mobilisation law of *Frank and Zhao*) and Finite Element Method. The constitutive laws of soil structure interaction, from elastic to plastic model, are addressed to develop the macro-element method. Furthermore, the previous studies of macroelement method, used in the shallow and deep foundation, are synthesised.

---

## I.1 REVIEW OF PILE DESIGN

Piles foundation has been used in construction since prehistoric as a method of overcoming the difficulties of founding the construction on soft soil, but the design was based on experience entirely until the last of the nineteenth century.

From the experimental observation of foundation, the interaction between soil and structure or known as soil-structure interaction theory can be comprehended. Also, behaviour of pile foundation while the load acting on the pile can be predicted. Some calculation methods have been proposed due to these comprehensions to predict the load-displacement analysis.

The loads that are transmitted from the upper structure determining the movement of the pile. Then the interaction between pile and soil, and also pile to another pile (in case of piles group) occurs. The embedded piles reinforce and increase load capacity of soil which is the same way as the steel reinforcement in concrete. For the vertical load, the failure of pile foundation occurs at the interface between sides of the pile and soil, and at the pile base. The total shear stress at the shaft-soil interface and the base of pile achieves a limit value which is varying with depth and soil type. For the horizontal failure is resulted from lateral load or moment, the normal stress at the interface achieves a limit value which is varying with depth. The possibility of understanding the behaviour of piles are several methods proposed to analyze the complexity that exist in soil-structure interaction of pile foundation under monotonic axial and lateral load.

Nowadays, there are many kinds of literature have been proposed as an approach formula for the capacity of the pile. The result of field experiences and empirical data of the piles performance have been published. Numbers of theories used to analyse the interaction between pile and soil due to the balancing approach between empirical experiences and theory. It is common progress in foundation engineering. Among them, the numerical modelling, using finite element method and load transfer method (hyperstatic reaction methods), is the most suitable method because of its capability to solve the problem by taking into account the above several complexities.

In practical engineering, **the load transfer method** is commonly used in design purpose. Initially, It proposed by *Coyle and Reese, 1966*. In the construction of load transfer method, there are many proposed mobilisation theory from Frank and Zhao method, hyperbolic, etc. However, most methodologies are still not applicable to routine calculation. There is much particular interpretation to define the parameter used in this method such as pile material, type of soil, installation method and compressibility of the pile where it is provided in many codes

such as API (American Petroleum Institut), Eurocode 7 and 8, AFNOR, etc. The load-displacement response is the result of this method.

The **Finite Element Method** is used in SSI analysis where it is possible to define more complex interactions at the local level in detail for all elements (soil, foundation, structure, etc.). However, it requires high cost in calculation time, complexity in mesh construction and also difficulty in post-processing result due to the complexity of SSI problems involved with.

## I.2 BEHAVIOUR OF PILE UNDER MONOTONIC LOAD

The prediction of displacement-stress or displacement-load on the pile is influenced by many parameters of soil and type of pile. From experimental observation, the pattern of soil-structure behaviour can be shown by a stress-displacement curve as a simple way to understand the performance of pile. The governing equation of settlement prediction in an elastic state or a plastic state in many models that proposed by many researchers is very important as the constitutive law of calculation method in the stress-displacement prediction.

### I.2.1 Experimental Observation of the Soil-Structure Interaction

Many studies carried out on pile load testing, most of them focused on the relationship of soil reaction and axial/lateral pile displacement. The relationship knows as the  $T$ - $z$  curve for axial loading and  $P$ - $y$  curve for lateral loading. Figure I.1 describes the soil-structure reaction for axial loading (Figure I.1.a) and reaction for lateral loading (Figure I.1.b). Where shaft friction and end-bearing reaction work on axial loading mechanism. The lateral reaction of soil dealing with depth works on lateral loading mechanism.

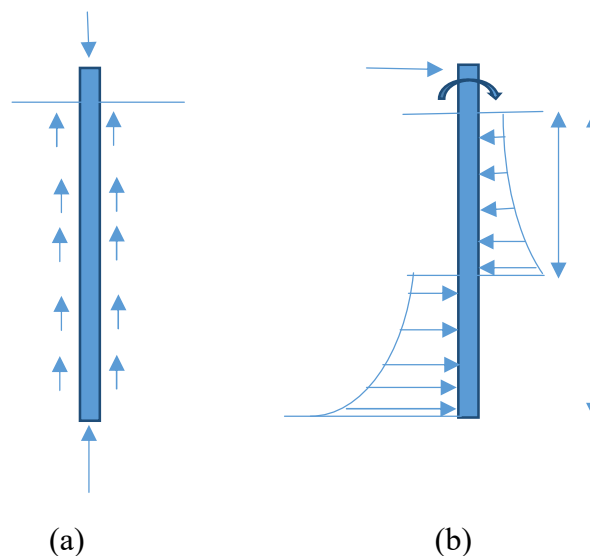


**Figure I.1.** Piles capacity mechanism (a) axial loads (b) lateral load

In the practical test, the pile can be instrumented to define normal stress along the pile and obtain the result for each depth. Bi-directional loading test, introduced by *Osterberg* in 1986s (*Osterberg, 1989*), is one of loading test method (Figure I.2).

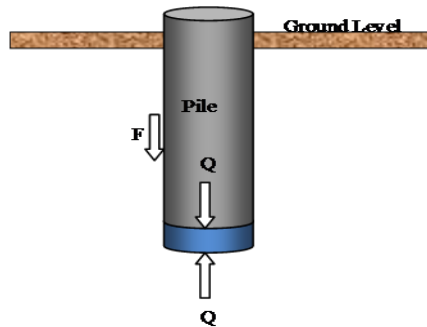


Figure I.2. Bi-directional loading test

This test loads the pile in compression from the bottom of pile. As the cell in the bottom expands, the end bearing  $Q$  provides reaction for the side shear  $F$  bi-directional static loading tests calculating the pile head settlements by the side shear load-displacement curve. It is obtained from the upward movement of the top of the load cell. The downward movement of the bottom of the load cell obtains the end bearing load-displacement curve.

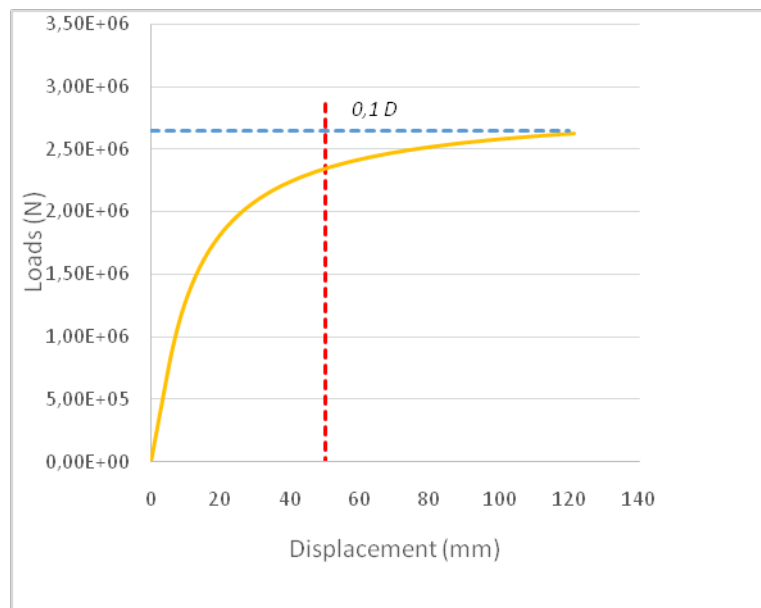


Figure I.3. Loads-Displacement curve, pile is loaded until Ultimate state

In axial static load tests (Figure I.3) is an illustration while the load applied on pile effecting to the displacement of the pile until the pile-capacity reached ( $R_c$ ) and the peak resistance for bearing capacity of pile assuming 10% Diameter of the pile (*API, 1993*). Those relationship is described by equation I.1 to I.3.

$$R_c = R_s + R_b \quad (I.1)$$

$$R_s = \sum q_{si} h_i P_i \quad (I.2)$$

$$R_b = q_b A_b \quad (I.3)$$

The experimental observation shows the contribution of shaft friction and end bearing of the pile to the force that is applied on pile. Figure I.4 illustrates the contribution of the pile-capacity between shaft resistance ( $R_s$ ) and bearing capacity ( $R_b$ ). The result of the  $T$ - $z$  method is assumed as experimental test showing that the normal stress decreases with the depth. The reduction of normal stress along the pile due to the mobilised friction on the interface is very influenced to pile-capacity.

When the applied load on pile reaches the top of pile-capacity ( $R_c$ ), then the difference between Ultimate pile-capacity and bearing capacity is shaft friction (equation I.1). Bearing capacity ( $R_b$ ) is calculated according to equation I.2, where  $A_b$  is cross-section area of the pile at base and  $q_b$  is a unit end-bearing resistance. And shaft resistance ( $R_s$ ) is calculated according to equation I.3, where  $P_i$ ,  $q_s$  and  $h_i$  are the perimeter of the pile at  $i$  section, unit skin resistance and thickness of the section.

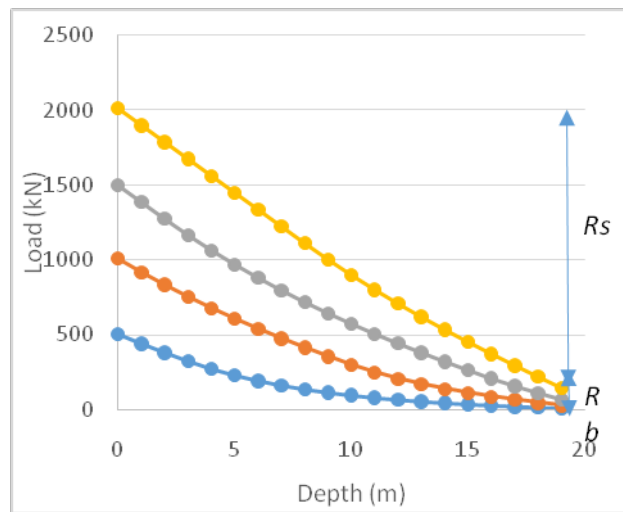


Figure I.4. Loads transfer curve (shaft and tip)

The full-scale lateral load test performed to develop a load-displacement relationship. The horizontal movement occurs in field test cause of lateral load. Its relationship is recorded between lateral load dealing with depth  $z$ .

During a load test, the lateral load act on the head of pile then displacement occur dealing with dept (Figure I.5.a). The displacement of the pile can be measured (Figure I.5.b). The slope of pile dealing with depth data is recorded. The load-displacement graphic that result of the field test is described in Figure I.6. Increasing of load will influence the increase of displacement.

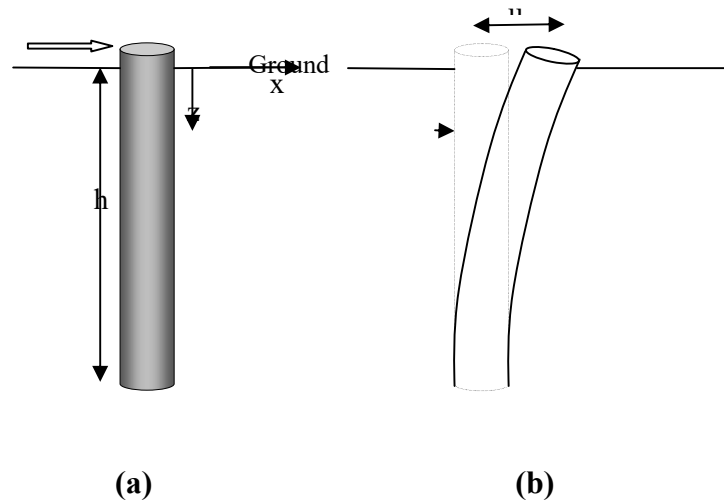


Figure I.5. Lateral load test layout

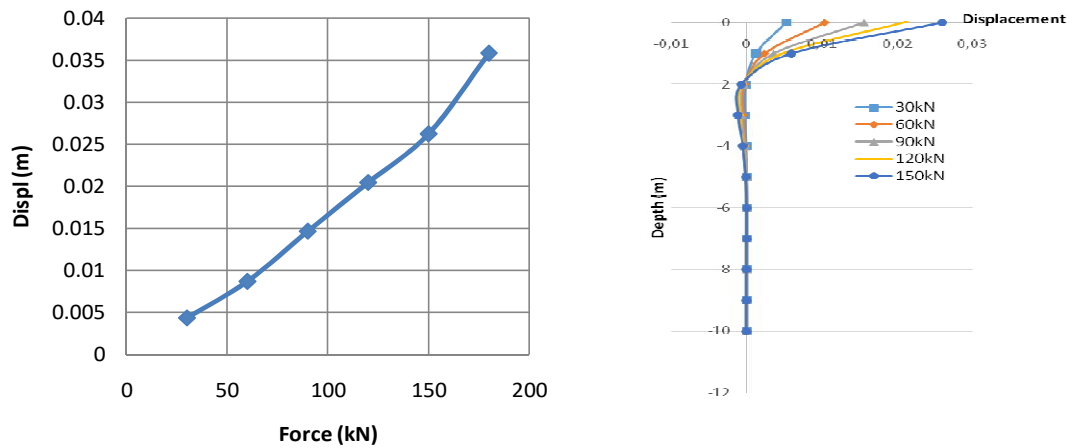


Figure I.6. Lateral load test layout

### I.2.2 Load Distribution On Pile Group

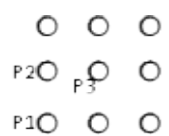
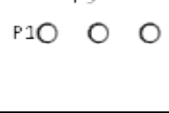
It has been known that the load, for the stiff pile-caps, is highest at the corners then edges. But for the flexible pile-caps, the load is distributed more evenly but often at the cost of higher settlements at the centre caused by a dishing effect of the pile-cap (*Rose, 2012*). *Whitaker (1957)* reported that at the large of loading, the corner piles take the largest and the centre of the pile takes the smallest proportion. *Cook (1974)* also demonstrated the interaction between pile in a group. In 25-piles square group at the corner found carrying five times as much as the centre pile load. *Poulos (1980)* reported the load distribution test between theoretical and test result which is tested by *Koizumi and Ito (1967)* in 3x3 pile group (Table I.1). *Comoros et al (2009)* gave the summarise result of simulation by 3D non-linear analysis providing the precise response of characteristic of the pile in a group (Table. I.2). *Zhang et al (2013)* also reported the load distribution on 3x3 pile group at the center, edges and mid-edges

(Figure.I.7) where the largest is at corner , the second largest at edge and the smallest at the center. The stiff pile-cap would transfer the loads from the central piles and redistribute them to the outer piles, piles at the edge take up a higher fraction of the total loads and are subject to higher axial and bending loads. For large pile groups, the axial loads on piles with a flexible raft are relatively uniform distributed; however, with a rigid raft, the corner piles carry loads significantly higher than the centre piles (*Chow H and Poulos HG, 2015*).

Table I.1. Theoretical and measured load distribution tests of *Koizumi and Ito (1967)*

Pile Location	Pile Load/Average Pile Load	
	Theoretical	Measured
Center	0.35	0.46
Mid-side	0.82	0.86
Corner	1.35	1.2

Table I.2. Spring values simulating pile under vertical loading (*Comoros et al.,2009*)

Pile Layout	Pile Length (m)	Diameter (m)	Spring Stiffness (MN/m)		
			P1	P2	P3
	38	1	312	259	206
		1.2	382	316	264
		1.5	432	367	324
	42	1	342	291	246
		1.2	406	343	292
		1.5	476	417	363

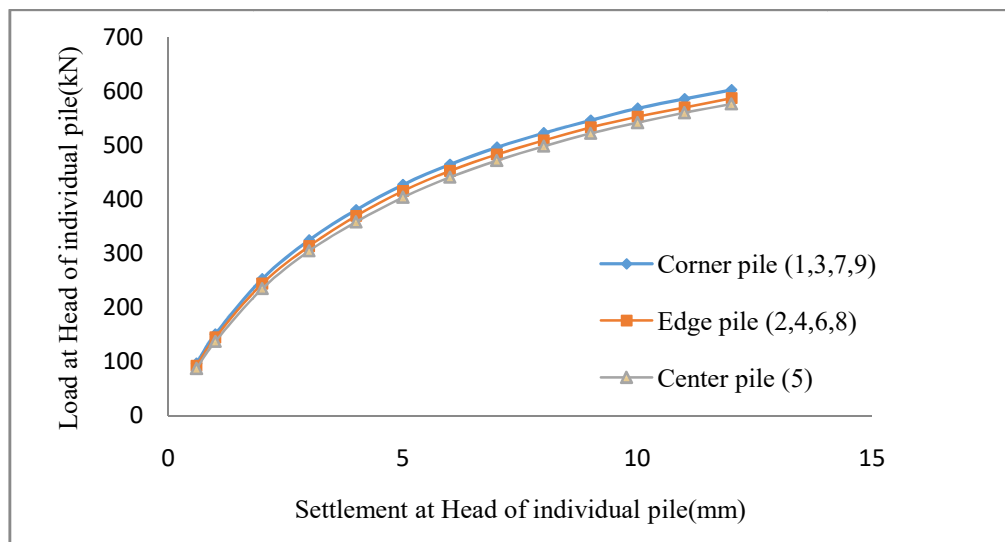


Figure I.7. Load settlement response of the piles at different location of nine-pile group connected to rigid pile-cap (*Zhang et al, 2013*)



### I.3 CONVENTIONAL PREDICTION METHODS

The popular prediction methods to account the soil-structure interaction for the pile foundation are the  $T-z$  method for vertical displacement, the  $P-y$  method for lateral displacement, the hyperbolic method as a more simple calculation until Finite Element method as the latest method that bases of the computer programming calculation.

#### I.3.1 Parameters Influence

In addition to soil properties, the behaviour of pile foundation essentially also depends on the installation method, the pile material and the compressibility.

##### I.3.1.1 Installations Effect

Three installations technique of piles are mentioned due to the displacement of soil during installation. The first technique of installation, relatively effecting big displacement on soil, is the large displacement pile such as wooden pile, spun pile, and driven steel closed end pile etc. The second technique, relatively effecting less displacement on soil than, is the small displacement such as micropile (Figure I.8.a). Then non-displacement pile is the third installation technique by boring such as bore pile etc (Figure I.8.b).

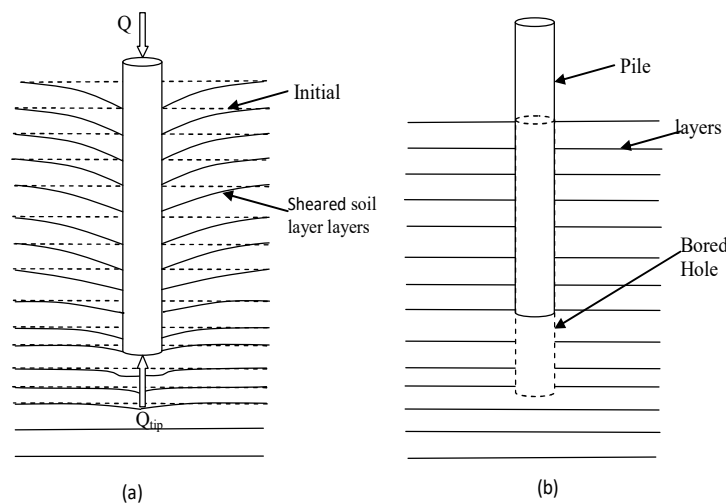


Figure I.8. (a) Soil layer deformation on Displacement pile on driving pile (b) Non-Displacement on bore pile

But, The standard NF P 94-262 (AFNOR, 2012) proposes two installation technique of piles as displacement pile and non-displacement pile followed by 20 type number of the pile which is divided into 8 group code (table I.3).

Table I.3. Classification of piles (AFNOR,2012)

Group code	Pile no.	Pile description	Category
1	1	Pile or barrette bored in dry	Non Displacement pile
	2	Pile or barrette bored with slurry	Non Displacement pile
	3	Bored and cased pile (permanent casing)	Non Displacement pile
	4	Bored and cased pile (recoverable casing)	Non Displacement pile
	5	Dry bored pile /or slurry bored piles with grooved socket /or pier (3 types)	Non Displacement pile
2	6	Bored pile with a single or a double rotation CFA (2 types)	Non Displacement pile
3	7	Screwed case in place	Displacement pile
	8	Screwed piles with casing	Displacement pile
4	9	Pre-cast or pre-stressed concrete driven pile (2 types)	Displacement pile
	10	Coated Driven Pile (concrete, mortar, grout)	Displacement pile
	11	Driven Cast-in-Place Pile	Displacement pile
	12	Driven Steel Pile, Closed End	Displacement pile
5	13	Driven Steel Pile, Open End	Displacement pile
6	14	Driven H Pile	Displacement pile
	15	Driven Grouted H Pile	Displacement pile
7	16	Driven Sheet Pile	Displacement pile
1	17	Micropile Type I	Non Displacement pile
	18	Micropile Type II	Non Displacement pile
8	19	SGP Micropile (Type III) / or SGP Pile	Non Displacement pile
	20	MRP Micropile (Type IV) / or MRP Pile	Non Displacement pile

### I.3.1.2 Time effect

The soil disturbance occurs during the installation. The reformation of soil strength around the pile depends on the time, especially on clay as an effect of the consolidation process. The increasing of soil capacity decreases after the installation of the pile that is installed on clay, sand or fine sand. This phenomenon known as "*soil setup*" effect. But sometimes, the pile which is installed on the saturated sand and compacted silt, the soil capacity decreases shortly after installation. This phenomenon is known as "*relaxation*".

The pore water pressure increases while the pile is driven into the saturated cohesive soil. The increment of the diameter of pile effects to the increase of pore water pressure. It is a part of the effect of the shear and the deflection, and another part is affected by the radial compression that occurs while driving the pile. Increasing water pressure reduces the effective pressure of soil, and also decreasing the shear strength of soil. It effects to the decreasing of the pile-capacity during installation and a short time after. After installation, the pore water pressure decreases through radial flow around the pile (the soil compacted because of the pore water flows away). It known as consolidation process that effects to increase the shear strength. The increasing of the shear strength and the soil capacity are known as "*soil setup*". The variation of pile-capacity with time depends on type soil, type of pile and the dimension of the pile.

Figure I.9 shows the variation of pile-capacity with time that compiled by *Fleming et al., 2008*. There are three piles driven into the soft clay. That Figure describes where the pile-capacity increases dealing with time.

The opposite to above phenomenon, the pile-capacity also can decrease with time after installation. It calls "relaxation". This phenomenon occurs when the pile is installed to the saturated stiff fine granular soil such as dense silt and fine cohesionless soil. The relaxation occurs because of the densification of granular around the pile that is effected by driving pile. At the beginning of installation, the increasing of negative pore water pressure effects to the increase of shear strength of soil at the moment. After the installation, the negative pore water pressure decreases gradually to the positive pore water pressure, and the effective pressure of soil also decreases. These also effect on decreasing of the pile-capacity.

Because of the decreasing of pile-capacity after installation due to relaxation effect, it is very important to assess the capacity of the pile after the equilibrium occurs in the soil. Federal Highway Administration (*FHWA, 2006*) proposes a static loading test for the saturated silt and stiff

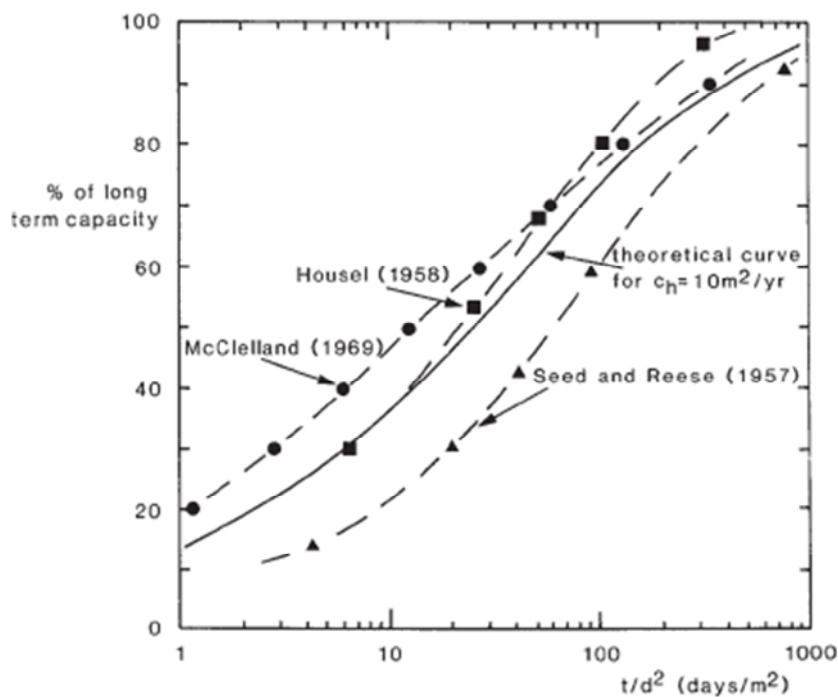


Figure I.9. Variation of pile-capacity with time (*Fleming et al, 2009*)

### I.3.1.3 Compressibility of Pile

The load-deformation response of pile has been examined in any calculation method such as numerical method, finite element method or boundary element method (*frank, 1974 and Randolph, 1977*). The development methods show that the settlement of pile depends on various parameters such as pile geometry and stiffness, and soil stiffness.

The shaft compression occurs during loading, and the deflection of pile can be estimated (Fleming, 2008). The movement due to slip occurs 0.5 to 2% of the pile diameter in clay and 0.2% in the sand where It starts at  $P_{slip}$  of pile load. The ratio between  $P_{slip}$  and ultimate shaft capacity  $Q_s$  usually is taken between 0.5 to 0.6 (Fleming,2008). It shows that the failure around the pile can occur at the load level which is lower than maximum axial friction. This phenomenon is related to the compressibility of the pile and rigidity (Murff, 1980). In the flexible pile, a failure is achieved gradually through the pile. The failure may occur at the top of soil surrounding the pile while at the lower layer of soil has not reached the failure yet. But for the rigid pile, the friction peaks are mobilised along the pile surrounding the pile at the same time. The behaviour of this mobilisation is shown in Figure I.10. Where the value of  $R_f$  is affected by the value of the flexibility ratio  $K$ .

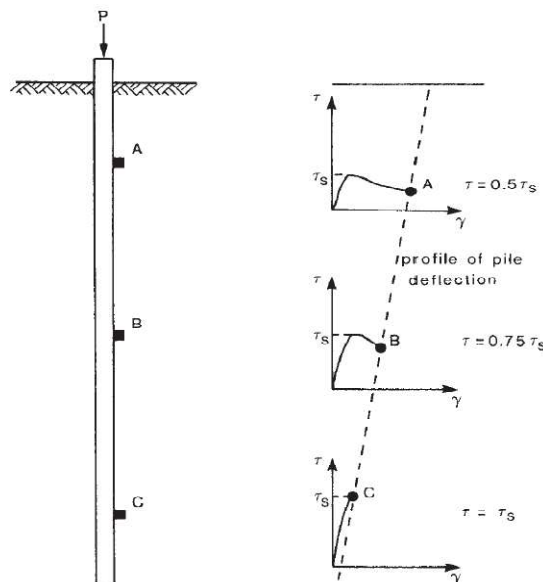


Figure I.10. The progressive failure of along pile

Randolph (1983) introduced the equation for the ratio of flexibility as equation I.4.

$$K = \frac{\pi d q L^2}{(EA)_p \Delta w_{res}} \quad (I.4)$$

Where,  $\Delta w_{res}$  is the relative movement from peak to residual,  $d$  is diameter of pile,  $L$  is length of pile and  $(EA)_p$  is the parameter of modulus young and area of pile. In order to allow the progressive failure of the pile, the value of reduction factor should be applied to shaft pile-capacity base on peak value of shaft friction that is shown in Figure I.11.

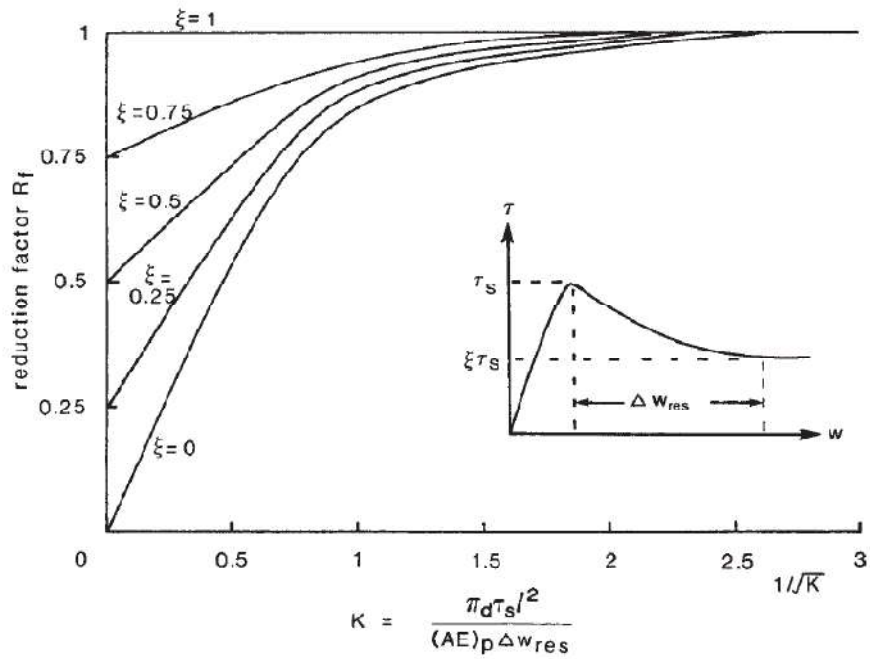


Figure I.11. Variation of reduction factor with pile stiffness ratio

### I.3.2 Loads Transfer T-z Method

The load-displacement relationship for axial load piles can be described through two loading mechanism, soil skin friction along the shaft and end-bearing of soil. The pile-capacity ( $R_c$ ) is the ability of pile supporting the load which is a combination between shaft resistances ( $R_s$ ) and bearing capacity ( $R_b$ ) of the pile for axial load pile (Figure I.12.a and equation I.1).

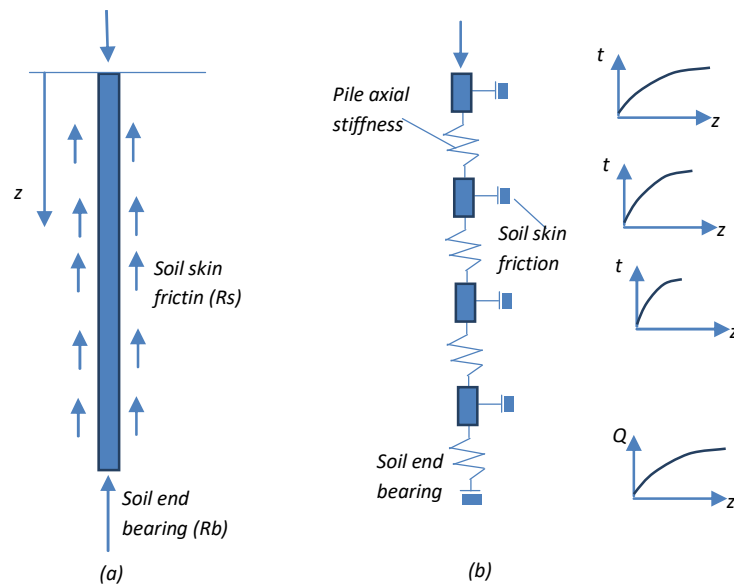


Figure I.12. The mechanism on axially monotonic load (a) transfer mechanism and (b) spring-mass model

The shaft resistances ( $R_s$ ) is total resistance along the pile calculated from equation I.3 where  $q_{si}$  is unit load transfer in skin friction at segment  $i$  (normally varies with depth),  $h_i$  is length at segment  $i$  and  $P_i$  is perimeter of pile at segment  $i$ . the bearing resistance ( $R_b$ ) is calculated from equation I.2 where  $q_b$  is unit end-bearing resistance and  $A_b$  is cross section area of pile. For an open tube pile, there are two condition of pile in bearing capacity mechanism which are plugged and unplugged condition (Figure I.13). The plugged condition (Figure I.13.a) happen when the open tube on tip of pile is compacted with the soil then the load transfer mechanism using full cross section area ( $A_{plugged}$ ). And for unplugged condition (Figure I.13.b) consist of soil against the pile cross section area and internal skin friction ( $q_{s,internal}$ ) from the soil movement inside the shaft of pile. The equation I.5 is used for plugged condition ( $R_{b,plugged}$ ), and the equation I.6 is used for unplugged condition ( $R_{b,unplugged}$ ).

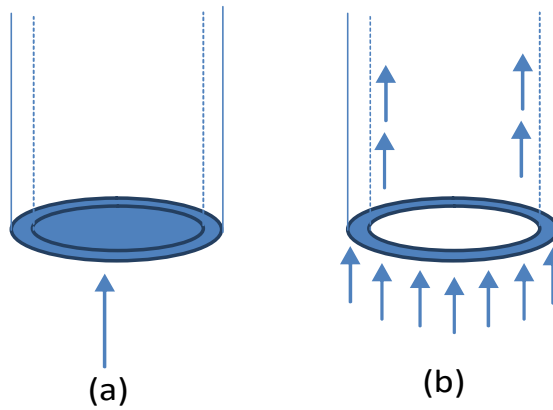


Figure I.13. End bearing resistance considering (a) plugged condition and (b) unplugged condition

$$R_{b,plugged} = q_b A_{b,plugged} \quad (I.5)$$

$$R_{b,unplugged} = q_b A_{b,unplugged} + q_{s,internal} A_{s,internal} \quad (I.6)$$

Where,  $A_{b,unplugged}$  is unplugged cross section area at the pile toe and  $A_{s,unplugged}$  is surface area of the pile segment inside the shaft interior in contact with soil in shear.

On  $T$ - $z$  curve method, the stress-strain relationship can be described through three loading mechanisms (Figure I.14) that are an axial deformation of the pile, soil skin friction and soil end-bearing. Springs present the interaction between pile and soil, the mobilisation of shaft friction described by non-linear springs distributed along the shaft and single spring at the base. The pile is divided into several segments due to the axial stiffness.

The equation for the load transfer of external force on pile taken from the reaction at skin friction and pile deformation, the equilibrium of force can be seen at free body diagram of pile segment at depth  $z$  in Figure I.14.

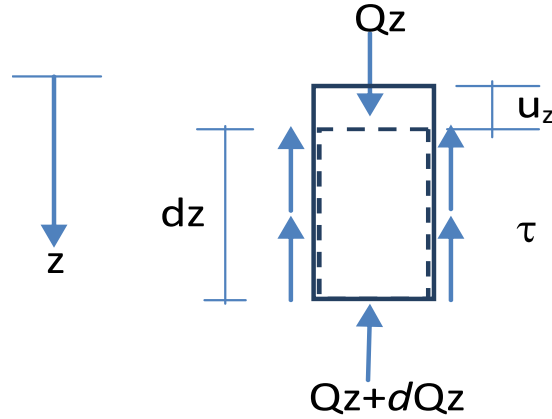


Figure I.14. Free body diagram of pile segment

While the load applied on the segment, the reaction from shaft friction and internal pile force balance the load and then deformation occurs ( $u_z$ ). These situation expressed by the following equation:

$$Q_z = Q_z + dQ_z + \tau.C.dz \quad (I.7)$$

$$-\frac{dQ_z}{dz} = \tau.C \quad (I.8)$$

And the following equation for axially loaded beam describes the development of internal force in pile due to deformation,

$$Q_z = -EA \frac{du_z}{u_z} \quad (I.9)$$

where,  $Q_z$  = internal pile force at depth  $z$

$\sigma$  = soil unit friction at depth  $z$

$C$  = circumference of pile at depth  $z$

$E$  = Modulus elasticity of pile at depth  $z$

$A$  = Cross section area of pile at depth  $z$

$u_z$  = Displacement of pile segment at depth  $z$

Substitution the equation I.8 which is differentiated by  $z$  into equation I.9 yields to be the governing equation for the pile and soil as the following equation,

$$EA \frac{d^2u_z}{uz^2} = \tau.C \quad (I.10)$$

$$\tau.C - EA \frac{d^2u_z}{uz^2} = 0 \quad (I.11)$$

In this method, the force which is produced by the unit weight of pile is negligible.





$$z_{si} = \left(\frac{B}{\lambda_{si}}\right) q_{si} \tag{I.13}$$

And the sloop is controlled by  $k_s$  for the  $T$ - $z$  curve and  $k_b$  for the  $P$ - $y$  curve. Both  $k_s$  and  $k_b$  are the functions of the Pressure-meter modulus  $E_m$ , which is governed by equation I.14 and I.15

For fine soils  $k_s = 2.0 \frac{E_m}{B}$  and  $k_b = 11 \frac{E_m}{B}$  (I.14)

For granular soil  $k_s = 0.8 \frac{E_m}{B}$  and  $k_b = 4.8 \frac{E_m}{B}$  (I.15)

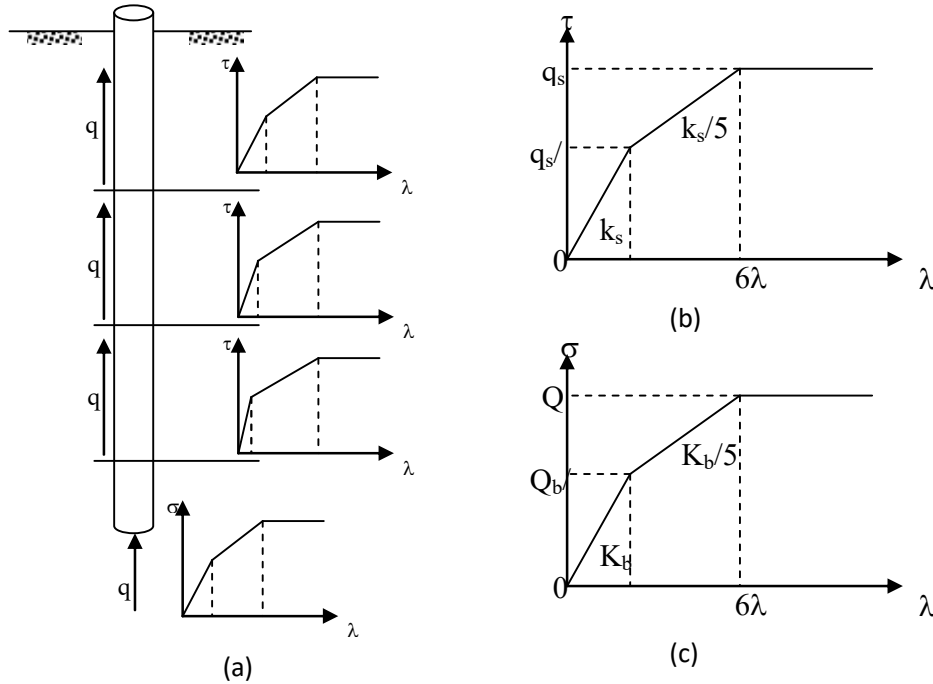


Figure I.16. (a) Load-Transfer mechanism (b) the T-z curve (c) the q-z curve (after Frank and Zhao,1982)

Since 1993, The calculating rules of pile-capacity from Pressure-meter test adopted from the new code of practice for foundations (MELT, 1993) known as the Fascicule 62-V. Bustamante et Gianceselli (2006) proposed the possibility of installation technique that made the possibility of re-adjusting the parameter of calculation of the axial limit coefficient. They proposed from 17 categories of the pile in Fascicule 62-V into 20 categories which have been grouped into eight classes.

Burlon et al. (2014) revised the previous calculation that presented by Bustamante et Gianceselli (2006). The revision proposed for compliance in France standard with the requirements of Eurocode 7. The standard is relating to the dimensioning of the deep foundation NF P 94-262 (AFNOR,2012).

Generally, the bearing capacity of the pile is expressed by equation I.16. But to express the value of  $R_b$  (tip bearing capacity) and  $R_s$  (shaft resistance) with PMT result are;

$$Rb = A k_p P l e^* \tag{I.16}$$

Where  $A$  = the pile tip area, where for steel driven piles are illustrated on Figure I.17.

$k_p$  = the tip bearing factor

$P l e^*$  = the net equivalent Menard limit pressure under and around the pile tip

$$P l e^* = \frac{1}{b + 3a} \int_{D-b}^{D+3a} P l^*(z) dz \tag{I.17}$$

$$a = \max \left\{ \frac{B}{2}; 0,5 \right\}$$

$$b = \min \{ a; h \}$$

Where  $h$  = the thickness of soil that is contained the carrier formation (resisting layer).

$a$  = the limit above the pile tip

$b$  = the limit below the pile tip

$B$  = Diameter of pile

$D$  = Depth of pile

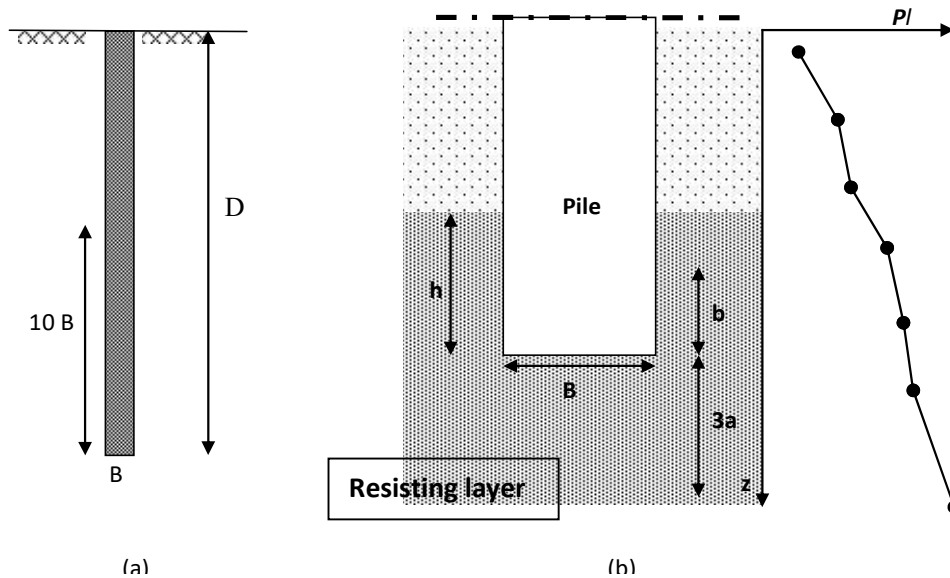


Figure I.17. Model of the full pile (a) model of the base of pile (b)

$$D_{ef} = \frac{1}{P l e^*} \int_{D-10B}^D P l^*(z) dz \tag{I.18}$$

Where,  $D_{ef}$  = effective depth of pile

When the value of  $D_{ef}/B$  is bigger then 5 and  $k_p$  is equal to  $k_{pmax}$  where the value is depend on soil type and pile class (table II.1). If the value of  $D_{ef}/B$  is less then 5, use equation I.19 for the value  $k_p$ , as described at Figure I.18.

$$k_p = 1.0 + \frac{(k_{pmax} - 1.0) D_{ef}}{5B} \quad (I.19)$$

At least, the embedded pile is equal to 3 times of diameter or 1,5 meters depth for the pile with the diameter greater than 0,5 meter.

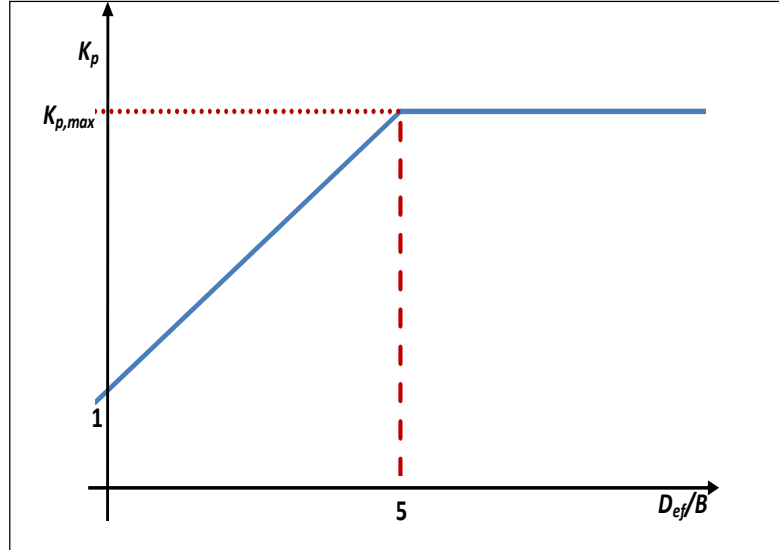


Figure I.18. Value of  $k_p$  and  $D_{ef}/B$

Table I.4. Value for the tip bearing resistance factor  $k_{p,max}$  for  $D_{ef} \geq 5$  (Burlon et al, 2014)

Group code	Clay & Silt	Sand , Gravel	Chalk	Marl and Limestone	Weathered Rock
1	1.25	1.2	1.6	1.6*	1.6
2	1.3	1.7	2.0	2.0	2.0
3	1.7	3.9	2.6	2.3	2.3
4	1.4	3.1	2.4	2.4*	2.4*
5	1.1	2.0	1.1	1.1*	1.1*
6	1.4	3.1	2.4	1.4*	1.4*
7	1.1	1.1	1.1	1.1*	1.1*
8	1.4	1.6	1.8	1.8	1.5*

\* A higher  $k_p$  value can be used but must be proven by a load test

The ultimate skin friction is expressed by equation I.20.

$$R_s = \sum A_{si} q_{si} \quad (I.20)$$

$$A_{si} = P_i \cdot h_i \quad (I.21)$$

Where,  $A_{si}$  is the side surface area at segment  $i$ ,  $P_i$  is the perimeter of pile and the developed perimeter for calculation is illustrated on Figure I.19, and  $h_i$  is thickness of segment at segment  $i$ .

And,  $q_{si}$  is the ultimate unit skin friction at segment  $i$  where the value gives empirically considering the category of the pile, type of soil and pressure limit  $p_l^*$ . The expression for unit skin friction at equation I.23. where the minimum value from both calculations are taken.

$$q_s = \text{Min} \{(\alpha_{\text{spile-soil}} f_{\text{soil}}(p_l^*)), (q_{s-\text{max}})\} \tag{I.22}$$

$$f_{\text{soil}}(p_l^*) = (a_i + b_i \cdot p_l^*) (1 - e^{-c_i \cdot p_l^*}) \tag{I.23}$$

The parameter of  $f_{\text{soil}}$  are defined by three parameters  $a_i$ ,  $b_i$  and  $c_i$  where the value depends on the soil type (presented on table I.5 and Figure I.19). These parameters and the installation factor  $\alpha_{\text{soil-pile}}$  (table I.6) are adjusted to optimize functions of the ratio of the calculated values to the measured values for the three quantities of  $R_b$ ,  $R_s$  and  $R_c$ .

The maximum Value ultimate skin friction  $q_{s-\text{max}}$  for each soil type and installation methods are presented in table I.7.

Table I.5. Selecting the  $Q_i$  line to obtain the limit unit skin friction value  $q_s$  (Burlon et al,2014)

Type of soil	Clay (%CaCO3<30%) silt soil itmediate	Sand , Gravel	Chalk	Marl and Limestone	Weathered Rock
Curve	Q1	Q2	Q3	Q4	Q5
a (MPa)	0.003	0.01	0.007	0.008	0.01
b (MPa)	0.04	0.06	0.07	0.08	0.08
c (MPa)	3.5	1.2	1.3	3	3

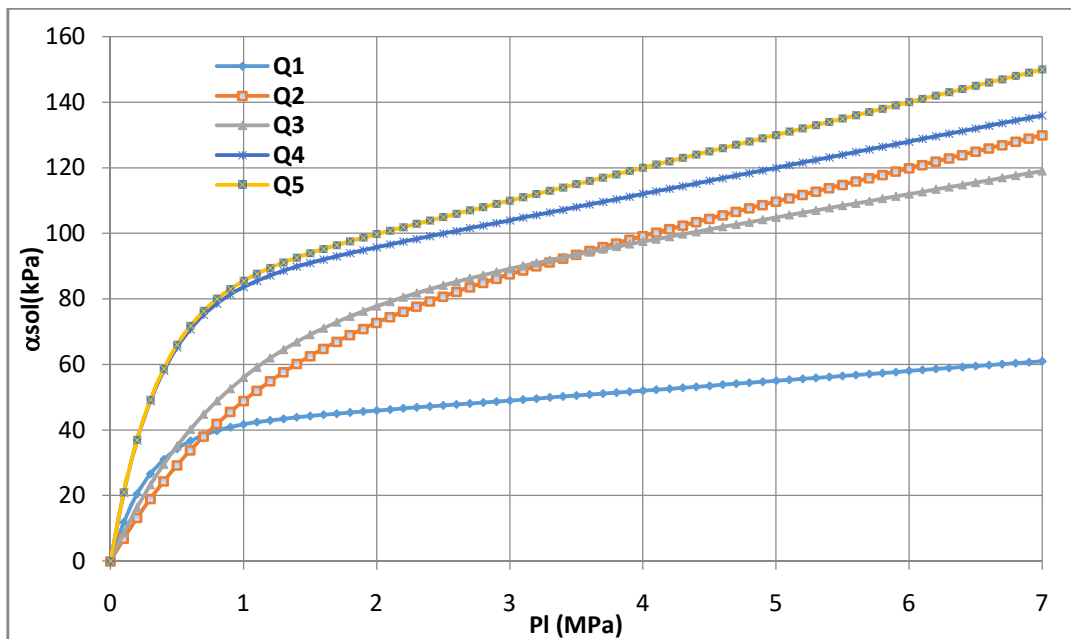


Figure I.19. Friction curve  $f_{\text{soil}}(p_l^*)$

Table I.6. Value of installation factor  $\alpha_{\text{soil-pile}}$  (Burlon et al, 2014)

No	Installation methods	Clay (%CaCO <sub>3</sub> <30%) silt soil intermediate	Sand , Gravel	Chalk	Marl and Limestone	Weathered Rock
1	Pile or barrette bored in dry	1.1	1	1.8	1.5	1.6
2	Pile or barrette bored with slurry	1.25	1.4	1.8	1.5	1.6
3	Bored and cased pile (permanent casing)	0.7	0.6	0.5	0.9	0.9
4	Bored and cased pile (recoverable casing)	1.25	1.4	1.7	1.4	1.6
5	Dry bored pile /or slurry bored piles with grooved socket /or pier (3 types)	1.3	1.4	1.8	1.5	1.6
6	Bored pile with a single or a double rotation CFA (2 types)	1.5	1.8	2.1	1.6	1.6
7	Screwed case in place	1.9	2.1	1.7	1.7	1.7
8	Screwed piles with casing	0.6	0.6	1	0.7	0.7
9	Pre-cast or pre-stressed concrete driven pile (2 types)	1.1	1.4	1	0.9	0.9
10	Coated Driven Pile (concrete, mortar, grout)	2	2.1	1.9	1.6	1.6
11	Driven Cast-in-Place Pile	1.2	1.4	2.1	1	1
12	Driven Steel Pile, Closed End	0.8	1.2	0.4	0.9	0.9
13	Driven Steel Pile, Open End	1.2	0.7	0.5	1	1
14	Driven H Pile	1.1	1	0.4	1	0.9
15	Driven Grouted H Pile	2.7	2.9	2.4	2.4	2.4
16	Driven Sheet Pile	0.9	0.8	0.4	1.2	1.2
17	Micropile Type I	1.25	1.4	1.8	1.5	1.6
18	Micropile Type II	1.25	1.4	1.8	1.5	1.6
19	SGP Micropile (Type III) / or SGP Pile	2.7	2.9	2.4	2.4	2.4
20	MRP Micropile (Type IV) / or MRP Pile	3.4	3.8	3.1	3.1	3.1

Note. For the categories 9 to 16, the above value are multiplied by 0.75 when the piles are vibro-driven instead of being driven.

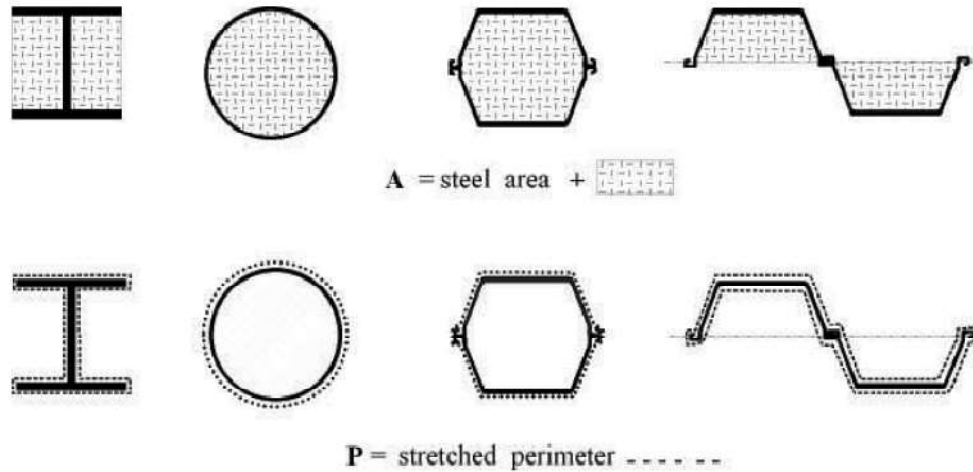


Figure I.20. Area A and perimeter P to be used for open-end steel piles & sheet piles

Table I.7. The maximum Value ultimate skin friction  $q_{s-max}$

No	Instalation methods	Value in kPa				
		Silt and clay, percentage Calcium carbonate (CaCO3) < 30%	Sand , Gravel	Chalk	Marl and Limestone	Weathered Rock
1	Pile or barrette bored in dry	90	90	200	170	200
2	Pile or barrette bored with slurry	90	90	200	170	200
3	Bored and cased pile (permanent casing)	50	50	50	90	---
4	Bored and cased pile (recoverable casing)	90	90	170	170	---
5	Dry bored pile /or slurry bored piles with grooved socket /or pier (3 types)	90	---	---	---	---
6	Bored pile with a single or a double rotation CFA (2 types)	90	170	200	200	200
7	Screwed case in place	130	200	170	170	---
8	Screwed piles with casing	50	90	90	90	---
9	Pre-cast or pre-stressed concrete driven pile (2 types)	130	130	90	90	---
10	Coated Driven Pile (concrete, mortar, grout)	170	260	200	200	---
11	Driven Cast-in-Place Pile	90	130	260	200	---
12	Driven Steel Pile, Closed End	90	90	50	90	---
13	Driven Steel Pile, Open End	90	50	50	90	90
14	Driven H Pile	90	130	50	90	90
15	Driven Grouted H Pile	200	380	320	320	320
16	Driven Sheet Pile	90	50	50	90	90

### I.3.3 Loads Transfer P-y Method

The most application used for lateral deflection analysis of pile is the  $P$ - $y$  method. This method has been widely used because represents the calibration of actual conditions obtained from the full-scale test. Figure I.21.a, the cylindrical pile under lateral load, shows that the distribution of unit normal stress around the pile is uniform before displacement occurs (Figure I.21.b). When the deflection occurs at the distance  $y_1$  and the depth  $z_1$ , the distribution of stress looks like Figure I.21.c. By resisting force ( $P_1$ ) at the opposite direction of the load which the stress decreases on the backside of the pile and increases on the front and also at the left and right side of the pile which has both normal and shearing stress as the displaced soil tries to move around the pile.

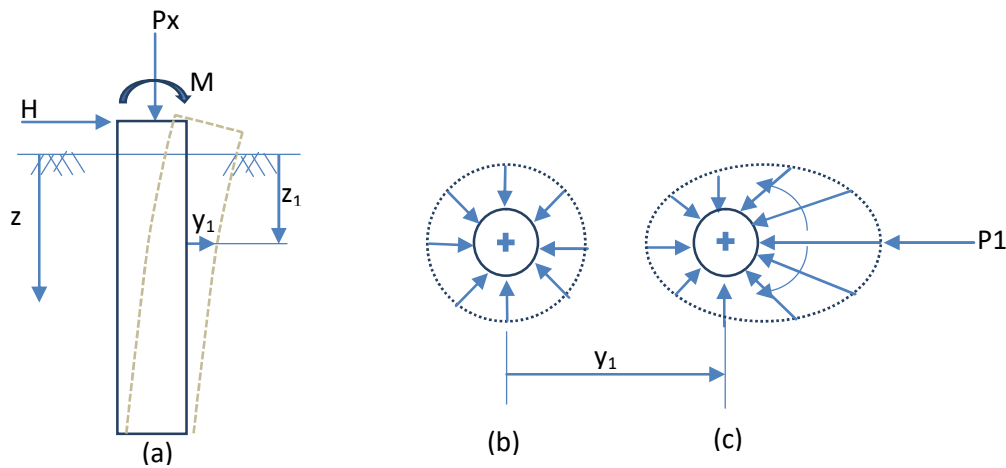


Figure I.21. Unit stress distribution in lateral load

The  $P$ - $y$  method defines the relationship between lateral load and deflection which occurs between soil and pile described in a curve.

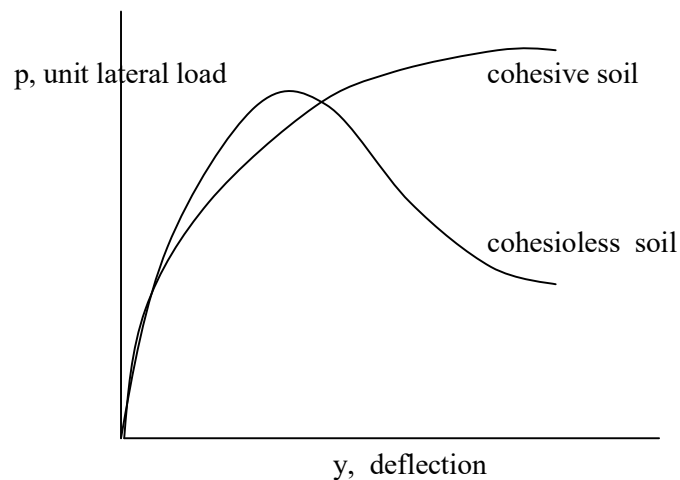


Figure I.22. Behavior of P-y curve (Coduto, 1994)

The axis-p is unit lateral load, and the axis-y is a lateral deflection of the pile. The behaviour of  $P$ - $y$  curve showed in Figure I.22 which is describing the relationship on the  $P$ - $y$  curve for cohesive soil and cohesionless soil.

The influence parameter on the  $P$ - $y$  curve is the type of soil, type of load (short/long term, monotonic or dynamic), the diameter of the pile, shaft friction, depth of pile, installation method and interaction pile to pile in a group of the pile. The analysis in the  $P$ - $y$  method is done by considering the behaviour of  $P$ - $y$  curve throughout the pile (Figure I.23). It can be solved by Finite difference analysis which divides the pile into  $n$  segments. For the analysis, the boundary condition is needed. There is two boundary condition at the tip of the pile, shear stress and zero moments. Boundary condition on top of pile depends on the type of connection of piles head with pile-cap (unrestrained/free-head pile and restrained/fix-head pile), as follows:

- Unrestrained/free-head pile, horizontal shear strength ( $V$ ) and moment ( $M$ ) are determined. On piles head, there is rotation and deflection ( $S_t \neq 0$  and  $y_t \neq 0$ )
- Restrained/fix-head pile, horizontal shear strength ( $V$ ) and slope ( $S_t$ ) are defined. For the first assumption,  $S_t$  is null, but it can have value.

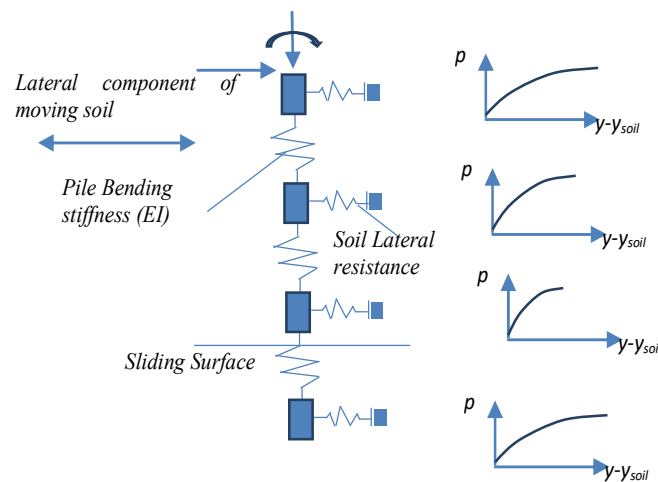


Figure I.23. Pile segment discretization pile element and soil element.

The differential equation for a beam column is described by equation I.24 solving the implementation of the  $P$ - $y$  method.

$$E_p I_p \frac{d^4 y}{dx^4} + P_x \frac{d^2 y}{dx^2} + E_{p-y} y - W = 0 \quad (I.24)$$

where,  $y$  = displacement of pile

$E_p I_p$  = bending stiffness of pile



$P_x$  = axial load on pile head

$E_{p-y}$  = soil reaction modulus based on P-y curve

$W$  = distribution load of pile on segment

Further formulas define behaviour of pile in each segment,

$$S_z = \frac{dy}{dx} \tag{I.25}$$

$$M_z = E_p I_p \frac{d^2 y}{dx^2} \tag{I.26}$$

$$V_z = E_p I_p \frac{d^3 y}{dx^3} + P_x \frac{dy}{dx} \tag{I.27}$$

where,  $S_z$  = slope of the curve defined by the axis of pile

$M_z$  = bending moment of the pile

$V_z$  = shear in pile

As mentioned before, the discretisation of the pile to be some nodes from 0 at the top of the pile until  $n$  segment to the tip of the pile by  $h$  length (Figure I.24). It is done on the pile to define the differential equation on the finite difference form into the numerical term and allows the solution to be achieved the iteration. It provides the solution for variation of bending stiffness of pile ( $E_p I_p$ ) down along the pile and the of soil reaction ( $E_{p-y}$ ) varied with pile deflection, required for P-y method. During the discretisation, the additional nodes and the imaginary nodes are required respectively 2 nodes above the pile and 2 nodes below the toe of pile. These nodes are only used to obtain the solution in iteration.

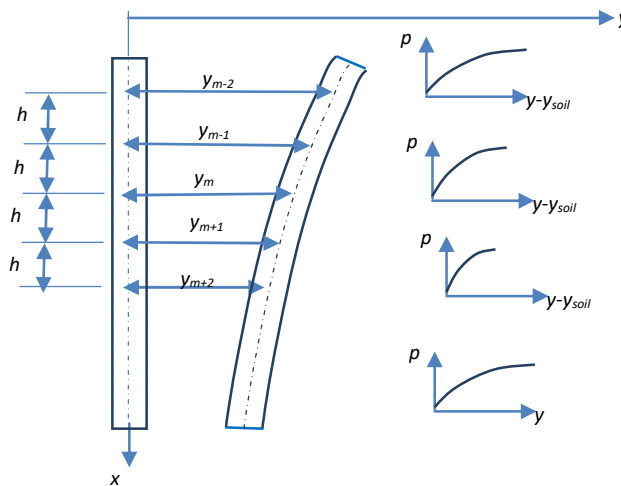


Figure I.24. The P-y curve at pile segment adjusts with depth

The imaginary nodes are used to define boundary condition of iteration. In this iteration, there are five boundary conditions can be derived from pile head: shear ( $V$ ), moment ( $M$ ), slope ( $S$ ),

rotation stiffness ( $\frac{M}{S}$ ), and deflection ( $y$ ). Since only two boundary condition can be identified that are employed at the piles toe based on moment and shear. The moment is set to zero at the toe and assuming the value of deflection ( $y$ ) to define the value of shear stress ( $V$ ). In lateral load analysis, differential method is made by solving the differential equation using the assumptions that the pile is geometrically straight, eccentric loads are not considered, transverse deflection deflections are small and also deflections due to shearing stress are small.

### Predicting Pile Lateral Behaviour by Frank & Zhao method (Pressure Meter Test)

The Winkler theory for the horizontal beam on the elastic support is,

$$EI \frac{d^4y}{dz^4} + k \cdot B \cdot y = 0 \quad (I.28)$$

Then, the value of  $k$  is obtained from settlement equation  $w=f(Em)$  (Menard, 1963) for an infinitely long strip footing, of width  $B$ , since  $k \cdot B = p/w$ .

The value of  $E_s$  is expressed by equation I.29 where  $E_s$  is in average, for  $B$  larger than 0,6 meters, below the critical depth.

$$k \cdot B = E_s = \frac{18E_m}{4 \left(2.65 \left(\frac{B_0}{B}\right)\right)^\alpha \left(\frac{B_0}{B}\right) + 3\alpha} \quad (I.29)$$

Where,  $\alpha$  is the Menard rheological factor ( $1/4 < \alpha < 2/3$ ) and  $B_0$  is reference diameter equal to 0,6 m. In the difference loading condition using the generalized  $P$ - $y$  curve (Figure I.25), Frank (1999) mentions that the decrease of  $k$  as  $y$  depends on the creep (or yield) pressure  $p_c$  (which can be estimated as  $p_c = P_l/2$  (Viana, 2012))

Figure I.31 explains the soil reaction due to type of load where Figure I.25(a) is the graph for permanent actions at pile head, (b) is for short time actions at pile head, (c) is for soil lateral thrust, and (d) mimics an unexpected instant actions at pile head.

Base on the parameter proposed by Menard et al. (1969) and Tuna et al. (2008,) the equation for  $B < B_0$  is,

$$\text{for } B < B_0; \quad E_s = \frac{18E_m}{4(2.65)^{\alpha+3\alpha}} \quad (I.30)$$

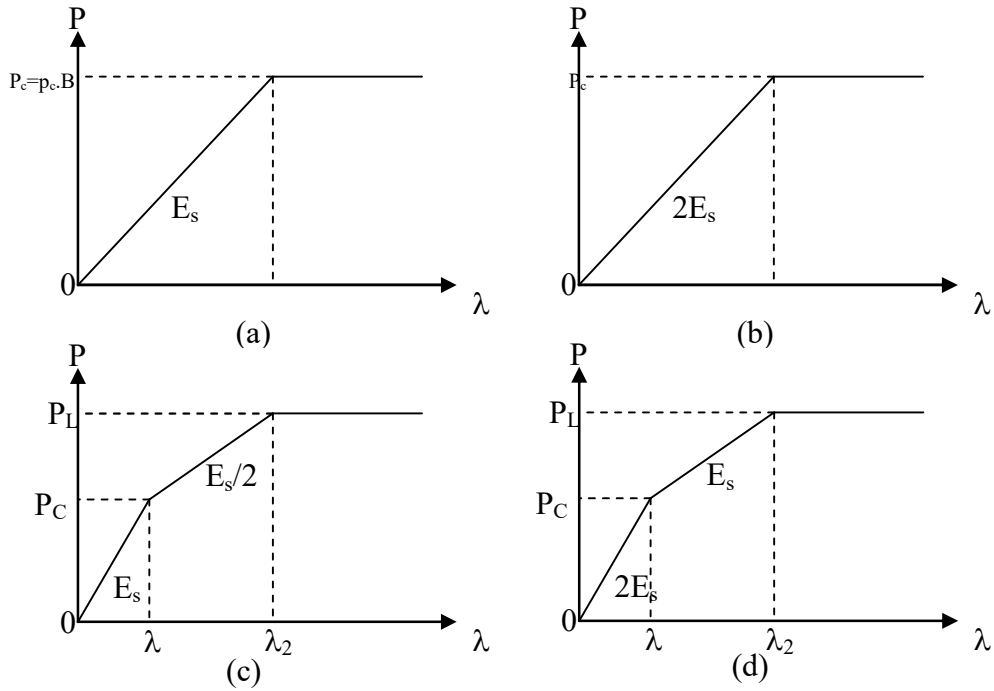


Figure I.25. Soil reaction against lateral displacement (after Frank, 1999)

### I.3.4 Hyperbolic Method

The hyperbolic model is a simple stress-strain relationship, it is based on the concept of the incrementally non-linear elastic behaviour. This model can be used for analysis of dams, excavation and various types of soil-structure interaction, but it is not suitable for predicting the instability or collapse loads (Kareem, 2007).

The hyperbolic stress-strain curve, both for clay and sand, can represent the stress-strain behaviour of soil reasonably accurately (Kondner, 1963) by the equation,

$$(\sigma_1 - \sigma_3) = \frac{\varepsilon}{\frac{1}{E_i} + \frac{\varepsilon}{(\sigma_1 - \sigma_3)_{ult}}} \quad (I.31)$$

Where,  $E_i$  is the initial slope of a stress-strain curve,  $(\sigma_1 - \sigma_3)_{ult}$  is the asymptotic value of the strength, and  $(\sigma_1 - \sigma_3)$  is the compressive strength of soil which is less than the value of the asymptotic value (Figure I.26.a). Figure I.26.b is the transformed stress-strain curve on a hyperbolic, where  $E_i$  and  $(\sigma_1 - \sigma_3)_{ult}$  values can be determined easily. Where, the curve presents the linear relationship between  $\frac{\varepsilon}{(\sigma_1 - \sigma_3)_{ult}}$  and  $\varepsilon$ .

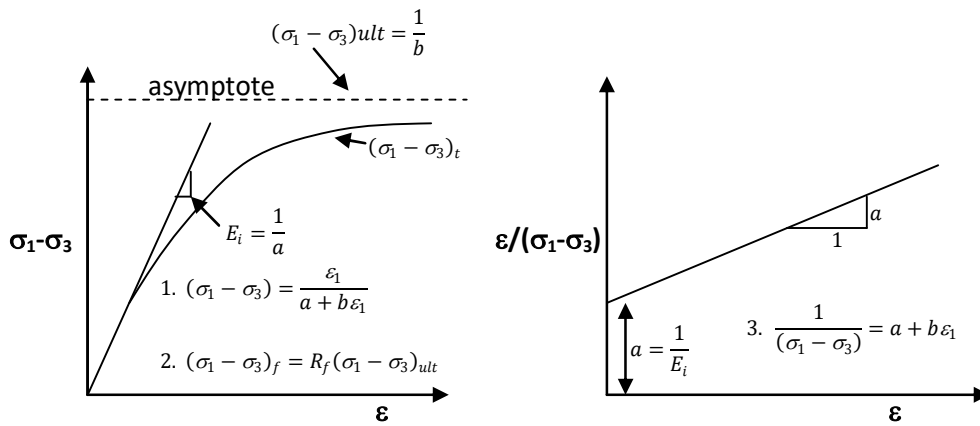


Figure I.26. Hyperbolic representation of stress-strain, *Kondner (1963)* (a) real curve (b) transformed curve

From the measured results (Figure I.27 and I.28), *Zhang (2013)* plots a curve of the load-displacement response of both the pile base (Figure I.27) and the shaft (Figure I.28). The load-displacement curve is taken to be hyperbolic in non-linearity.

The ultimate unit skin friction and initial gradient of the response are required to define the shaft response. Also on the pile base response where the ultimate unit end-resistance and the initial gradient are required to construct these curve.

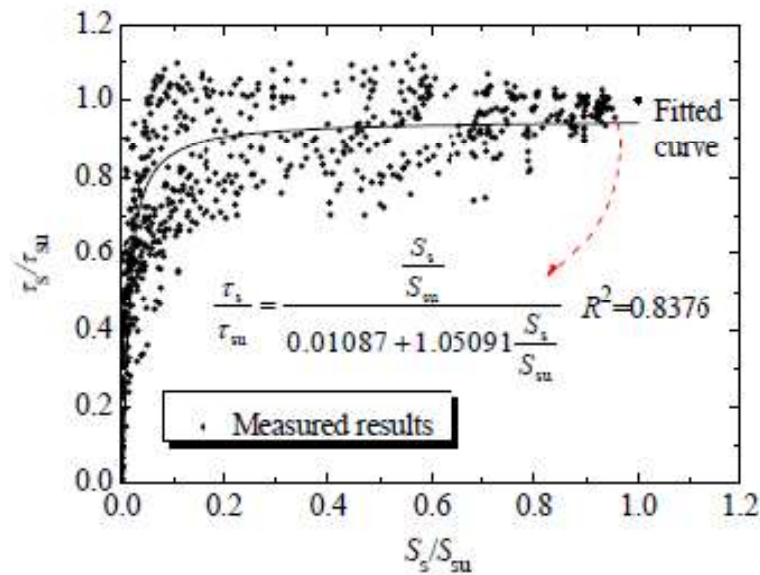


Figure I.27. Observed and theoretical relationship between shaft resistance and displacement (*Zhang et al. 2013*)

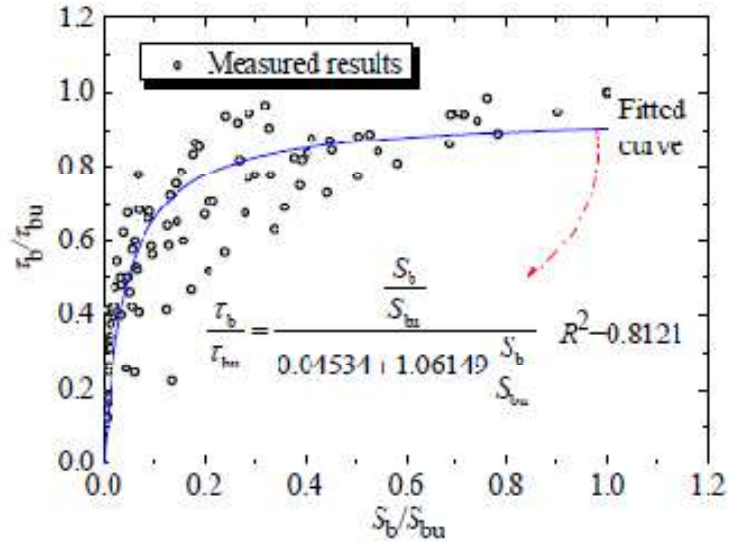


Figure I.28. Observed and theoretical relationship between end-bearing resistance and displacement ( Zhang et al. 2013)

In laterally load, Bouafia A (2007 and 2017) proposed the hyperbolic method using Pressure-meter test result and cone penetration test. The Pressure-meter test provides the  $E_m$  and  $P_l$  parameters respectively to Menard deformation modulus and the PMT limit pressure and for the cone penetration test provides  $q_c$  cone resistance that relates to  $E_{ti}$  and  $P_u$  in P-y curve parameters (Figure I.29)

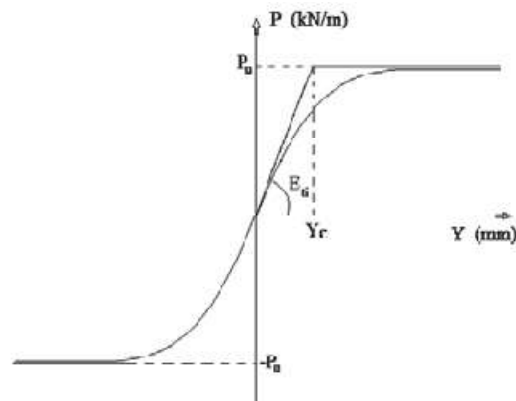


Figure I.29. Schematic shape of the P-Y curve (Bouafia A, 2013)

The equation of characteristic lateral reaction ( $E_{ti}$ ) is composed by equation I.32 (for PMT) and equation I.33 (for CPT) where  $K_E$  is the modulus number defined by equation I.34

$$E_{ti} = k_E \cdot E_m \tag{I.32}$$

$$E_{ti} = k_E \cdot q_c^* \tag{I.33}$$

$$k_E = a \cdot k_R^n \tag{I.34}$$

And the asymptote  $P_u$  is composed by equation I.35 (for PMT) and equation I.36 (for CPT) where  $K_P$  and  $K_C$  are the lateral resistance factor defined by equation I.37 and I.38.  $P_l^*$ ,  $q_c$  and  $B$  are PMT pressure limit, cone resistance from Cone penetration test, and  $B$  is diameter of pile.

$$P_{ui} = k_p P_l^* B \quad (I.35)$$

$$P_{ui} = k_c q_c^* B \quad (I.36)$$

$$k_p = b + c \cdot k_R^m \quad (I.37)$$

$$k_c = b \cdot k_R^m \quad (I.38)$$

The modulus number and lateral resistance factor are governed by the pile slenderness ration  $K_R$  (equation I.39 for PMT and equation I.40 for CPT) or called the lateral pile/soil stiffness ratio and these modulus are also varying of a, b, c, n and m due to limited data (Table I.8 and I.9) proposed by *Bouafia A*, 2013.

$$k_R = \frac{E_p \cdot I_p}{E_c \cdot D_e} \quad (I.39)$$

$$k_R = \frac{E_p \cdot I_p}{q_c \cdot D_e} \quad (I.40)$$

Table I.8. Value of the coefficient a,b,c,n and m for PMT (*Bouafia A*. 2013)

Soil	D/B	KR	a	n	b	c	m
Sand	≥ 10	≥ 0.01	0.33	-0.5	0.0	3.0	0.5
		< 0.01	3.40	0.0	0.0	0.31	0.0
Clay	≥ 5		1.85	-0.2	0.3	1.0	1.0
Silt			5.50	0.0	2.30	0.0	0.0
Organic clay			3.70	0.0	0.14	0.0	0.0

Table I.9. Value of the coefficient a,b,n and m for Cone penetration test (*Bouafia A*. 2017)

Soil	D/B	KR	a	n	b	m
Sand	≥ 10	≥ 0.02	0.1	-1.1	1.4	0.83
		< 0.02	7.00	0.0	0.06	0.0
Clay	≥ 7.5	≥ 0.03	3.00	-0.33	7.70	1.38
		< 0.03	3.00	-0.33	0.06	0.00
Silt			10.80	0.0	0.10	0.0
Organic clay			25.30	0.0	0.04	0.0

#### I.4 FINITE ELEMENT METHOD

The special form of finite element method is matrix analysis which is discretising the whole continuum element into a finite number of an element connected by difference nodal point. In the finite element analysis on soil solution, the  $T$ - $z$  curved is used to solve the governing differential equation that allows for simulation of the non-linear stress-strain behaviour of soil. It can be taken by employing non-linear stiffness curve denoted by the  $T$ - $z$  curve for soil skin friction and  $q$ - $z$  curve for end bearing resistance which computes at each iteration base on displacement value. The discretisation of the pile into segments term is used in the Finite Element Method. It is consist of two piles element and one soil shear element (Figure I.30). The effect of skin friction between pile and soil is characterized by single spring that selected on the midpoint of each pile segment, and the length of each shear element represents to the full length of each since there is one shear element per segment. The length of pile is divided into half per segment to represent two pile elements in the calculation of the pile axial stiffness.

Springs assumption at each segment on axial load analysis (Figure I.30.a) is made by solving the governing differential equation using finite element method. There is as follow four assumptions: geometrically of the pile is straight such that the second-order effects are not considered as the first assumption, the eccentric loads are not considered, the pile material is isotropic, and the deformation of the pile will not significantly change throughout the simulation to alter the initial pile geometry.

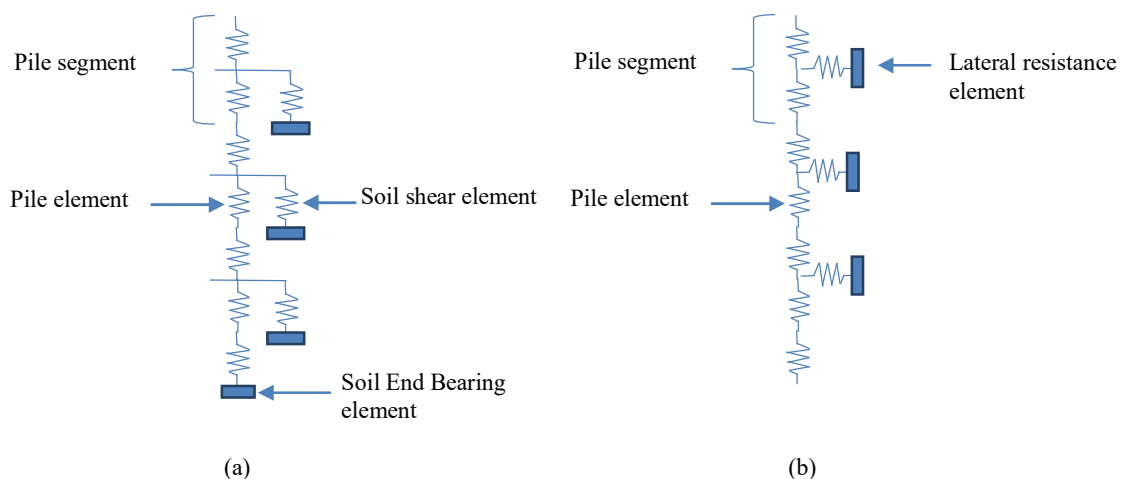


Figure I.30. Pile segment discretization into pile element and soil element.

under axial compression, the pile is assumed to be linear perfectly elastic and perfectly plastic. And the assumption of pile axial stiffness  $k_{pile,axial}$  in the elastic range of each element is calculated using equation I.41.

$$k_{pile,axial} = \frac{E_{pile} A_{pile}}{L_{pile}} \quad (I.41)$$

where  $E_{pile}$  is pile modulus of elasticity,  $A_{pile}$  is cross-section area of pile element, and  $L_{pile}$  is the length of pile element.

By using  $T$ - $z$  curve, the stiffness of each soil skin element  $k_{soil, shear}$  is found to obtain the unit skin friction corresponding the soil displacement of the current iteration using equation I.42

$$k_{soil, shear} = \frac{\tau_{segment} A_{s,ext}}{z_{segment}} \quad (I.42)$$

where,  $\tau_{segment}$  is soil unit skin friction in unit force per area,  $A_{s,ext}$  is surface area of the pile segment exterior in contact with soil in shear and  $z_{segment}$  is soil displacement of the current iteration on segment.

At the tip of pile, the stiffness is found using  $q$ - $z$  curve to obtain the end bearing resistance on elastic state corresponding to the soil displacement of the current assumption by equation I.43.

$$k_{soil,tip} = \frac{q A_{pile}}{z} \quad (I.43)$$

where,  $q$  is soil unit end-bearing capacity in unit force per area,  $A_{pile}$  is surface area of the tip of pile and  $z$  is soil displacement of the current assumption.

There are six steps involved in Finite Element Method. The first step is element discretization which has been explained above. The second step is determination of primary variable such as displacement, stresses, etc. The third is element equation derived using an appropriate variation principle as,

$$[K_E]\{\Delta d_E\} = \{\Delta R_E\}$$

Where,

$[K_E]$  = element stiffness matrix

$\{\Delta d_E\}$  = Vector of incremental element nodal displacements

$\{\Delta R_E\}$  = Vector of incremental element nodal forces

The fourth is global equation which is combined to form global equation;

$$[K_G]\{\Delta d_G\} = \{\Delta R_G\}$$

Where,

$[K_G]$  = Global stiffness matrix

$\{\Delta d_G\}$  = Vector of incremental Global nodal displacements

$\{\Delta R_G\}$  = Vector of incremental Global nodal forces



The fifth is boundaries condition which is modified by formulating the boundary condition such as point load and direction, pressure, the effect of incremental global nodal force and the displacement effect. The sixtieth is the solving of the global equation. It solves the displacement at all nodes that are used to evaluate the soil-structure interaction.

While the load subjected to the model then the displacement occurs, the state of the model in Flac3D can be identified by the pattern of Plasticity Flow indicator according to the stress-strain curve (Figure I.31) that is indicating the system still adjusting elastically or has been in the plastic state.

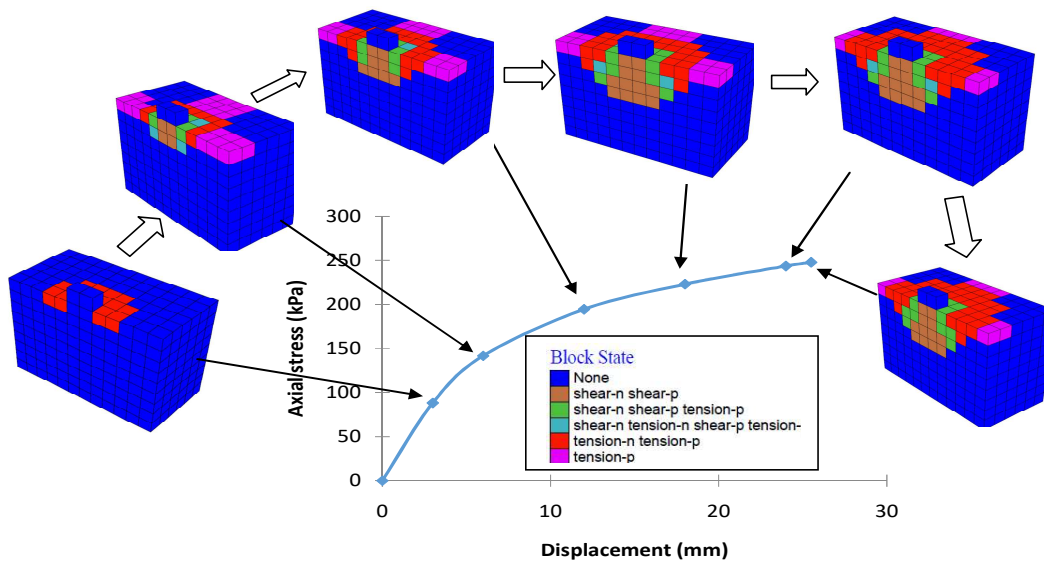


Figure I.31. The pattern of Plasticity Flow indicator on Flac3D

The plasticity state plot indicates two types of failure mechanism: shear failure and tensile failure where each type is designated by a different color. In which, indicating the failure has occurred in now (shear-n and tension-n for the shear and tension failure now) or past (shear-p and tension-p for the shear and tension in elastic state but previously at failure in the past).

## I.5 MACRO-ELEMENT MODELING

The concept of Macro-element had been widely used to simulate the macroscopic behavior of structural element connection such as for beam-column connections of steel, concrete and wooden structure. Likewise in geo-mechanic, this concept has been developed by *Nova and Montrasio (1991)* in the first time to simulate the nonlinearities in Soil-Structure Interaction. Then, other contributions were carried out in the context of the shallow foundation by *Pelluci, 1997, Cremer, 2001, Chatzigogos et al. 2007, Grange et al., 2008, Abboud et al. 2017.* Afterwards, in deep foundation context, *Tachiroglu 2006, Rha 2007 Li 2015, and Zheng Ji, 20019* presented the soil-structure interaction for vertical single pile.

### I.5.1 Macro-element Method for Shallow foundation

The scheme of macro-element structures (Cremer, 2001) are presented in Figure I.32. The soil domain is divided into two parts as far field and near field. The far-field remains the linear system and the nonlinearities of material and geometric (rocking and uplift) are lumped in the near field. Conceptually, these fields are separated by a boundary.

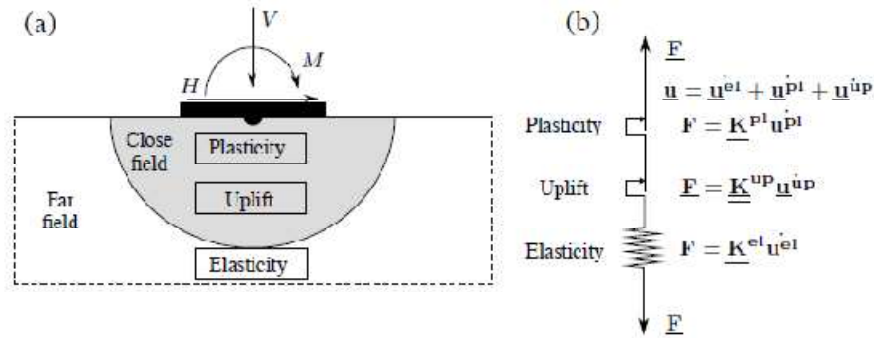


Figure I.32. General structure of macro-element a. Structure of macro-element b. System analogy

Each mechanism creates a part of displacement. The total displacement of the foundation can be written as equation I.44:

$$\dot{u} = \dot{u}^{el} + \dot{u}^{pl} + \dot{u}^{up} \quad (I.44)$$

where this decomposition considers three mechanisms (elasticity, plasticity and uplift). The elastic behavior can be written by following way,

$$F = K^{el} \cdot u^{el} \quad (I.45)$$

where  $K^{el}$  is the elastic stiffness matrix and  $u^{el}$  is the elastic displacement vector. The elastic stiffness matrix is defined as follows:

$$K^{el} = \begin{bmatrix} K_{zz}^{el} & 0 & 0 \\ 0 & K_{xx}^{el} & 0 \\ 0 & 0 & K_{\theta\theta}^{el} \end{bmatrix} \quad (I.46)$$

The nonlinearities of material and geometric exist in near field where three elements need to be established in plastic model. There are the ultimate loading, yield surface and flow rules.

The yield criteria is expressed by the formula,

$$f_{\infty} \equiv \left( \frac{H'}{aV'^c(1-V')^d} \right)^2 + \left( \frac{M'}{bV'^e(1-V')^f} \right)^2 - 1 = 0 \quad (I.47)$$

Where,  $a, b, c, d, e$  and  $f$  are the parameters for constitutive law.

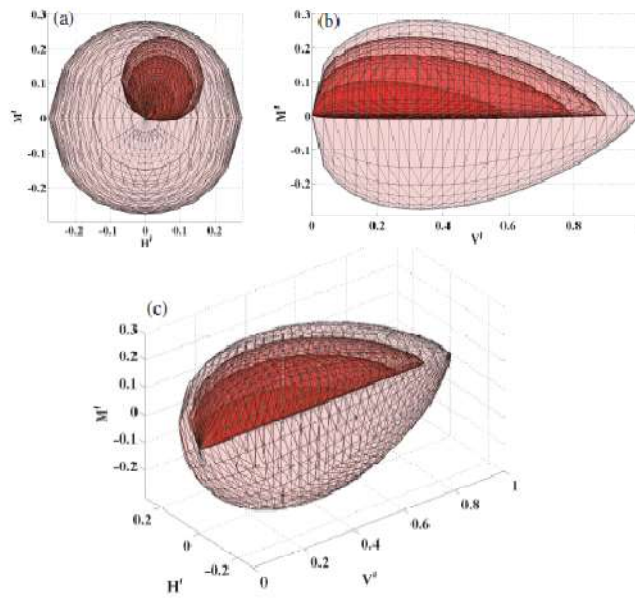


Figure I.33. Evolution of the charge surface within the rupture criterion of the Crémer model  
(Grange, 2008)

Chatzigogos, 2007 proposed a mechanism of macro-element (Figure I.34) where the uplift mechanism is less complete than Cremer, 2001 because he considers that uplift mechanism is in elastic non-linear mechanism.

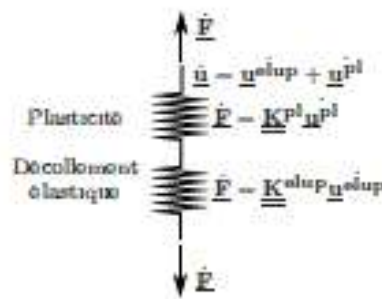


Figure I.34. General structure of macro-element of Chatzigogos, 2007.

By the framework of Chatzigogos, 2007 approach, three elements are established for the plastic model of uplift and soil yielding: (i) ultimate surface (ii) yield surface with the hardening law and (iii) the flow rules (Figure I.35).

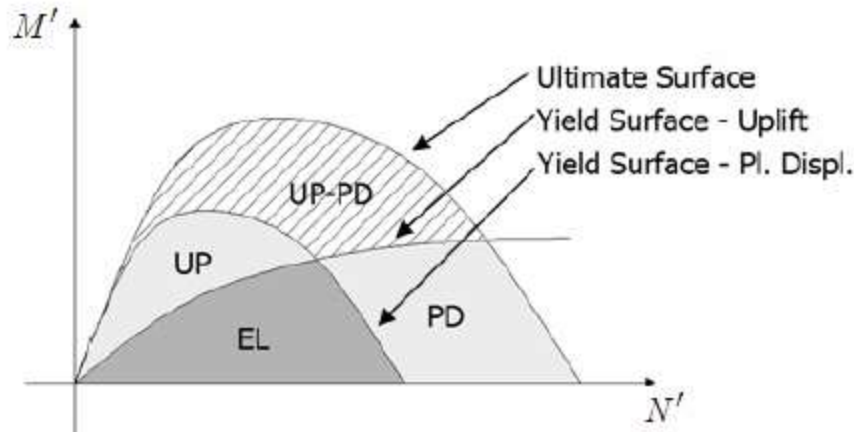


Figure I.35. Ultimate and yield surface by Chatzigogos,2007.

Grange et al, 2008 proposed a simpler mechanism of macro-element in 3D by integrating five mechanisms (Figure. I.36) into a constitutive equation are formulated in rate-for:

$$\dot{\underline{F}} = \underline{K}^{plup}(\underline{F}, \underline{q}) \dot{\underline{u}} \quad (48)$$

where  $K^{plup}$  is the tangent stiffness of the system depending on the system state and loading reaction and  $q$  is a pseudo-vector of internal variable accounting for the effect of previous loading history.

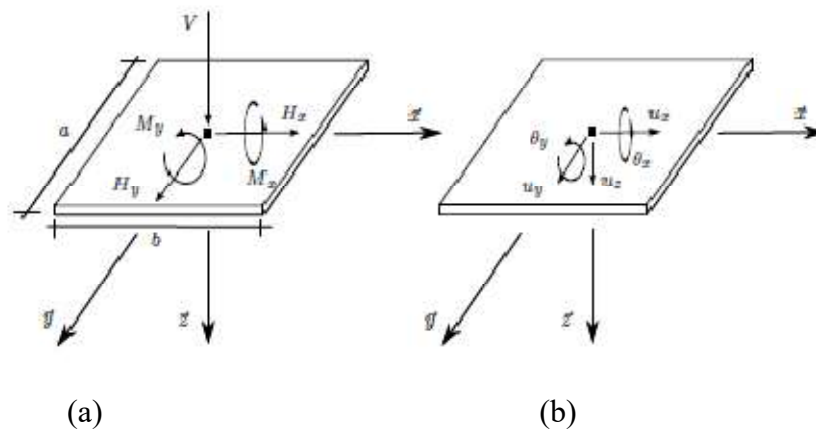


Figure I.36. Layout of variable global studied a. efforts b. displacement (Grange, 2008)

Abboud et all, 2017 developed a 3D macro-element to model the seismic behavior in elastoplastic term. The non-linear behavior was presented yield surface from the Eurocode criteria which is implemented to the Finite Element Method framework.

In the implementation of macro-element, Abboud et al, 2017, is divided into three types (i) single macro-element model (Figure I.37), (ii) Distributed macro-element model (Figure I.38), and (iii) Hybrid macro-element model (Figure I.39).

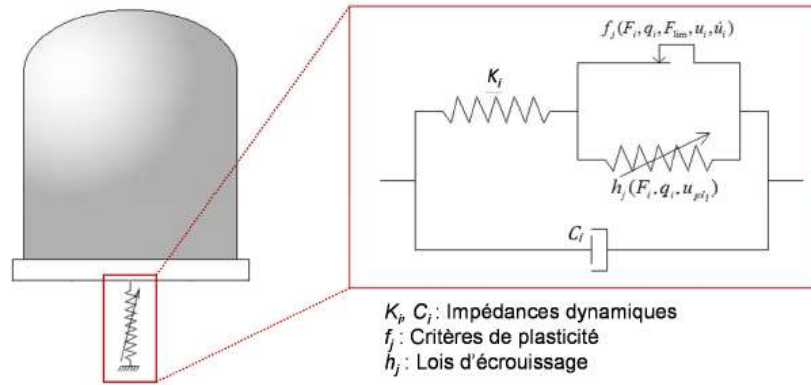


Figure I.37. Single Macro-element model (Abboud et al, 2017)

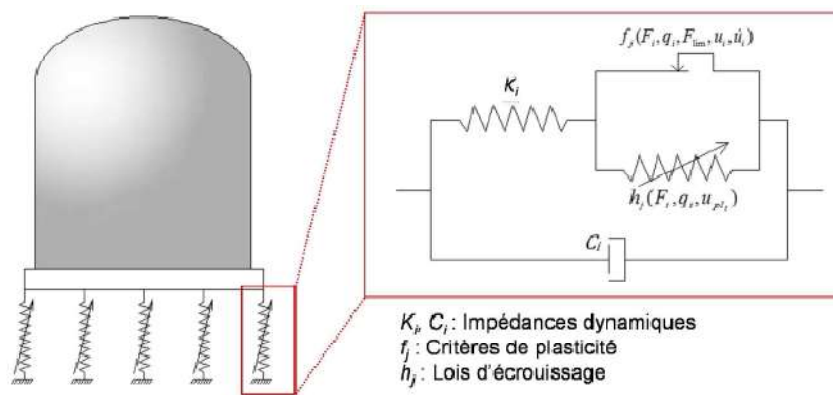


Figure I.38. Distributed Macro-element model (Abboud et al, 2017)

In hybrid model, the foundation rests on the groundmass discretized in Finite Element. The behaviour of foundation is formulated by means of generalized variable (force and displacement) in several nodes of the interface (Figure I.45).

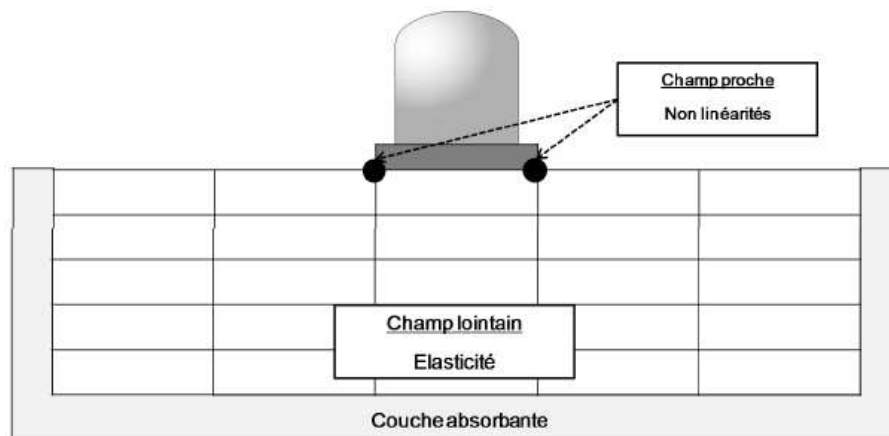


Figure I.39. Hybrid Macro-element model (Abboud et al, 2017)

The parameter of macro-element are shown in table I.10, it is determined base on the static response.

Table I.10. Parameter of Macro-element (*Abboud, 2017*)

Parameters	Description
$K_{hx}$	Horizontal stiffness according to x
$K_{hy}$	Horizontal stiffness according to y
$K_v$	Vertical stiffness
$K_{mx}$	Rotation stiffness according to x
$K_{my}$	Rotation stiffness according to y
$c$	Cohesion at interface
$\phi$	Friction angle at interface
$V_{lim}$	Elastic limit for vertical load
$V_r$	Ultimate of bearing capacity for vertical load
$v_r$	Settlement failure
$H_h$	Slope of the non-linear part of the H-h curve that Equal to the horizontal stiffness of the foundation
$\gamma$	Maximum horizontal displacement

### I.5.2 Macro-element Method for deep foundation

Macro-element on deep foundation has been proposed by many researchers after the macro-element on a shallow foundation, such as *Nogami et al. (1992)* who combined spring and dash spot to incorporate damping into the basic elastoplastic soil response represented by the  $P$ - $y$  model. And *Boulanger et al. (1999)* who simulated the drag force as well as the formation gap. Also, *Taciroglu et al. (2006)* proposed the interaction element by assembling three basic elements of leading element, rear face element and drag element for soil structure interaction on lateral load.

#### Lateral Load Transfer Element by Taciroglu et al. (2006)

In the term of load transfer element, *Taciroglu et al. (2006)* proposed an assembly of three components for macro-element in lateral force. The interaction element is described in Figure I.40, where the interaction element is an assembly of various sub-elements which are consist of drag element, rear-face element and leading-face element.

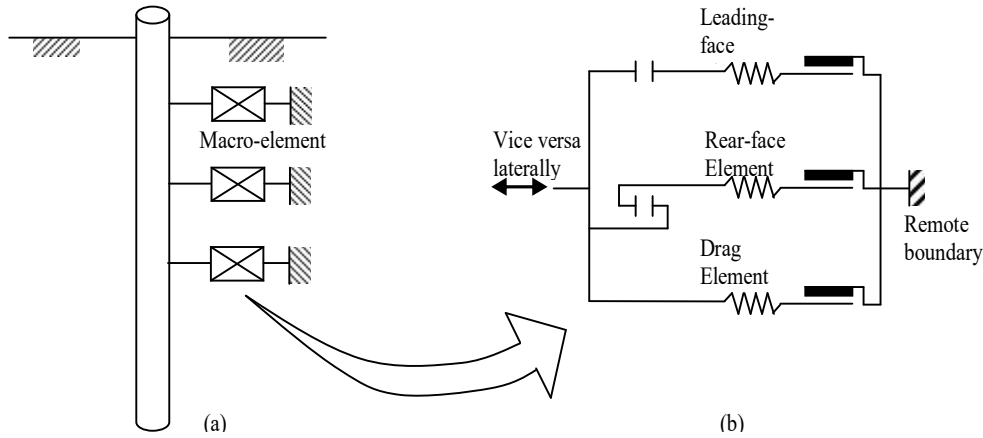


Figure I.40. (a) Macro-element on lateral load, (b) components of macro-element (Tacioglu, 2006)

The conventional rate-independent plasticity is used in  $T$ - $z$  and  $q$ - $z$  elements model to approach the vertical macro-element model (Rha et al., 2007). Each macro-element consists of the elastic spring  $E_s$  that connects to the elastoplastic element in series (Figure I.37). It mimics the skin friction and end bearing macro-element behaviour before reaching limit load. The elastoplastic element is composed of constant yield force ( $\sigma_y > 0$ ) and hardening ( $\kappa$ ). Where the relationship can be expressed as;

$$\sigma = E_s(z - z^p) \quad (I.98)$$

Where,  $\sigma$  is the axial resistance,  $z$  is total axial displacement, and  $z^p$  is axial plastic displacement. And the relationship between hardening and yield force for the model are given by,

$$f(\sigma, \kappa) = |\sigma| - (\sigma_y + \kappa) \leq 0 \quad (I.50)$$

$$\dot{\kappa} = |\dot{\sigma}| \quad (I.51)$$

$$|\dot{z}^p| \cdot f = 0, \quad |\dot{z}^p| \cdot \dot{f} = 0, \quad \text{if } f = 0 \quad (I.52)$$

Where,  $\dot{z}^p$  and  $\dot{\sigma}$  are rate of displacement and rate of force in plastic. And then the evolution equation of them in stress and hardening variable is,

$$((\dot{\sigma}, \dot{\kappa})) = \begin{cases} (E_s \dot{z}, 0) & \text{if } f < 0 \\ (C_{(z)} \dot{z}, |\dot{\sigma}|) & \text{if } f = 0 \end{cases} \quad (I.53)$$

Where,  $C_{(z)}$  is plastic tangent stiffness.

### Coupled Load Transfer Element Rha et al. 2007

Since the vertical and horizontal load applied simultaneously on a pile, the mechanism of load transfer both axially or laterally from the shaft intuitively be affected. It has been explained above in single axial load or single lateral load. Event the effect of vertical load on lateral behaviour is weak (Rha et al. 2007).

The multiaxial macro-element consists of the axial component and a lateral component. In Figure I.41 shows that the configuration of macro-element between vertical and lateral element is connected in parallel.

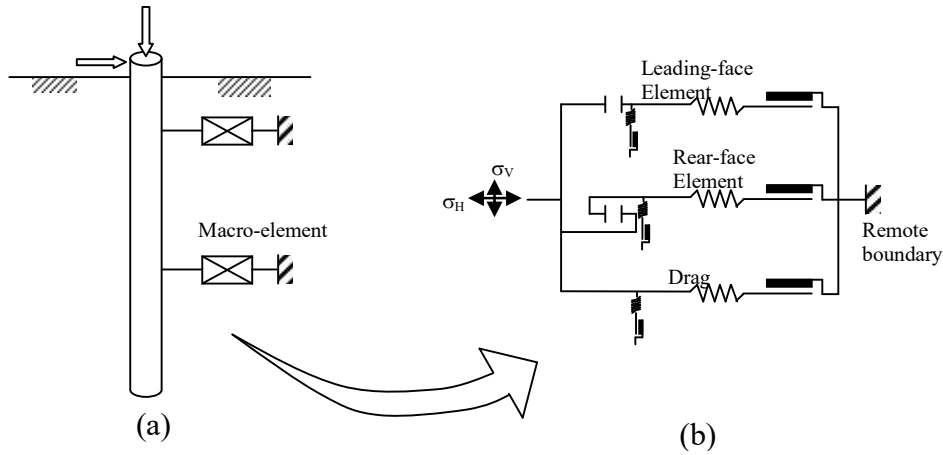


Figure I.41. (a) Macro-element on multi-axial load (b) basic element on multi-axial model  
(Rha and Taciroglu, 2007)

**Macro-element of Zheng li, 2015 and Zhuang Ji, 2019 in the Hypoelasticity framework.**

The macro-element model for single vertical pile has proposed by Zang li, 2015. The pile is embedded in sand with pile-head on the ground surface. It develops within the framework of hypoelasticity. The incremental of the constitutive equation of the non-linearity is defined in terms of generalized forces, displacement and rotation. The mechanical response, for the monotonic loading, is described by means of generalizing displacement  $\mathbf{u}$  and load vector  $\mathbf{t}$ .

$$\mathbf{t} := \{V, H, M\}^T \tag{I.54}$$

$$\mathbf{u} := \{w, u, \theta\}^T \tag{I.55}$$

where,  $H$ ,  $V$  and  $M$  are the resultant force (horizontal and vertical) and the moment acting on the pile head. The  $w$ ,  $u$  and  $\theta$  are the respective displacement and rotation. For the general velocity vector is introduced as:

$$\mathbf{d} := \dot{\mathbf{u}} \tag{I.56}$$

Then, the basic structure of macro-element in hypoelastic term are:

$$\dot{\mathbf{t}} = \kappa(\mathbf{t}, \mathbf{q}, \eta) \tag{I.57}$$

Where,

$$\mathcal{K} = \mathcal{L}(\mathbf{t}, \mathbf{q}) + \mathbf{N}(\mathbf{t}, \mathbf{q})\eta^T \tag{I.58}$$

$$\eta = \mathbf{d}/\|\mathbf{d}\|$$

where,  $\mathcal{K}$  is tangent stiffness matrix,  $\mathcal{L}$  is elastic stiffness matrix, and  $\mathbf{N}$  is constitutive vector.

The elastic stiffness matrix is defined by:



$$\mathcal{L} = \frac{1}{m_R} \mathcal{K}^e \quad (I.59)$$

$$\mathcal{K}^e := \begin{bmatrix} k_v & 0 & 0 \\ 0 & k_{hh} & k_{hm} \\ 0 & k_{hm} & k_{mm} \end{bmatrix} \quad (I.60)$$

where and  $k_v$ ,  $k_h$ ,  $k_{mm}$  and  $k_{hm}$  the vertical, horizontal, rotational and coupled horizontal-rotational stiffness in,  $\mathcal{K}^e$ , the elastic stiffness matrix of the foundation system. The non linear function  $N$  can be expressed as:

$$N_{(t)} = -Y_{(t)} \mathcal{L} m_{(t)} \quad (I.61)$$

where  $Y(t)$  is the scalar function which controls the degree of nonlinearity; and  $m(t)$  is the unit gradient which describes the plastic flow direction.

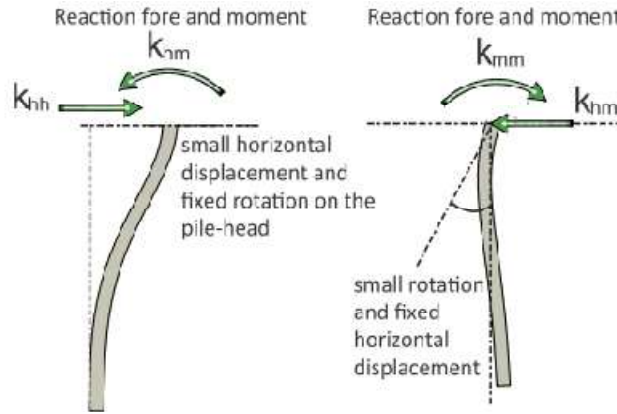


Figure I.42. Determining The initial stiffness parameter of the hypoplastic macro-element (Zheng li, 2015)

Zhuang Ji, 2019 proposed a macro-element model to investigate the soil-structure interaction for caisson foundation in sand under combined monotonic loading for offshore wind turbines. The macro-element was developed within the framework hypo-elasticity. It has the same framework as the macro-element that was constructed by Zhiang li, 2015.

The failure surface in the H:M/D loading plane is described by a mathematical formula as equation below:

$$F = \left(\frac{H}{h_i V_0}\right)^2 + \left(\frac{M}{D m_i V_0}\right)^2 + 2e \frac{H}{h_i V_0} \frac{M}{D m_i V_0} - 1 = 0 \quad (I.62)$$

where  $V_0$  is the vertical bearing capacity of the foundation, the fitting parameters  $h_i$  and  $m_i$  represent the intersection of each ellipse with the  $H/V_0$  and  $M/(DV_0)$  axes respectively and  $e$  is the eccentricity of the ellipse. And the failure curve is presented in Figure I.43.

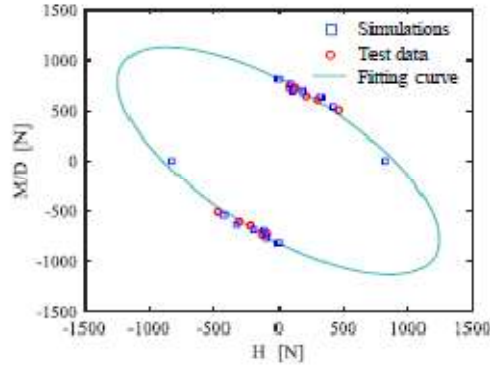


Figure I.43. Failure envelope in the H:M/D loading plane: fitting curve based on model tests data and numerical simulation (Zhuang Ji, 2019)

For the failure surface in 3D H-M-V space is expressed by the equation I.62 and the failure envelope is shown in Figure I.44.:

$$F = \left(\frac{H}{h_i V_0}\right)^2 + \left(\frac{M}{Dm_i V_0}\right)^2 + 2e \frac{H}{h_i V_0} \frac{M}{Dm_i V_0} - Fv(V, Vt, V_0) = 0 \quad (I.63)$$

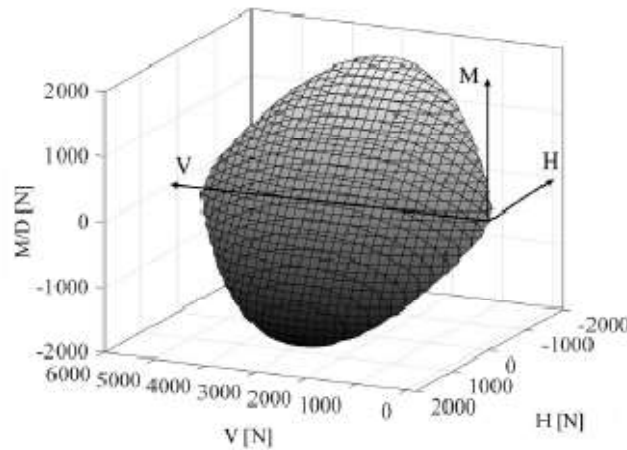


Figure I.44. Failure surface in 3D H-M-V space (Zhuang Ji, 2019)

## I.6 RESULT

The bibliography study shows Complexity in soil-structure analysis and design. Thanks to simple models like macro-elements can achieve excellent results. The works have made it possible to improve the application of macro-element having reliable and adequate result to experiment.

However, There is no macroelement model for the deep foundation that concentrated the nonlinearities of interaction into a single particular point of the computational model.

The macro-element model of *Abboud et al., 2017* and *Rha et al. 2007* that synthesized previous work seems to be a reasonable basis for the development of a new robust macro-

element that is capable of analyzing the soil-structure interaction for deep foundation, either the single pile or pile group. The formulation in forces and displacements facilitates its use for the justification of the foundations (bearing capacity, sliding, detachment, settlements, translations, distortions and rotations).

## **CHAPTER II: DEVELOPMENT OF MACRO-ELEMENT**

---

This chapter presents the development of macro-element. The construction of this tool is based on the elastoplasticity theory. Development is started from the determination of the governing equation and the boundary conditions of macro-element to the obtaining of relative displacement. The relative displacement has been developed for elastic state, elastic-perfectly plastic, and plasticity.

---

### II.1 CONCEPT OF MACRO-ELEMENT

The proposed macro-element assumes the heterogeneities of local element along the pile (Figure II.1.a) into a homogeneities single macro-element (Figure II.1.b). The macro-element must be representative of local heterogeneities properties sufficiently (due to the state of hardening of local properties) with the aim of reproducing the general foundation behaviour. This simple mathematical processing of the result is an advantage of uncoupled springs. However, this model has a drawback in the calibration of the spring parameters.

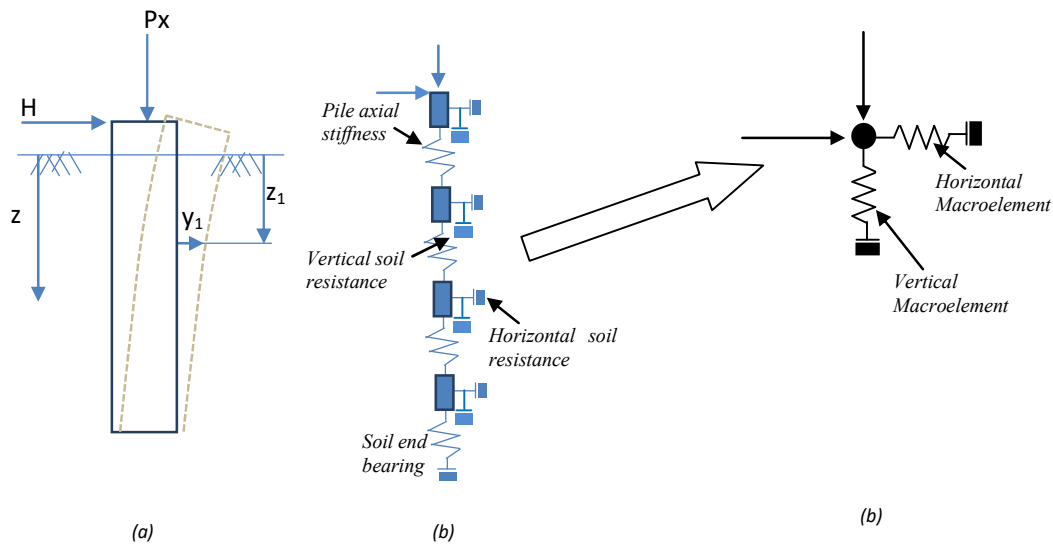


Figure II.1. The concept of Macro-element that work on single macro element.

Using Flac3D, the macro-element model can be embedded in the main program as a Fish function. The model is constructed by the model of soil and model pile which is followed by both properties. In the proposed model, the model is constructed as ground only with macro-element parameters which are attached to grid points on ground surface as shown in Figure II.2 and II.3. For a single pile, the properties of soil and pile are represented by a single macro-element on the ground mesh (Figure II.2). For pile group, it is presented by a single macro-element for every member of pile group with the distance center-to-center of pile then these macro-elements are connected by a pile cap (Figure II.3).

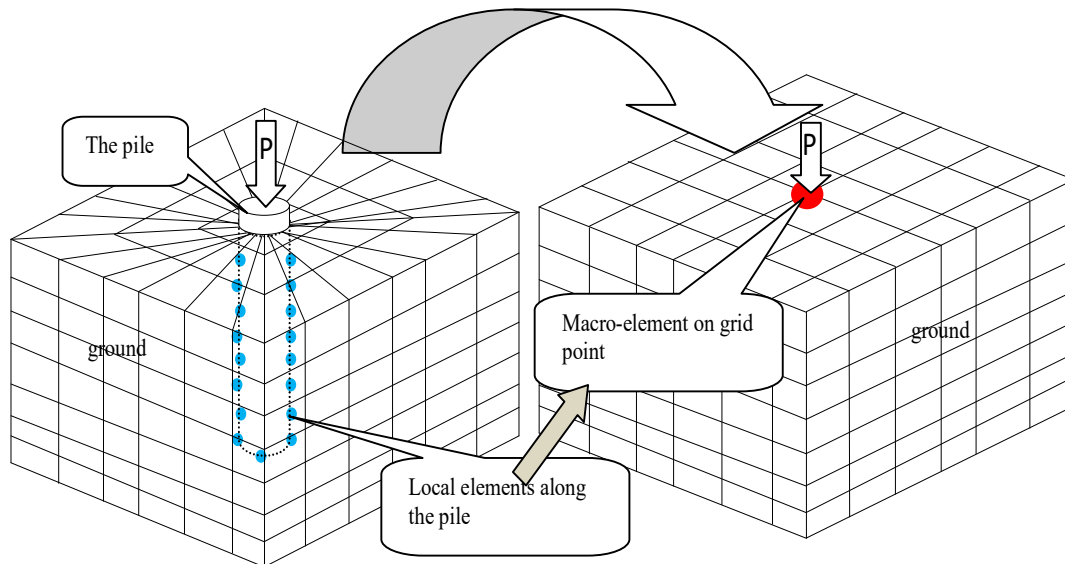


Figure II.2. The concept of Macro-element that is attached on Flac3D for the single pile

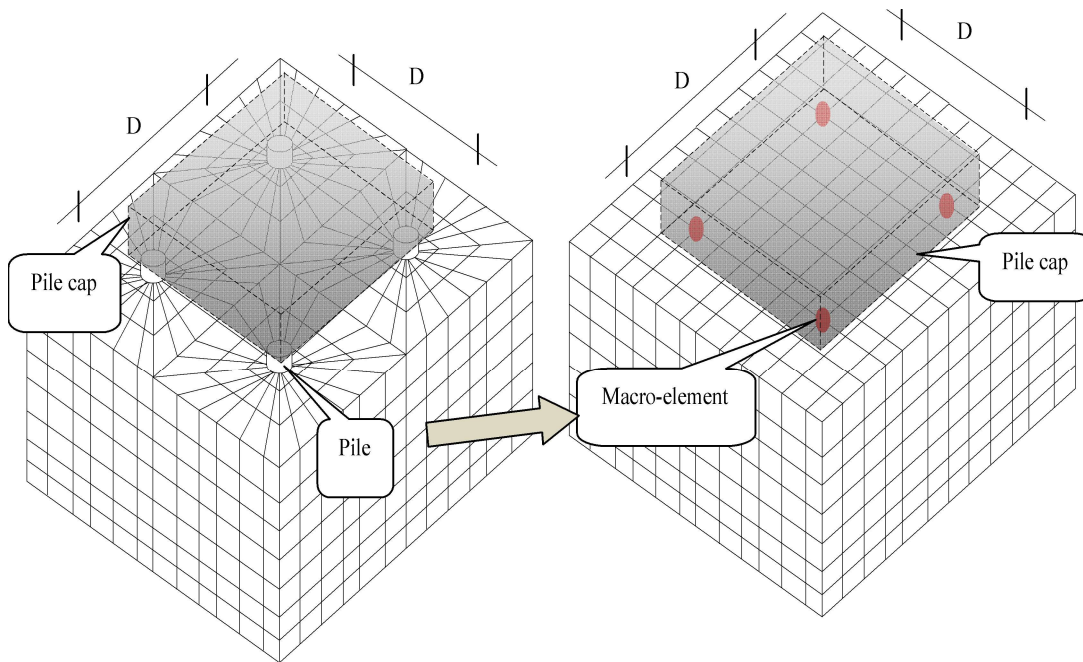


Figure II.3. The concept of Macro-element that is attached on Flac3D for the Group pile

## II.2 THE ELASTOPLASTIC LOAD-DISPLACEMENT LAW

The elasto-plastic is the branch of theory about behaviour of material. Initially, It goes under elastic deformation but upon reaching the yield limit, the permanent (irreversible) deformation occurs. Mathematically, the strain additive decomposition is:

$$\varepsilon = \varepsilon^e + \varepsilon^p \quad (II.1)$$

Where,  $\varepsilon$  is the total strain,  $\varepsilon^e$  and  $\varepsilon^p$  are the elastic and plastic strain respectively.

In term of macro-element, the stress-strain behaviour at local element is changed to the load-displacement response to Figure the global element (Figure II.4). This type of curve is defined from every field loading test to measure the capacity of pile. There are divided into two zones, elastic zone and plastic zone. The relative displacement response  $du$  develops load-displacement curve in elastic state and plastic state under the boundaries condition control, respectively.

The elastic zone occurs before the yield strength limit reached where the slope of curve is governed by elastic stiffness  $K_{v/h}$  (horizontal or vertical stiffness) and elastic displacement  $u^e$ .

It is illustrated in Figure II.5 that the boundary condition of elastic zone can be expressed by,

$$f:f(P)-fy < 0 \tag{II.2}$$

where, the function of load  $f(P)$  is less than the yield strength limit  $fy$ .

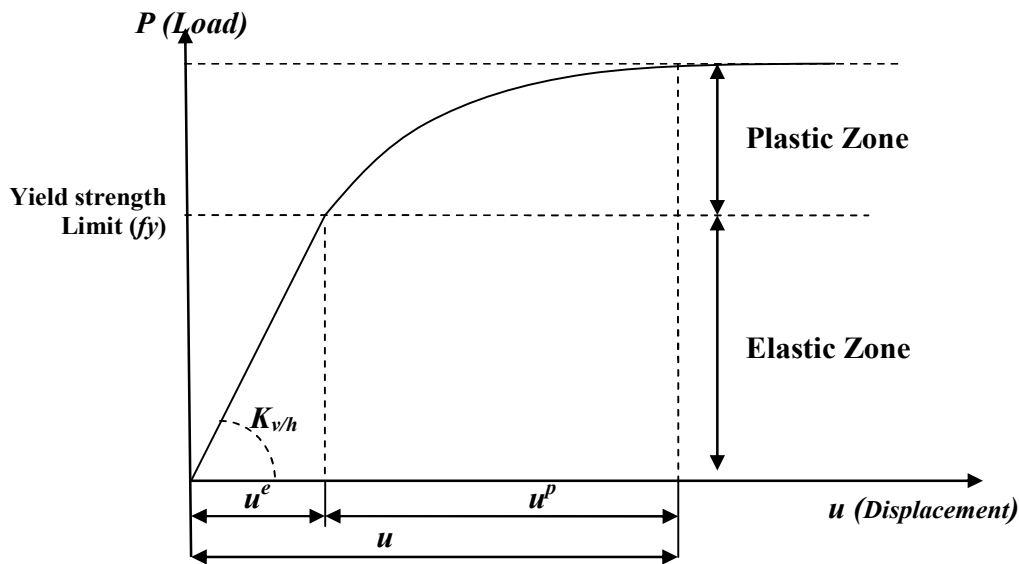


Figure II.4. Elastic and plastic zone in the stress-strain curve

After the yield strength limit has been reached, the plastic zone occurs. In the equilibrium condition of plastic state, the function is equal to zero. It can be expressed,

$$f:f(P)-fy = 0 \tag{II.3}$$

where, the equilibrium comes from the function of load  $f(P)$  to the yield strength limit  $fy$  that is controlled by the hardening law in every increment of displacement.

The relative displacement response for each state of macro-element model is formulated in detail to the mathematical model subsequent developed upon the boundary condition of state.

There is three constitutive models which underlies in construction of this macro-element model. These are arranged into elastic, elastic-perfectly plastic, and Elastoplasticity with hardening.

### II.2.1 Relative Displacements in Elastic Response

On **Linear Elastic State** the Constitutive equations of elasticity (*Hook's law*) is:

$$P^e = k \cdot du \quad (II.4)$$

Where,  $P^e$  is the load in elastic zone,  $k$  is stiffness and  $du$  is the relative displacement. From Figure II.5. can be explained that in elastic zone the curve is in linear state. In every mechanism, the multiplier  $\lambda$  is calculated. It is used to define the displacements generated by applying law of normality that is proposed by *Simo and Hughes (1998)*.

$$u = \lambda \frac{\partial f}{\partial f(x)} \quad (II.5)$$

Where,  $u$  is the displacement and  $\lambda$  is the multiplier.

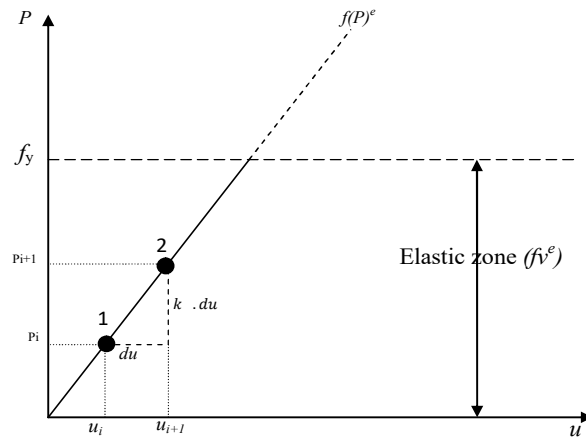


Figure II.5. Elastic and plastic zone in the stress-strain curve

From Figure II.5, when the total load in  $P_{i+1}$ , at point 2, is a combination of the value of load at  $P_i$  and value of relative displacement ( $du$ ) is multiplied by stiffness ( $k$ ) of elasticity.

$$P_{i+1} = P_i + k \cdot du < 0 \quad (II.6)$$

In mathematical law, the equation of  $df(x)$  can be write as,

$$df(x) = f(x) \cdot f'(x) \quad (II.7)$$

due to Figure II.6 the equation II.7a can be written as,

$$df(P) = \lambda^e \cdot k (\partial f / \partial f(P)) \quad (II.8)$$

where the value of  $(\partial f / \partial f(x))$  is equal to 1

So it can be written as,

$$df(P) = \lambda^e \cdot k (1) \quad (II.9)$$

in elastic limit condition,

$$f((P)^e - df(P)) = 0 \quad (II.10)$$

Then, the formula can be derived from *Taylor series* that the first-order approximation is,

$$f((P) - df(x)) = f(P)^e - (\partial f / \partial f(P)) df(P) \quad (II.11)$$



by substituting equation II.8, II.9 and II.10, it becomes

$$0 = f(P)^e - (\partial f / \partial f(P)) \cdot \lambda^e \cdot k \cdot (\partial f / \partial f(P)) \quad (II.12)$$

$$0 = f(P) - 1 \cdot \lambda^e \cdot k \cdot 1 \quad (II.13)$$

$$f(x)^e = 1 \cdot \lambda \cdot k \cdot 1 \quad (II.14)$$

$$\lambda^e = f(P)^e / (1 \cdot k \cdot 1) \quad (II.15)$$

Where  $f(P)^e$  is elastic force,  $f(P)^c$  is correction force in elastic state,  $\lambda^e$  is multiplier in elasticity,  $k$  is the slope constant at elastic state, and  $f_y$  is the yield strength limit. And then correction for vertical load on Flac3D is  $f(P)^e$  subtracted initial internal load from Flac3D.

The concept of macro-element at a mass of element are explained in Figure II.6:

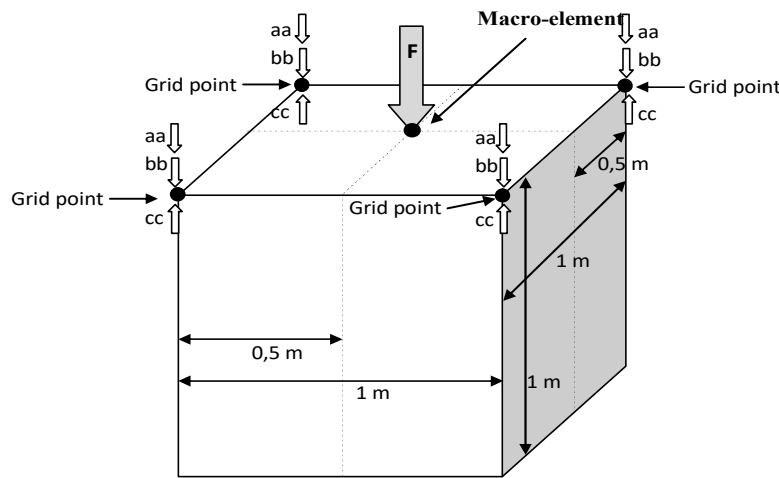


Figure II.6. Model of macro-element at a mass

All of the forces and the reaction applied to the element is spread only into grid points on the surface of elements such as the internal force and the external force and marked as  $aa$ ,  $bb$  and  $cc$ . The  $aa$  is the internal force which comes from the unit weight of soil. The volume of the element is  $1 \text{ m}^3$ . The shallow foundation has a surface wherein this model is equal to  $1 \text{ m}^2$ . And the value of  $aa$  on each grid point is equal to the density of soil ( $\gamma$ ) multiplied by the surface area of the element ( $1 \text{ m}^2$ ) and then multiplied by half of wide ( $0.5 \text{ m}$ ) then the result of  $aa$  is equal to  $0.5 \gamma \text{ kN}$ . The  $bb$  comes from the external force that is applied to element divided by the number of grid points on the surface (in this element has four grid points). If the stress is applied  $F \text{ kPa}$  on the element then the force works  $F$  on single grid point multiplied by area of element then divided by number of grid on surface of element or can be written as  $F/4 \text{ kN}$ . And the  $cc$  is the reaction at a grid point. If the stress applied is  $F \text{ kPa}$ , so the calculation is  $cc=(aa)+(bb)/4$  or can be written as,

$$cc = (0,5\gamma)kN + \left(\frac{F}{4}\right)kN \quad (II.16)$$

**Case Study and Validation in elasticity**

In order to verify this macro-element method, a simple model is constructed with a dimension of the element as Figure II.7 with a unit weight of soil is  $20 \text{ kN/m}^3$  and the variation of stress increase gradually every 50 kPa from 100 kPa to 500 kPa.

The value of  $aa$  on each grid point is equal to the density of soil ( $20 \text{ kN/m}^3$ ) multiplied by the surface area of the element ( $1 \text{ m}^2$ ) and then multiplied by half of wide (0,5 m) then the result of  $aa$  is equal to  $10 \text{ kN/m}^3$ . The value of  $bb$  is the force that works on the element 100 kPa multiplied by  $1 \text{ m}^2$  and then divided by number of grid point on surface of element. So the value of volumetric force at the grid point is  $2,5 \cdot 10^4 \text{ N}$ . And the  $cc$  is the reaction at a grid point. If the stress ( $F$ ) applied is 100 kPa, due to equation II.14 the value of  $cc$  is  $cc=(0.5 \times 20\text{kN}) + (100/4 \text{ kN})$  where the result is  $3.5 \cdot 10^4 \text{ N}$ , and for further calculation is presented in table II.1.

Table II.1. The analytic calculation of internal forces on elastic state

Applied Stress (F) (Pa)	External force at the grid point (aa) (N)	Volumetric force at the grid point (bb) (N)	Internal force at the grid point (cc) (N)
1.00E+05	2.50E+04	1.00E+04	<b>3.50E+04</b>
1.50E+05	3.75E+04	1.00E+04	<b>4.75E+04</b>
2.00E+05	5.00E+04	1.00E+04	<b>6.00E+04</b>
2.50E+05	6.25E+04	1.00E+04	<b>7.25E+04</b>
3.00E+05	7.50E+04	1.00E+04	<b>8.50E+04</b>
3.50E+05	8.75E+04	1.00E+04	<b>9.75E+04</b>
4.00E+05	1.00E+05	1.00E+04	<b>1.10E+05</b>
4.50E+05	1.13E+05	1.00E+04	<b>1.23E+05</b>
5.00E+05	1.25E+05	1.00E+04	<b>1.35E+05</b>

And then the following model is constructed in Flac3D model in elastic state at the same element by following soil properties: Young's modulus E, Poisson ratio  $\nu$ , and the unit weight  $\gamma$  are 10 MPa, 0,3,  $20 \text{ kN/m}^3$ . Considering data above, a model in Flac3D is constructed with dimension  $1 \text{ m} \times 1 \text{ m}$  for every single element. The applied external force on the model is gradually increased every 50 kPa, , from 100 kPa to 500 kPa as explained in Figure II.8.

Since the conventional Flac3D calculation generate the value of external force ( $bb$ ), displacement ( $dz$ ) and internal force ( $cc$ ) at the grid. For the second step with the same element, the model is run by macro-element method by applying the same stress and generating the same output. The calculation result can be seen in table II.3.

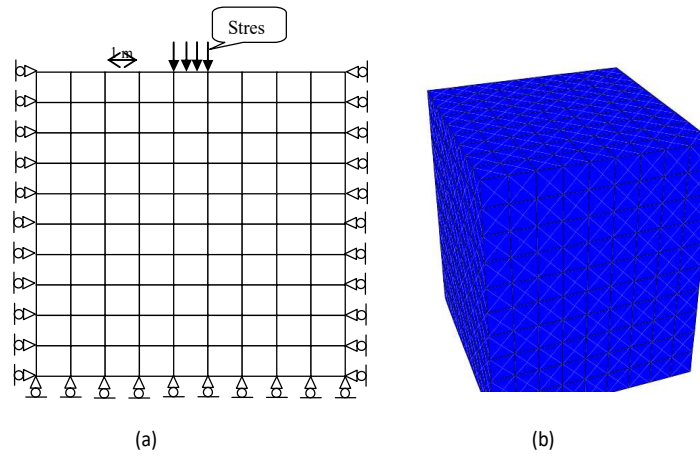


Figure II.7. (a) Sketch of mesh and boundary condition, (b) Model in Flac3D

From Table II.1, we can see that the reaction force (*cc*) from both analytical and Flac3D calculation are in the same result where the further calculation will be compared by these result.

The following calculation is the calculation that the macro-element is embedded into Flac3D programme as fish function and initialising into each grid points on the surface of the element (in this model there are four macro-element attached). And the calculation result with a macro-element attached in Flac3D by the fish function is showed in table II.3. by defining the value of *kv* is  $8.06 \cdot 10^6$  N/mm for elastic properties above, the value for internal force has been good checked and the result showed in table II.3.

Table II.3. Calculation on Flac3D with embedded Macro-element on elastic state

External force ( <i>bb</i> ) (N)	Internal force on grid point ( <i>cc</i> ) on Flac3D	
	Conventional (N)	Macro-element (N)
1.00E+05	3.50E+04	3.50E+04
1.50E+05	4.75E+04	4.75E+04
2.00E+05	6.00E+04	6.00E+04
2.50E+05	7.25E+04	7.25E+04
3.00E+05	8.50E+04	8.50E+04
3.50E+05	9.75E+04	9.75E+04
4.00E+05	1.10E+05	1.10E+05
4.50E+05	1.23E+05	1.22E+05
5.00E+05	1.35E+05	1.35E+05

And the comparison result of three calculations way shows that the result of Internal force on grid point (*cc*) is in the same value which is presented in Figure II.8. The calculation and comparison above indicated that the macro-element embedded works on Flac3D.

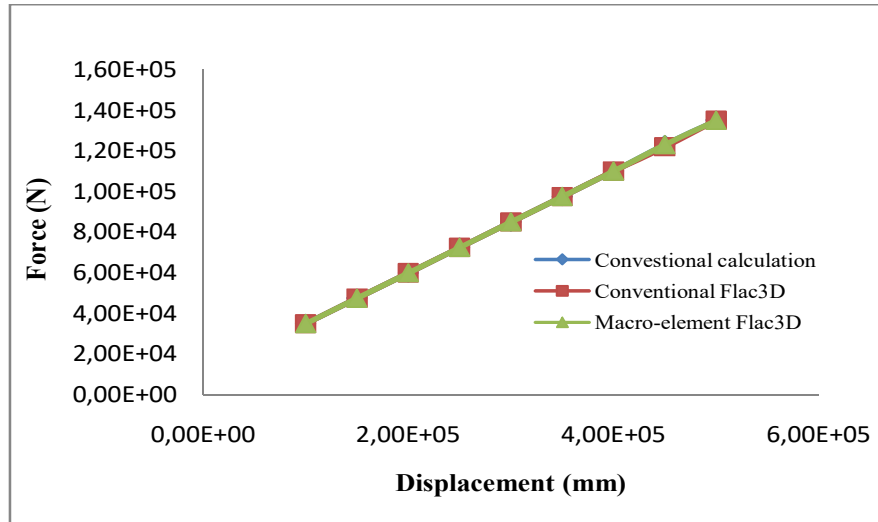


Figure II.8. The Stress-displacement curve for elastic state of three calculation type (analytical, Flac3D on model elastic, and macro-element in Flac3D)

### II.2.2 Relative Displacements in Elastic Perfectly-Plastic

Elastic-perfectly plastic model (Figure II.9) occurs when the yield strength limit  $f_y$  is in the same value as failure criterion where the yield conditions unchanged during displacement and then internal load (reaction for external load and volumetric force because of initial force from the unit weight of soil) will be corrected by equation II.16,

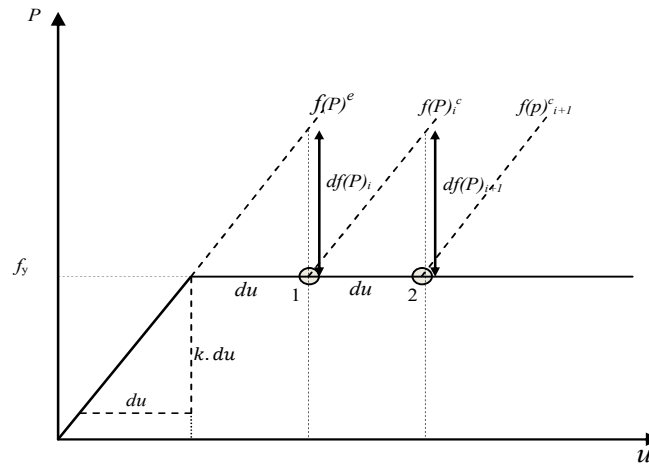


Figure II.9. Elastic-perfectly plastic zone in the stress-strain curve

At point 1, the correction is the function of elasticity subtracted by  $f_y$ .

$$df(P)_i = f(P)^e - f_y \tag{II.17}$$

thus, at the point 2, the correction is the corrected function of point 1 or in  $i$  ( $f(P)^c_i$ ) subtracted by  $f_y$ .

$$df(P)_{i+1} = f(P)^c_i - f_y \tag{II.18}$$

then, the equation II.8 can be rewrite as

$$df(P) = \lambda^{ep} \cdot k (\partial f / \partial f(x)) \quad (II.19)$$

and rewrite from equation II.15 can be written,

$$\lambda^{ep} = f(P) / \left( \frac{\partial f}{\partial f(P)} \cdot k \cdot \frac{\partial f}{\partial f(P)} \right) \quad (II.20)$$

where the value of  $(\partial f / \partial f(x))$  is equal to 1, then it can be written in,

$$\lambda^{ep} = (f(x)^c - f_y) / (1 \cdot k \cdot 1) \quad (II.21)$$

and then the corrected from internal load is the substitution of equation II.18,19 and 21,

$$f(x)^c = f(x)^e - (\partial f / \partial f(P)) \lambda^{ep} \cdot k (\partial f / \partial f(P)) \quad (II.22)$$

then, the correction function at  $i$  is

$$f(P)_i^c = f(P)^e - 1 \cdot \left( \frac{f(P)^c - f_y}{1 \cdot k \cdot 1} \right) k \cdot 1 \quad (II.23)$$

and, the new correction function at  $i+1$  is the correction load at  $i$  ( $f(P)_i^c$ ) subtracted by relative correction load ( $df(P)_{i+1}$ ). It can be written as,

$$f(P)_{i+1}^c = f(P)_i^e - 1 \cdot \left( \frac{f(P)^c - f_y}{1 \cdot k \cdot 1} \right) k \cdot 1 \quad (II.24)$$

### Case Study in Elasticity-perfectly Plastic on Flac3D

The purpose of this case study is to verify that the macro-element model which is embedded into Flac3D is work well. By the same model of the element above, the macro-element embedded in Flac3D and following soil properties: Young's modulus  $E$ , Poisson ratio  $\nu$ , unit weight  $\gamma$ , cohesion  $c$ , friction angle  $\phi$ , dilatation  $\psi$ , and shear modulus  $G$  is 10 MPa, 0.3, 20 kN/m<sup>3</sup>, 0.1 MPa, 20°, 0 and 0.1 GPa. And for concrete properties are 10 GPa for  $E_c$  and 0.2 for  $\nu_c$ . Figure II.11 shows the result of macro-element with the value of  $K$  is  $8.06 \cdot 10^6$  and due to equation II.9 the  $f_y$  compression is  $8.57 \cdot 10^4$  N. By determining the value of  $k$  and  $f_y$ , the macro-element model works in accordance as expected (Figure II.10).

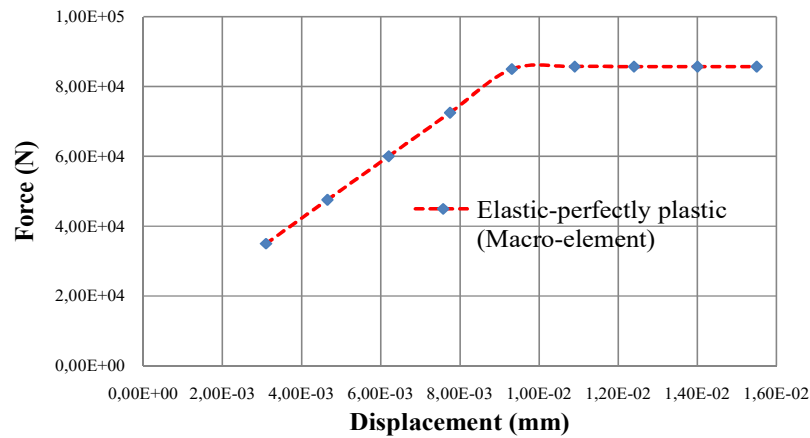


Figure II.10. The stress-displacement curve on Elastic-perfectly plastic state.

### II.2.3 Elastoplasticity With Hardening Law

Base on schematic diagram response shown in Figure II.11, the yield surface  $f(p)$  is assumed as a hyperbolic (equation II.25). The relationship between load and displacement are shown in Figure II.12.

The governing equation for the yield criterion can be defined explicitly as:

$$f(P)^{pl} = f_y + \left( \frac{a \cdot u^{pl}}{b + u^{pl}} \right) \quad (II.25)$$

Where  $u^{pl}$  is relative plastic-displacement,  $f(P)$  and  $f_y$  are unit force and yield strength limit criterion, and  $Rc$  is asymptote value of force.  $a$  and  $b$  are parameters of the governing the shape of hardening parameters. Therefore, these value can be obtained using the following equation.

$$a = (\sigma_1 - \sigma_3)_{ult} = Rc - f_y \quad (II.26)$$

And

$$b = \frac{a}{k} \cdot \alpha_b \quad (II.27)$$

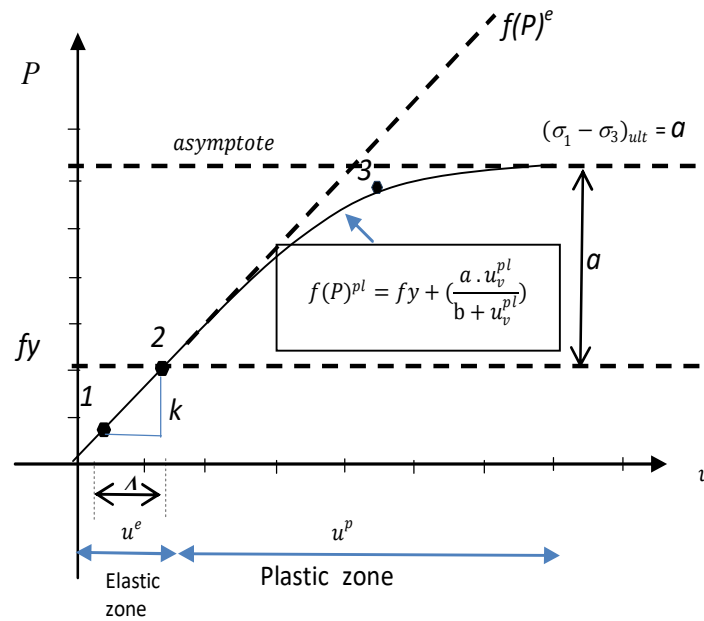


Figure II.11. Real Hyperbolic graphic

Where  $\alpha_b$  is the Coefficient of curvature that must be bigger than 1 to ensure the average result in Flac3D. The value of  $b$  governs the shape of the curve as described in Figure II.12 where the increasing the value of  $b$  effect to the decreasing the shape of the curve.

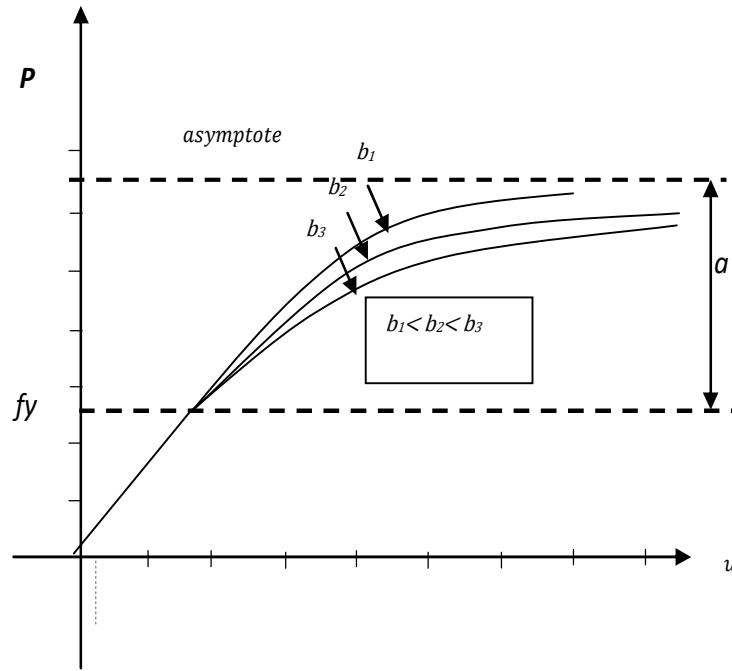


Figure II.12. Influence of coefficient  $b$  to the curve

#### II.2.4 Relative Displacement in Plastic Potential and Flow Rule

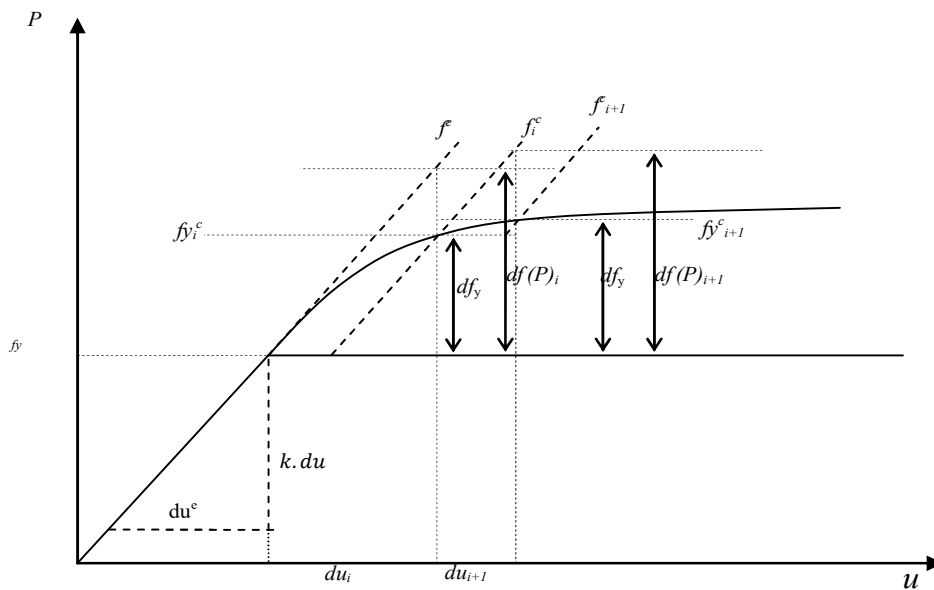


Figure II.13. The iterative development procedure of the mathematical tool plastic-hardening zone in the stress-strain curve

The hardening occurs after the onset of plastic yield (Figure II.13). Within the framework of deformation is expressed by equation II.26 in equilibrium, then the plasticity strain increment is obtained from the flow rule,

$$f(P - df(P) ; fy + dfy) = 0 \quad (II.28)$$

$$f(P ; fy) - \frac{\partial f}{\partial f_v} df(P) + \frac{\partial f}{\partial f_y} dfy = 0 \quad (II.29)$$

After the function of load correction occurred then it will be followed by the yield strength limit correction  $df_y^c$ . Where,

$$df_y^c = \frac{\partial f_y}{\partial u^{pl}} du^{pl} \quad (II.30)$$

Then, the substitution of equation II.7.b and II.28 to equation II.27 can be written as,

$$f(P ; fy) - \frac{\partial f}{\partial f(P)} \cdot \lambda^{pl} \cdot k \cdot \frac{\partial f}{\partial f(P)} + \frac{\partial f}{\partial f_y} \cdot \frac{\partial f_y}{\partial u^{pl}} \cdot du^{pl} = 0 \quad (II.31)$$

Where, the relative displacement is given by:

$$du^{pl} = \lambda^{pl} \frac{\partial f}{\partial f(P)} \quad (II.32)$$

Then, by combining equation II.31 and II.32, we obtain:

$$f(P ; fy) - \frac{\partial f}{\partial f(P)} \cdot \lambda^{pl} \cdot k \cdot \frac{\partial f}{\partial f(P)} + \frac{\partial f}{\partial f_y} \cdot \frac{\partial f_y}{\partial u^{pl}} \lambda^{pl} \frac{\partial f}{\partial f(P)} = 0 \quad (II.33)$$

$$f(P ; fy) = \left( \frac{\partial f}{\partial f(P)} \cdot k \cdot \frac{\partial f}{\partial f(P)} + \frac{\partial f}{\partial f_y} \cdot \frac{\partial f_y}{\partial u^{pl}} \cdot \frac{\partial f}{\partial f(P)} \right) \cdot \lambda^{pl} \quad (II.34)$$

$$d\lambda^{pl} = \frac{f(P^e; fy)}{\left( \frac{\partial f}{\partial f(P)} \cdot k \cdot \frac{\partial f}{\partial f(P)} + \frac{\partial f}{\partial f_y} \cdot \frac{\partial f_y}{\partial u^{pl}} \cdot \frac{\partial f}{\partial f(P)} \right)} \quad (II.35)$$

From equation above, the displacement in plastic state can be expressed as follow:

$$d\lambda^{pl} = \frac{(P, fy)}{\left( 1 \cdot k \cdot 1 + \frac{\partial f}{\partial u^{pl}} \cdot 1 \right)} \quad (II.36)$$

For the next step, the multiplier for relative displacement at  $\lambda_{i+1}^{pl}$  can be written as equation II.37. It is calculated at each plastic mechanism to define the plastic displacement:

$$d\lambda_{i+1}^{pl} = \frac{(P_i^c, fy_i^c)}{\left( 1 \cdot k \cdot 1 + \frac{\partial f}{\partial u^{pl}} \cdot 1 \right)} \quad (II.37)$$

Where,  $d\lambda_{i+1}^{pl}$  is the multiplier for relative displacement at point  $i+1$ ,  $P_i^c$  is the actual load in  $i$ ,  $fy_i^c$  is the correction yield strength limit at  $i$ ,  $k$  is stiffness in elastic state.

### II.3 SYNTHESIS OF ELASTOPLASTIC MACRO-ELEMENT PARAMETERS

The macro-element model needs the interpretation from every soil test result to fulfil the input data in model to determine the value of  $R_c$ ,  $f_y$ ,  $k_v$ ,  $a$ ,  $b$ , and  $C_s$ . The interpretation of PMT result is presented in Table II.4.



Table II.4. Parameters of elastoplastic macro-element model

Parameters	Description
$h_v$	Vertical Stiffness
$h_h$	Lateral Stiffness
$f_y$	Yield strength limit
$Rc$	Asymptote
$a$	Hardening parameter
$b$	Hardening parameter
$C_s$	Macro-element Slope Coefficient

### II.3.1 Vertical load

In order to define each parameter for the proposed macro-element method from pressure-meter test, the following sequence of calculation is presented:

1. Determine the value of  $Rc$  as the asymptote of stress from the PMT data by equation I.1.
2. Determine the value of  $f_y$  (yield strength limit), wherein this method define  $f_y = 0,5Rc$  as the first sloop in *frank and zhao* method (for vertical load) where the assumption is the elastic state occur at the first sloop.
3. Determine the value of  $k$  by equation II.38, where  $L$  is the depth of embedded pile,  $d$  is diameter of pile,  $E_m$  is Menard ratio, and  $z$  is the segment of the layer.

$$k = \frac{1}{L+1,5b} \int_0^{L+1,5b} E_m dz \cdot L \cdot d \quad (\text{II.38})$$

4. The value of  $k_v$  (slope in elastic state) is influenced by  $k$  and  $c_s$  (slope coefficient) in this method the value of slope coefficient on macro-element is proposed from 1 to 4. Where, the value of  $k_v$  is described at equation II.39

$$k_v = c_s \cdot k \quad (\text{II.39})$$

5. Determine the value of  $a$  by equation II.26 and  $b$  by equation II.27
6. Start the calculation by the equation II.4 until  $f(x)^e - f_y = 0$ .
7. If  $f(x)^e - f_y > 0$ , the yield is acting. Use the equation II.25 in this state considering equation II.37.

### II.3.2 Transversal load

The following sequence presents the calculation method for each parameter from Pressuremeter test for proposed macro-element method,:

1. Determine the value of  $D_{em}$  (effective depth on macro-element) taken six times diameter of pile.
2. Determine the value of  $P_{ui}$  for each segment, the asymptote of stress in segment  $i$  of the PMT data from equation I.35 or I.36, and  $P_u$  is total value in  $D_{em}$ .

3. Determine the value of  $f_y$  (yield), wherein this method define  $f_y = 0$ .
4. Determine the value of  $E_{ti}$  by equation I.32 or I.33.
5. The value of  $k_h$  (slope in elastic state) is influenced by  $E_{ti}$  and  $D_{em}$ . Where, the value of  $k_h$  is described at equation II.40 and  $R_c$  is total  $P_{ui}$  along  $D_{em}$  (Equation II.41).

$$k_h = \int_0^{0.5D_{em}} E_{ti} dz \quad (II.40)$$

$$R_c = \int_0^{D_{em}} P_{ui} dz \quad (II.41)$$

6. Determine the value of  $a$  by equation II.26 and  $b$  by equation II.27.
8. Start the calculation by the equation II.4 until  $f(x)^e - f_y = 0$ .
9. If  $f(x)^e - f_y > 0$ , the yield is acting. Use the equation II.24 in this state considering equation II.37.

## II.4 COMPARISON TO CONVENTIONAL LOAD TRANSFER METHOD

### II.4.1 Case Studies For Vertical Load Response

In order to verify the performance of macro-element on a deep foundation in vertical load, two cases are calculated by Frank and Zhao method to perform on the single pile to check the reliability at the proposed method for the single Macro-element analysis (Figure II.14.a), and the macro-element embedded into Flac3D (Figure II.14.b) of the load-settlement response of pile.

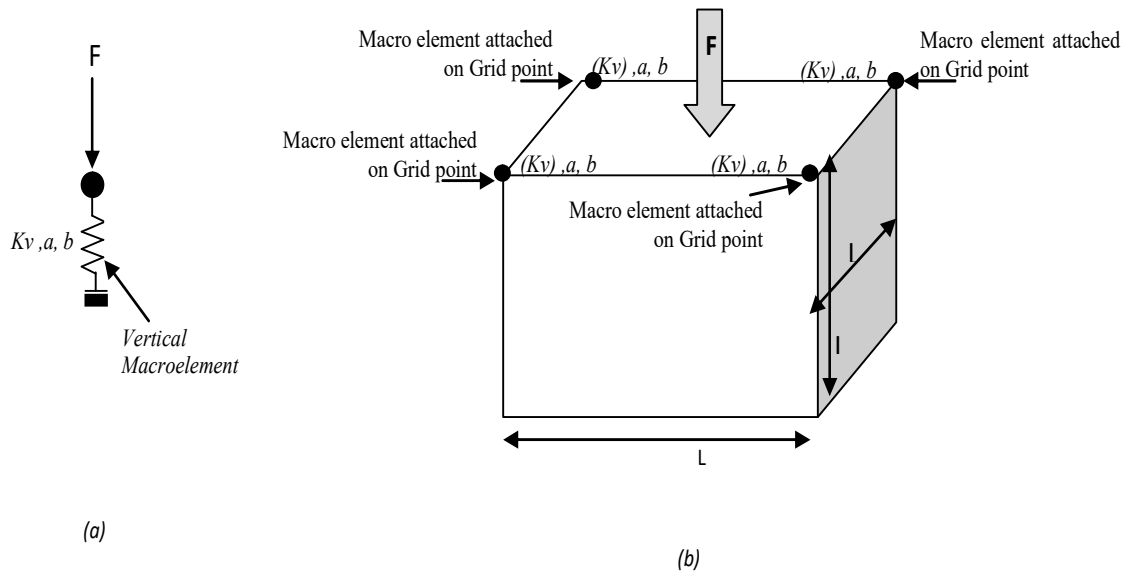


Figure II.14. (a) The single Macro-element for single pile and (b) Macro-element on Flac3D for pile group on vertically load

To compare the calculation results of the macro-element method then performed three types of calculations from data above for these model is done *T-Z* method using Frank and Zhao model, single macro-element (working on excel sheet) and the embedded macro-element into Flac3D.

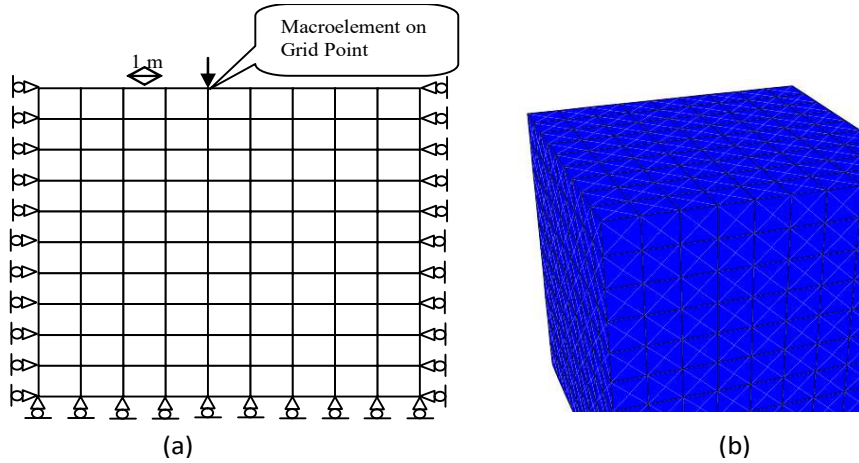
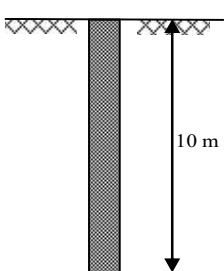


Figure II.15. (a) Sketch of mesh and boundary condition on the single Macro-element for single pile and (b) Model for Macro-element on Flac3D

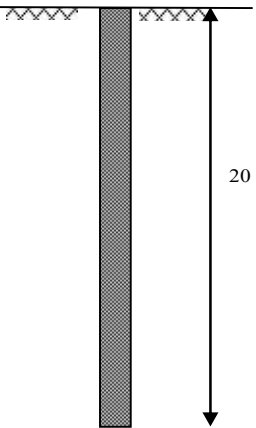
A simple model is used by following the two Menard Pressure-meter tests result which concrete pile are installed on soil (table II.4.a) 10m and 20m depth on soil (table II.4.b) and for concrete properties are 10 GPa for  $E_c$  and 0,2 for  $\nu_c$ . With eight variations of piles dimension for each depth of pile.

Table II.4. (a) Menard Pressure-meter test for type soil 1 (layered soil) and (b) type soil 2 (Homogeneous soil)

Depth m	Em mPa	PI* mPa
0	0	0
1	3.2	0.28
2	13.1	1.08
3	50	2.86
4	50.7	2.29
5	34.7	1.94
6	28.4	1.37
7	66.8	1.55
8	54.7	1.76
9	53.7	1.73
10	64.6	2.12
11	64.6	2.12
12	64.6	2.12



Depth m	Em mPa	PI* mPa	Depth m	Em mPa	PI* mPa
0	0	0	13	15	1.2
1	15	1.2	14	15	1.2
2	15	1.2	15	15	1.2
3	15	1.2	16	15	1.2
4	15	1.2	17	15	1.2
5	15	1.2	18	15	1.2
6	15	1.2	19	15	1.2
7	15	1.2	20	15	1.2
8	15	1.2	21	15	1.2
9	15	1.2	22	15	1.2
10	15	1.2			
11	15	1.2			
12	15	1.2			



(a)

Three types of the calculation methods are done to the calculation according to data of soil above and each dimension of the pile using Frank and Zhao method, macro-element in excel

sheet and macro-element embedded into Flac3D. For the first step in macro-element method is defining pile-capacity  $R_c$  using equation I.10, and the results of  $R_c$  in each dimension of piles are presented in table II.5 for soil type 1 and table II.6 for soil type 2.

**Table II.5.** The ultimate capacity of the pile head in each dimension of the pile in 10 m depth and soil type 1.a.

Dim (m)	0.3	0.4	0.5	0.6	0.7	0.8	0.9	1
Rc (N)	1.04E+06	1.66E+06	2.53E+06	3.70E+06	5.24E+06	7.20E+06	9.64E+06	1.26E+07

**Table II.6.** The ultimate capacity of the pile head in each dimension of the pile in 20 m depth and soil type 1.b.

Dim (m)	0.3	0.4	0.5	0.6	0.7	0.8	0.9	1
Rc (N)	1.57E+06	2.19E+06	2.86E+06	3.58E+06	4.35E+06	5.17E+06	6.03E+06	6.95E+06

For the next step is to determine the value of  $k_v$ ,  $a$ ,  $b$  and  $f_y$  with equation II.34, II.22, II.23 and  $f_y$  value define 0.5 of  $R_c$  and the value of  $c_{me}$  is defined 1. Those result is shown in table II.7 for soil type 1 in 10 m depth of pile and presented in each dimension of the pile from 0.3 cm to 100 cm.

**Table II.7.** Calculation results of the macro-element parameters at each dimension of the pile in 10 m depth and soil type 1.a.

Dim (m)	0.3	0.4	0.5	0.6	0.7	0.8	0.9	1
$k_v$ (N/m)	1.26E+08	1.68E+08	2.10E+08	2.52E+08	2.94E+08	3.36E+08	3.78E+08	4.20E+08
Rc (N)	1.04E+06	1.66E+06	2.53E+06	3.70E+06	5.24E+06	7.20E+06	9.64E+06	1.26E+07
$f_y$ (kN) (50% )	5.20E+05	8.30E+05	1.27E+06	1.85E+06	2.62E+06	3.60E+06	4.82E+06	6.30E+06
a (kN)(50% )	5.20E+05	8.30E+05	1.27E+06	1.85E+06	2.62E+06	3.60E+06	4.82E+06	6.30E+06
b (M) (a/ $k_v$ )	4.13E-03	4.94E-03	6.03E-03	7.34E-03	8.91E-03	1.07E-02	1.28E-02	1.50E-02

And the calculation for the value of  $k_v$ ,  $a$ ,  $b$  and  $f_y$  is shown in table II.8 for soil type 2 in 20 m depth of pile and presented in each dimension of the pile from 0,3 cm to 100 cm.

**Table II.8.** Calculation results of the macro-element parameters at each dimension of the pile in 10 m depth and soil type 1.b.

Dim (m)	0.3	0.4	0.5	0.6	0.7	0.8	0.9	1
$k_v$ (N/m)	9.00E+07	1.20E+08	1.50E+08	1.80E+08	2.10E+08	2.40E+08	2.70E+08	3.00E+08
Rc (N)	1.57E+06	2.19E+06	2.86E+06	3.58E+06	4.35E+06	5.17E+06	6.03E+06	6.95E+06
$f_y$ (kN) (50% )	7.85E+05	1.10E+06	1.43E+06	1.79E+06	2.18E+06	2.59E+06	3.02E+06	3.48E+06
a (kN)(50% )	7.85E+05	1.10E+06	1.43E+06	1.79E+06	2.18E+06	2.59E+06	3.02E+06	3.48E+06
b (M) (a/ $k_v$ )	8.72E-03	9.13E-03	9.53E-03	9.94E-03	1.04E-02	1.08E-02	1.12E-02	1.16E-02

The calculation result from *T-Z* method using Frank and Zhao model, single macro-element and the embedded macro-element into Flac3D are presented in Figure II.16 and II.17 for soil type in 10 m depth for each dimension of the pile.

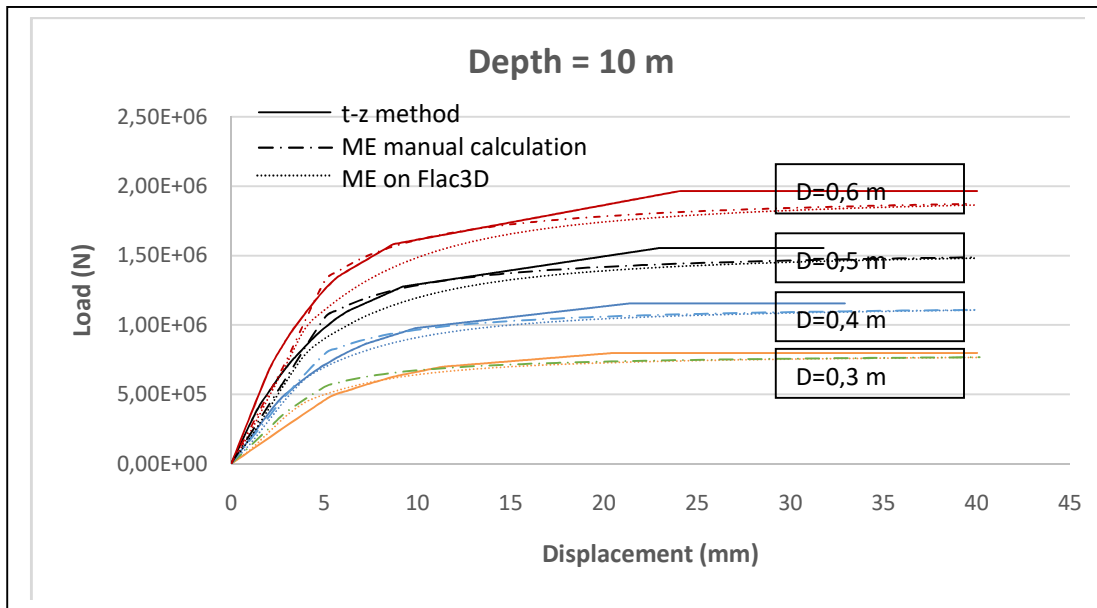


Figure II.16. The load-settlement curve at the pile head of single pile from soil type 1 from 10m depth (  $D= 30$  cm to  $D= 60$ cm)

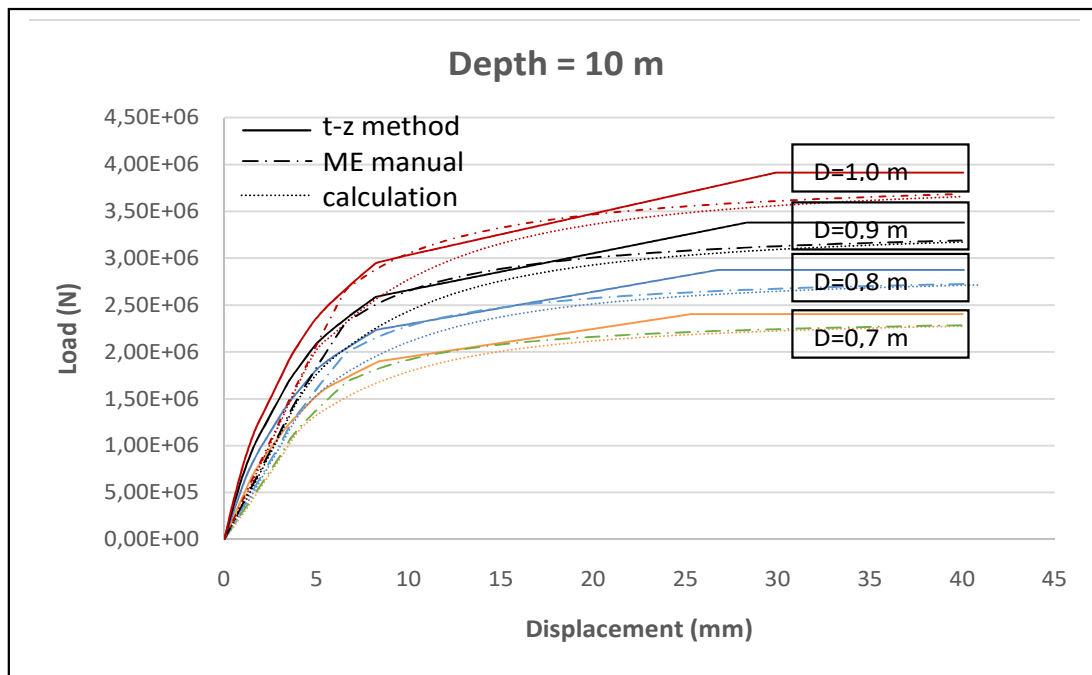


Figure II.17. The load-settlement curve at the pile head of single pile from soil type 1 from 10m depth (  $D= 70$  cm to  $D= 100$ cm).

The calculation result from T-Z method using Frank and Zhao model, single macro-element and the embedded macro-element into Flac3D are presented in Figure II.18 and II.19 for soil type 2 in 10 m depth for each dimension of the pile.

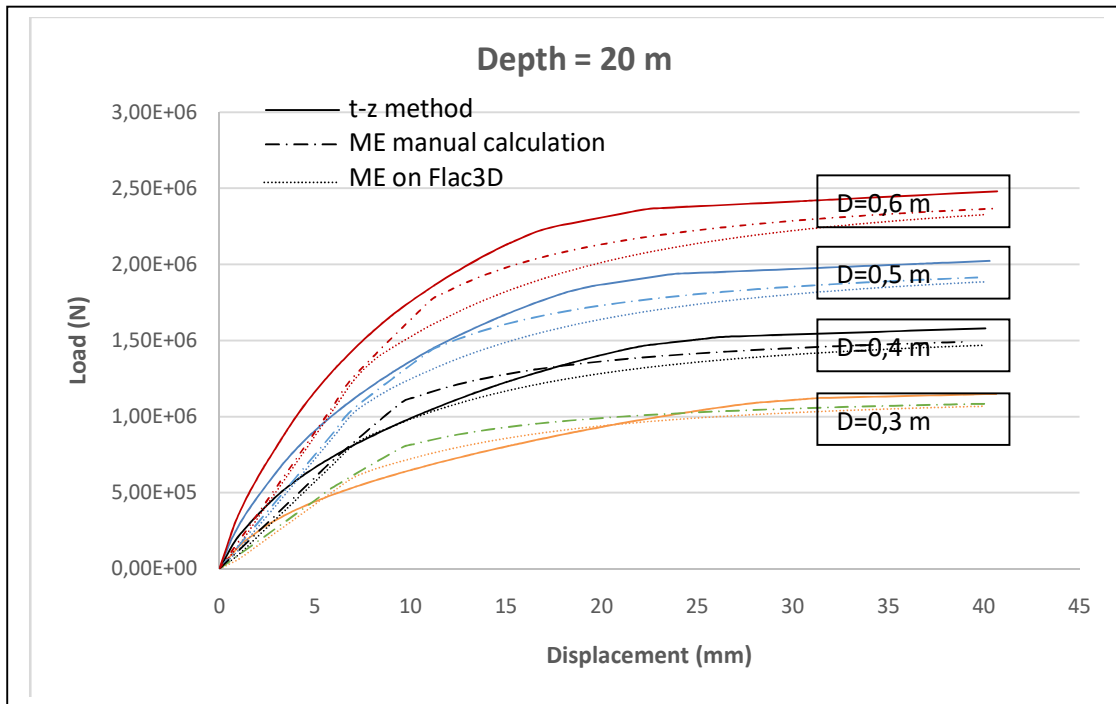


Figure II.18. The load-settlement curve at the pile head of single pile from soil type 2 from 20m depth ( D= 30 cm to D= 60cm).

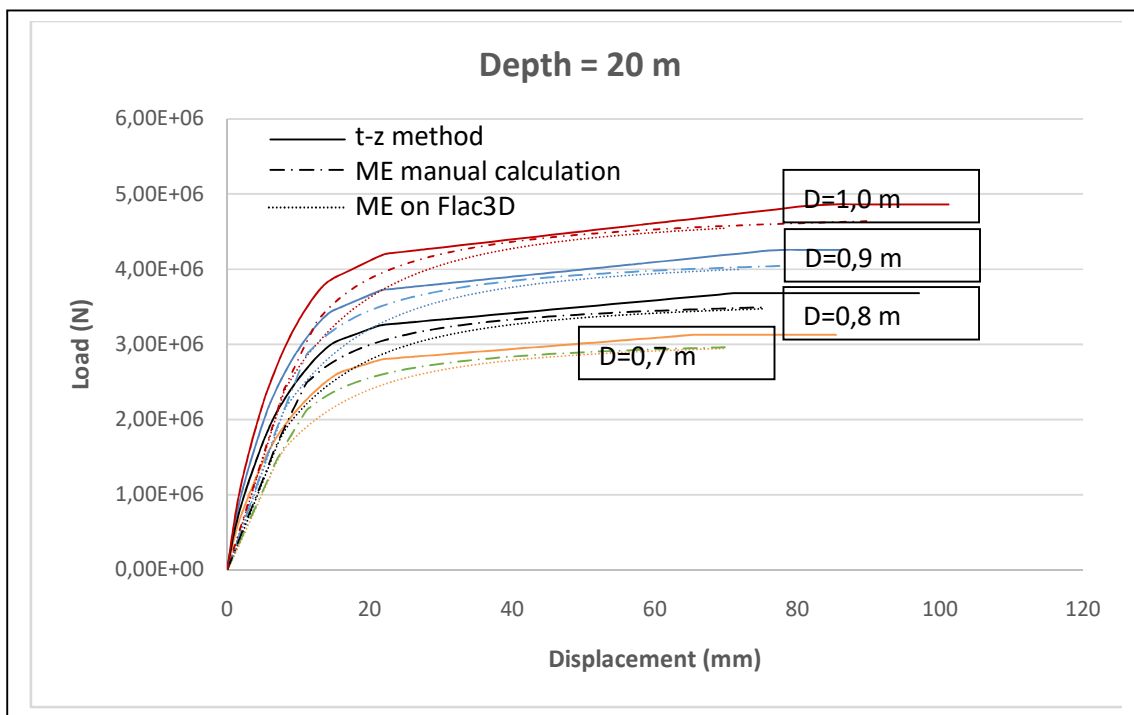


Figure II.19. The load-settlement curve at the pile head of single pile from soil type 2 and 20m depth ( D= 70 cm to D= 100cm).

Those Figures show that at low loading level the load-displacement curve at the pile head from the propose macro-element method is generally consistent with the load transfer method. At high loading level, the propose macro-element method is slightly larger than the load transfer method. And the result between the single macro-element and the embedded macro-element into Flac3D is in the consistent result.

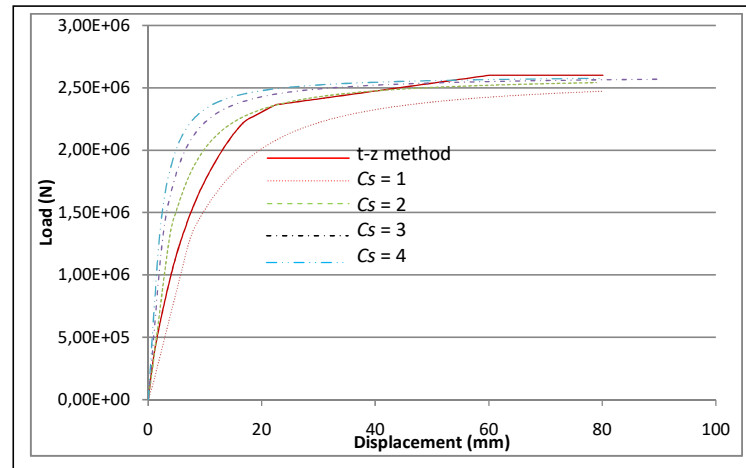


Figure II.20. The comparison curve between T-z method and the macro-element method due to the variation of slope coefficient on macro-element  $C_s$  (20m depth and diameter 70 cm )

Figure II.20 shows the calculation result for diameter 70 cm with 20 m depth by  $T-z$  method and macro-element method in which the shape variation curves are presented due to the variation of slope coefficient on macro-element  $C_s$ . By increasing of slope coefficient  $C_s$  influence to the slope of Loading-displacement curve, the coefficient is an effort to interpret the data from PMT into macro-element inputs so that the calibration value of the existing method and the results of loading test can be satisfactory.

One of a base concept in the proposed method is concentrating all of the reaction either in model elastic or model plastic on macro-element which is attached on Flac3D. Figure II.22a shows the mesh and boundary condition of the model constructed on Flac3D, and comparison of plasticity flow between the conventional model and macro-element model. For the first model is run by the conventional method of Flac3D where it runs by model Mohr-Coulomb, and the result of plasticity is shown in Figure II.22c where the plasticity flow exists on the model. The second model, The macro-element which is embedded on Flac3D as fish function runs the calculation by applying the displacement, and the result show that the plasticity flow doesn't exist on macro-element model (Figure II.22b), it is indicating that all of the reaction concentrated into macro-element.

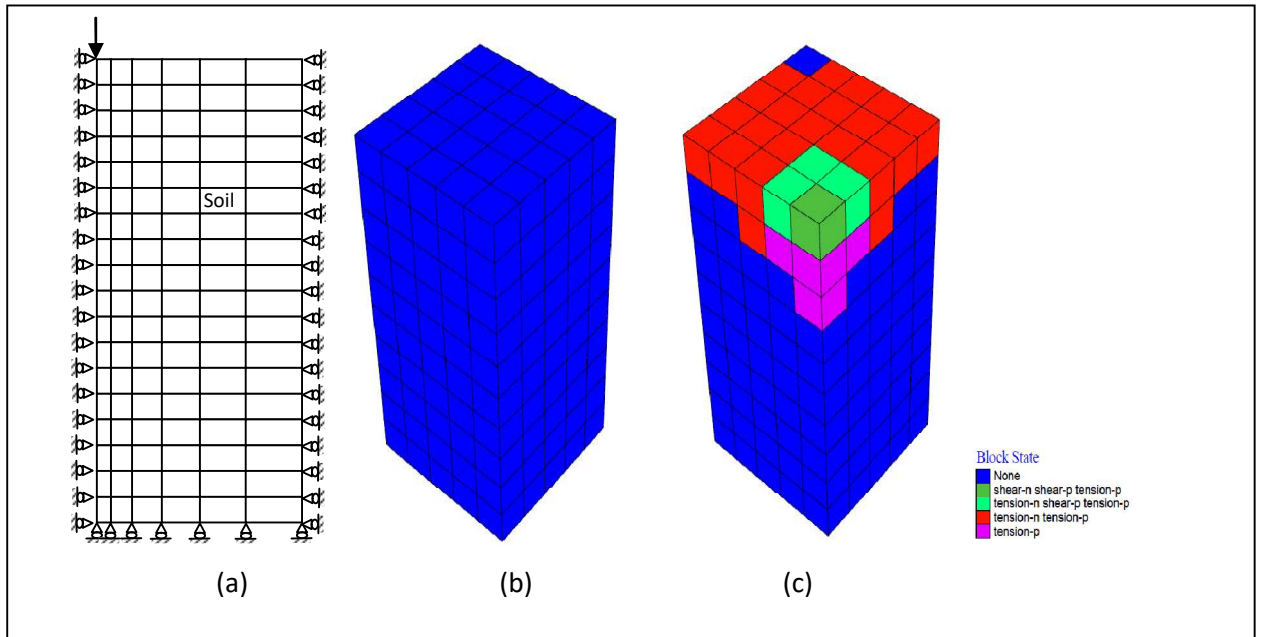


Figure II.22. (a) Mesh and boundary condition (b) The plasticity flow on Flac3D in macro-element method (c) The plasticity flow on Conventional Flac3D.

#### II.4.2 Case Studies For Transversal Load Response

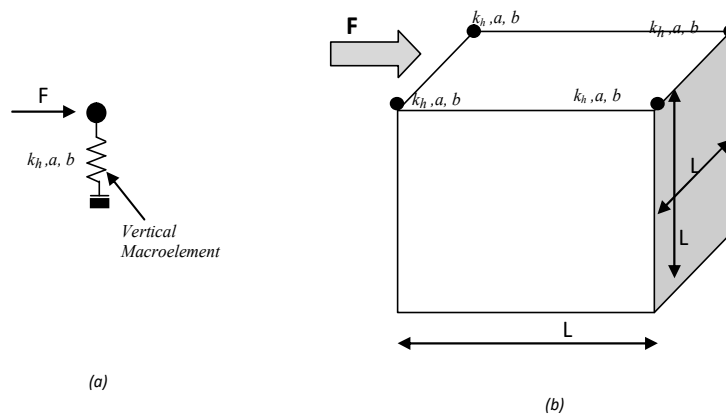


Figure II.23. (a) The single Macro-element for single pile and (b) Macro-element on Flac3D for pile group on Lateral load

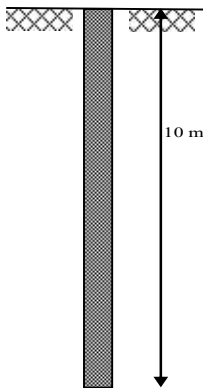
The macro-element model is also extended to analyse the response of the lateral load pile. The base concept of laterally loading on macro-element is similar to the vertical load in governing parameter, but the interpretation and the direction of load are different as explained in the interpretation of PMT result in macro-element method. The calculation of homogeneous soil is used data from table II.9, and for bi-layered soil is used data from table II.11. In order to verify this macro-element method on laterally loading, the calculation base on Frank and



Zhao method which is run by PILATE programming and the calculation in Flac3D base on Macro-element method are presented.

Table II.9. Menard Pressure-meter test for Homogenous soil

Depth	Em	pl
m	mPa	mPa
0	0	0
1	15	1.2
2	15	1.2
3	15	1.2
4	15	1.2
5	15	1.2
6	15	1.2
7	15	1.2
8	15	1.2
9	15	1.2
10	15	1.2
11	15	1.2
12	15	1.2



The model for vertical load is constructed in Flac3D as Figure II.16.a. by modifying the direction of load into the lateral load. The calculation presents eight diameter variation from 30 cm to 100 cm. By following Interpretation of PMT result in Macro-element Method on lateral load has been explained above then the result of each parameter needed in Flac3D is defined as presented in table II.10 for homogeneous soil and table II.12 for bi-layered soil. The interpretation value of  $\alpha_b$  is taken 2 to define the value of  $b$  for sand (equation II.23) on laterally load. From Figure II.24 and Figure II.25 show that generally the calculation results estimating the macro-element method is in good agreement with the results from P-y method and T-z method. In lateral load model, the yield of plasticity also doesn't exist by the same reason as vertically load.

Table II.10. Calculation results of the macro-element parameters for laterally load at each dimension of the pile in 10 m depth in homogeneous soil.

Diameter (m)	0.3	0.4	0.5	0.6	0.7	0.8	0.9	1
Eti (N/m <sup>2</sup> )	4.25E+07	4.45E+07	4.61E+07	4.27E+07	4.87E+07	4.97E+07	5.07E+07	5.15E+07
Pu(N/m)	2.71E+05	4.54E+05	6.82E+05	9.54E+05	1.27E+06	1.63E+06	2.04E+06	2.49E+06
D <sub>em</sub> (m)	1.8	2.4	3	3.6	4.2	4.8	5.4	6
Dem/2	0.90	1.20	1.50	1.80	2.10	2.40	2.70	3.00
k <sub>h</sub> (N/m)	3.83E+07	5.34E+07	6.92E+07	7.69E+07	1.02E+08	1.19E+08	1.37E+08	1.55E+08
a (N)	4.88E+05	1.09E+06	2.05E+06	3.43E+06	5.34E+06	7.83E+06	1.10E+07	1.49E+07

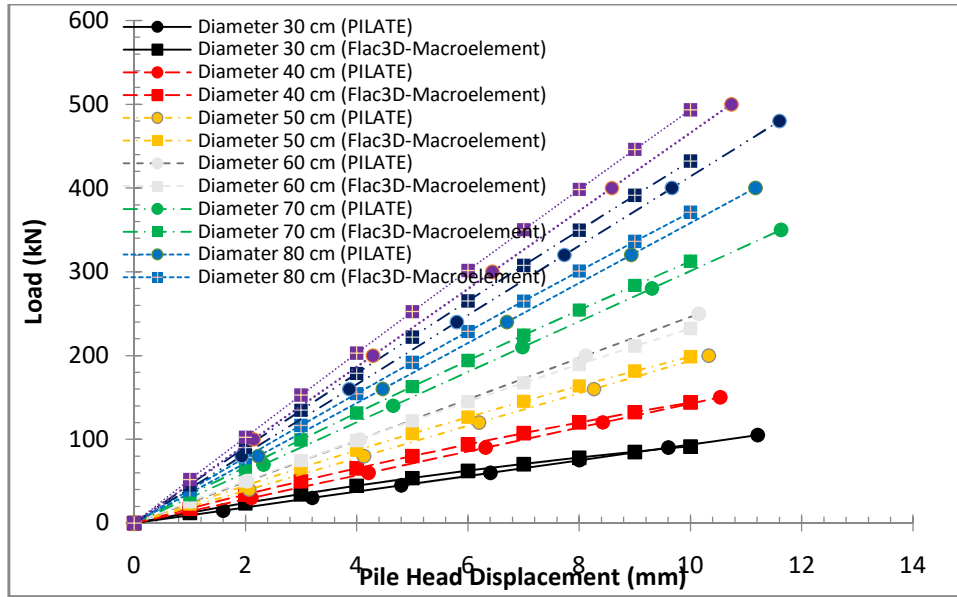
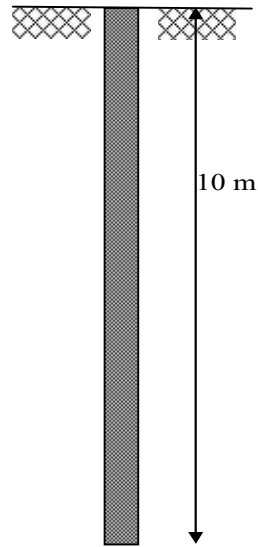


Figure II.24. The load-settlement curve for at the pile head of single pile from Homogenous soil with 10m depth ( D= 30 cm to D= 100cm).

Table II.11. Menard Pressure-meter test for Bi-layered soil

Depth	Em	pl
m	mPa	mPa
0	0	0
1	15	0.6
2	15	0.6
3	15	0.6
4	15	0.6
5	30	1
6	30	1
7	30	1
8	30	1
9	30	1
10	30	1
11	30	1
12	30	1



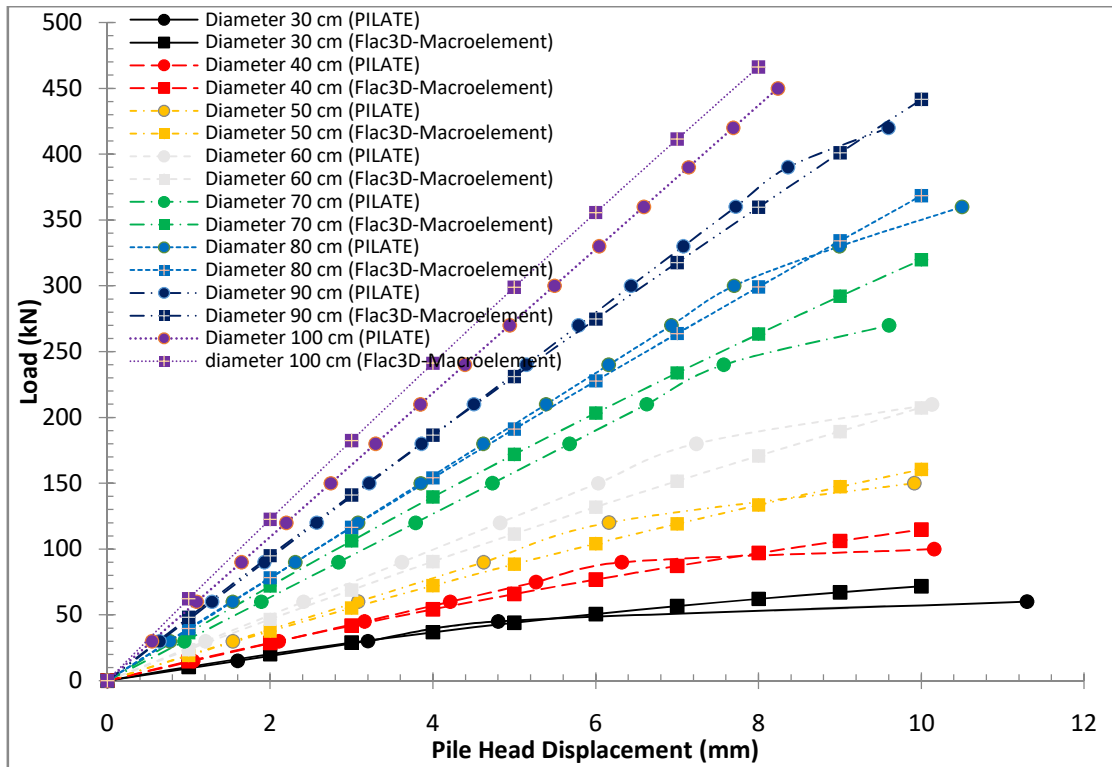


Figure II.25. The load-settlement curve for at the pile head of single pile from bi-layered soil with 10m depth ( D= 30 cm to D= 100cm).

Table II.12. Calculation results of the macro-element parameters for laterally load at each dimension of the pile in 10 m depth in bi-layered soil.

Diameter (m)	0.3	0.4	0.5	0.6	0.7	0.8	0.9	1
Eti (N/m <sup>2</sup> )	3.30E+07	3.80E+07	3.91E+07	4.00E+07	5.30E+07	4.94E+07	5.39E+07	6.22E+07
Rc(N/m)	1.78E+05	2.92E+05	4.32E+05	5.97E+05	7.95E+05	1.04E+06	1.32E+06	1.63E+06
D <sub>em</sub> (m)	1.8	2.4	3	3.6	4.2	4.8	5.4	6
Dem/2	0.90	1.20	1.50	1.80	2.10	2.40	2.70	3.00
k <sub>h</sub> (N/m)	2.97E+07	4.56E+07	5.87E+07	7.20E+07	1.11E+08	1.19E+08	1.45E+08	1.87E+08
a (N)	3.20E+05	7.00E+05	1.30E+06	2.15E+06	3.34E+06	4.98E+06	7.10E+06	9.78E+06

## II.5 RESULT

The methodology of the proposed macro-element model, step-by-step, was presented to define the parameter of macro-element method. The analysis result of macro-element has been compared and validated with the  $T-z$  method and the  $P-y$  method in load-deflection curve prediction.

The macro-element model gives more simple calculation than the model conventional in Flac3D because the model is constructed for soil parameter only and the parameter of the pile is presented in macro-element. It effects the running time of model which is faster than the conventional model.

From the comparison result which has been done on vertical load and lateral loads in eight diameter variation show the satisfactory result.

The macro-element model on Flaac3D can be applied to neither model elastic or model Mohr-coulomb that deliver the same result.

The plasticity flow doesn't exist in proposed macro-element model, because all of the reaction concentrate into macro-element.

## CHAPTER III: APPLICATION AND VALIDATION OF MACRO-ELEMENT

---

Three case histories are used to perform the case study. The embedded macro-element in Flac3D, as a tool, is used to develop a model. The developed model is intended to account the soil-structure interaction of deep foundation either single pile or pile group.

The history case that is reported by *Bustamante and Jezequel, 1989* and *Reiffsteck P, 2009* used to analyse the case study on the single vertically loaded pile. The second case is performed to a transversally loaded pile where the history case reported by (*Hadjaji T, 2002* and *Boufia A, 2017*) is used. The case study for pile groups is performed from the case history reported by *O'Neil et al., 1983, Castely and Maugeri, 2002 and Zhang et al., 2013*.

---

After making a comparison between  $T-z$  method and the  $P-y$  method with macro-element method, the validation with loading test result is importance of some interest. Four cases have been analysed for single pile and group pile analysis.

### III.1 SINGLE PILE

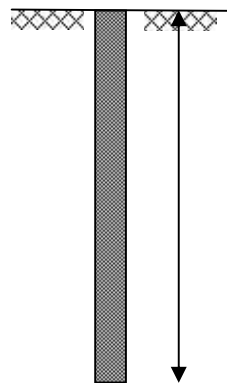
The implementation of macro-element in Flac3D under vertical and transversal load is validated to the loading test result. The field test results are taken from many places that reported by previous research.

#### III.1.1 Vertically Loaded Pile

Regarding the vertical loading test that was instrumented by  $LPC$  removable extensometers along its length of pile (*Bustamante and Jezequel, 1989*). LCPC (*Laboratoire Central des Ponts et Chaussees*) team did 9 PMT test and reported that participant number 8 and 9 gave the closest result to the reality (*Reiffsteck P, 2009*). The value of participant number 9 is used in this example case. It is used for this analysis data (Table III.1).

Table III.1 Soil parameter value from Pressuremeter test.

Depth (m)	Em (MPa)	PI (MPa)
1	4.5	0.34
2	4	0.32
3	4.75	0.41
4	10.8	0.76
5	10.5	0.81
6	16.5	1
7	19.1	1.08
8	18.5	1.09
9	22	1.2
10	20	1.32
11	23.1	1.37
12	22.5	1.42
13	28.2	1.62
14	31.2	1.63



The pile was installed at the experimental site located in North of France With 0.5 m diameter and 12 m deep, the soil is silt overlaying highly over-consolidated and fissured *Flander clay*. For this case, the models on Flac3D are made in two types, in the conventional model and macro-element model (Figure III.1) where the conventional model is constructed by soil and pile (Figure III.1), but for macro-element the model is constructed by ground only (Figure III.1.b).

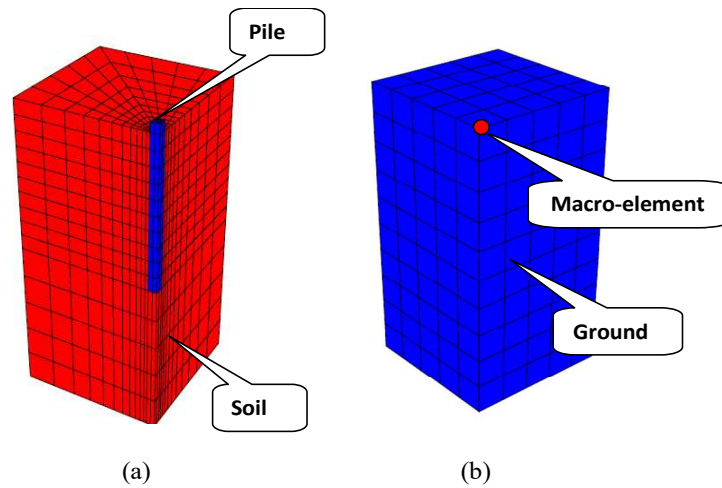


Figure III.1. Sketch of Flac3D mesh and boundary condition, (a) Conventional method (b) Macro-element method

On the conventional Flac3D model, the constructed model is described in Figure III.2.a where the model is constructed by soil and pile properties. It was run under Mohr-Coulomb criterion with the parameter as table III.2.

Table III. 2 Material properties

Material	$\gamma$ (kg/m <sup>3</sup> )	$E$ (Mpa)	$\nu$	$\phi$ (°)	$C$ (kPa)	$\psi$ (°)
Soil	1800	100	0.3	5	5000	5
Pile	2500	20000	0.2			

The program was run by applying the load on the pile and it needs 1 hour 13 minutes for 12 loading steps. Figure III.2b shows the displacement magnitude of model and the Plasticity flow of soil is showed in Figure III.2c.

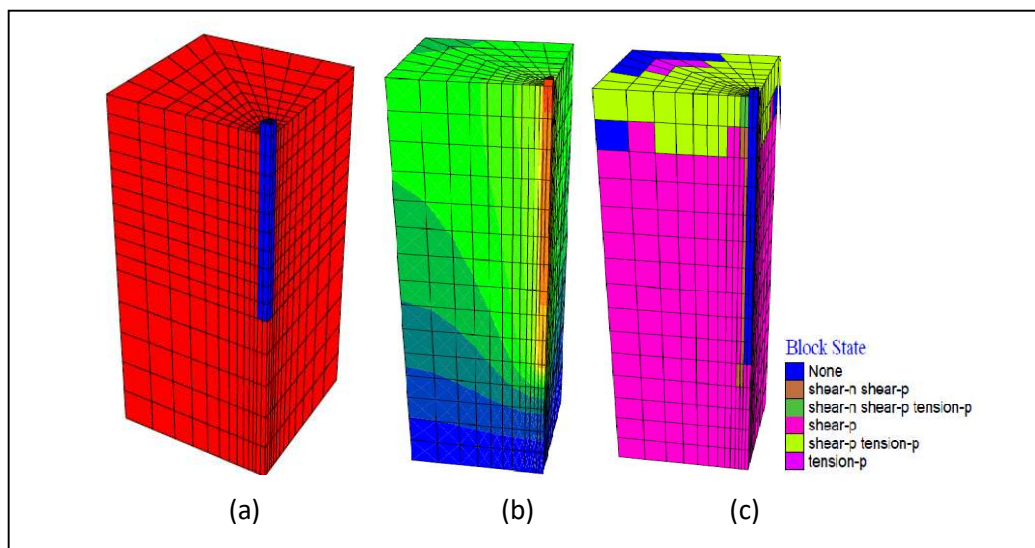


Figure III.2. (a) Model of the pile on flac3D (b) Displacement magnitude (c) Plasticity flow of soil

On macro-element model, the model is constructed for ground and the macro-element is attached on grid point (Figure III.3). From data PMT above defines the input data for macro-element by following step-by-step the interpretation of PMT result in macro-element method. The calculation defines the result as  $K_v=1,01 \cdot 10^8$ ,  $R_c=1.24 \cdot 10^6$  where  $f_y$  and  $a$  is taken  $0.5R_c$ ,  $c_s$  is adopted as 4 unit and to avoid divergence in Flac3D  $\alpha_b$  is adopted 1.01. the macro-element parameters are summarized in Table III.3. The proposed macro-element method needs less than 1 minute to finish the calculation in Flac3D. The calculation in macro-element has been done with two type calculations. It was in elastic-perfectly plastic state under Mohr-Coulomb criterion.

Table. III. 3 Macro-element parameters

Parameter	Unit	Value
$k_v$	Kg/m	1.01 E+8
$R_c$	Kg	1.24 E+6
$f_y$	Kg	6.2 E+5
$a$	Kg	6.2 E+5
$b$	m	6.2 E-3
$c_s$		4
$\alpha$		1.01

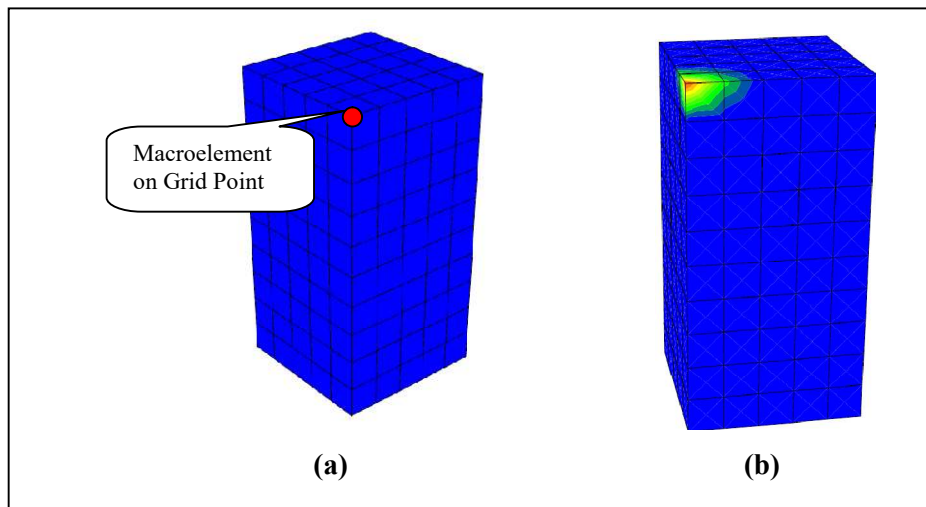


Figure III.3. (a) The simple model of the pile on flac3D for macro-element (b) Displacement magnitude

Figure III.4 shows that the Plasticity flow of soil doesn't exist when the macro-element works in elastic-perfectly plastic under Mohr-Coulomb criterion because all the processes are concentrated into macro-element.



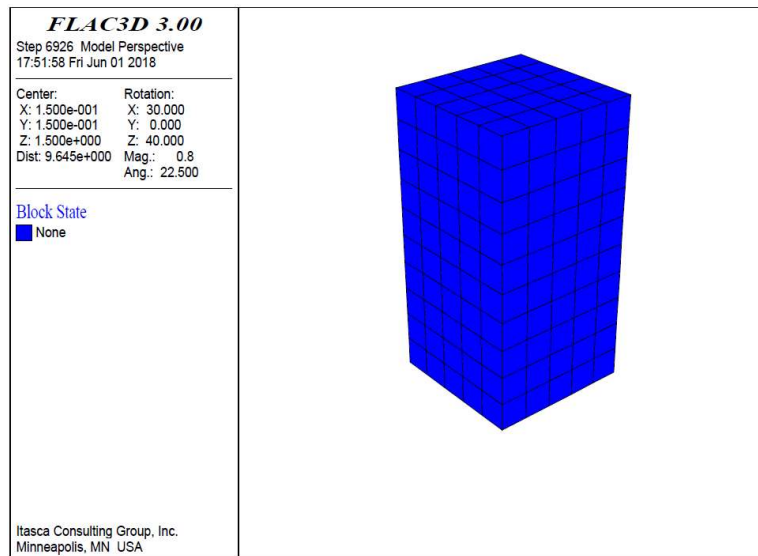


Figure III.4 Plasticity flow of soil on Flac3D for Macro-element method in Mohr-Coulomb criterion.

The comparison result between the Loading test and some theoretical calculation method are presented in Figure III.5. From that Figure shows that the macro-element model estimates in good agreement with the loading test result.

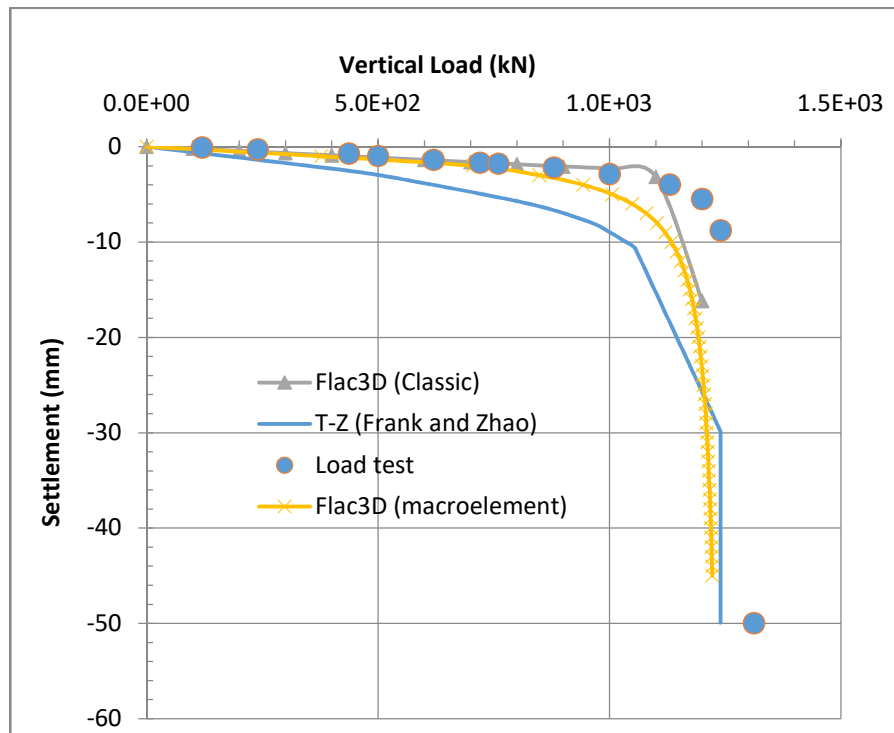


Figure III.5 Measured and calculated load-settlement curve at the pile head of single pile

### III.1.2 Transversally Loaded Pile

The experimental site located in *Plancoet* (cote du nord, France) in 1984 is a bi-layered soil. It was composed of four meters of clay (CL) and four meters of sand (SM) with diameter of pile

is 0.284 m by driven installation method,  $Ep.Ip$  is  $30 \text{ MNm}^2$ , the equivalent net cone resistance  $q_{ce}^*$  is 1.151 MPa and the lateral pile/stiffness ratio  $K_R$  is  $1.5 \cdot 10^{-2}$  (Hadjaji T, 2002 and Boufia A, 2017). According to the data and equation II.36 and I.43 defined the value of  $k_h$  and  $Pu$  are  $1.18 \cdot 10^7 \text{ N/m}$  and  $3.34 \cdot 10^4 \text{ N}$  and the value of  $\alpha_b$  is taken 2.

The value of  $Eti$  is defined by equation I.32 and then continue the calculation by following step-by-step Interpretation of PMT result in Macro-element Method on laterally load that has been explained above. And the result of these calculations are presented in Table III.4.

Table III.4. The macro-element parameters

Diameter (m)	0.284
Eti (N/m <sup>2</sup> )	1.38E+07
Pu(N/m)	1.96E+04
Dem	1.704
Dem/2	0.852
kh (N/m)	1.18E+07
a (N)	3.34E+04
b (m)	5.68E-03

The next step is constructing a simple model in Flac3D (Figure III.6) wherein this model initialled as soil properties only because the properties of pile are already expressed into macro-element parameters.

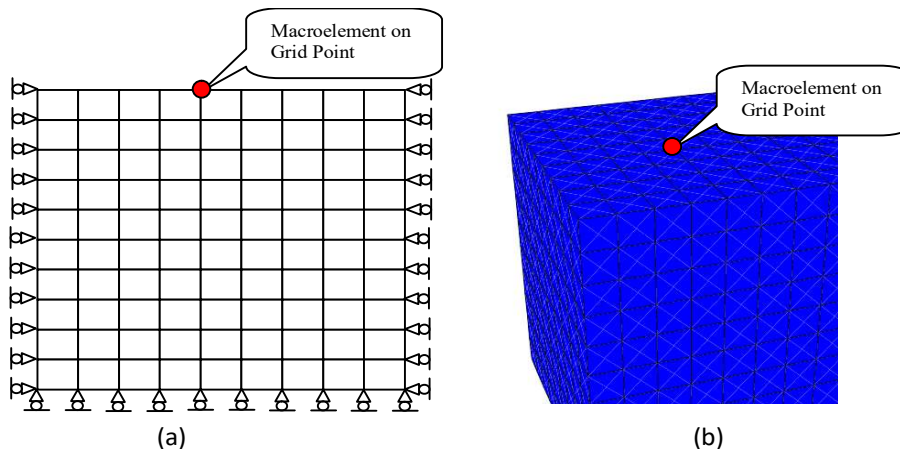


Figure III.6. (a) Sketch of mesh and boundary condition on the single Macro-element for single pile and (b) Model for Macro-element on Flac3d

A very good agreement is also notice in Figure III.7 between the propose macro-element method and measured displacement-load curve also presented other prediction methods for the comparison result (Boufia A, 2017).

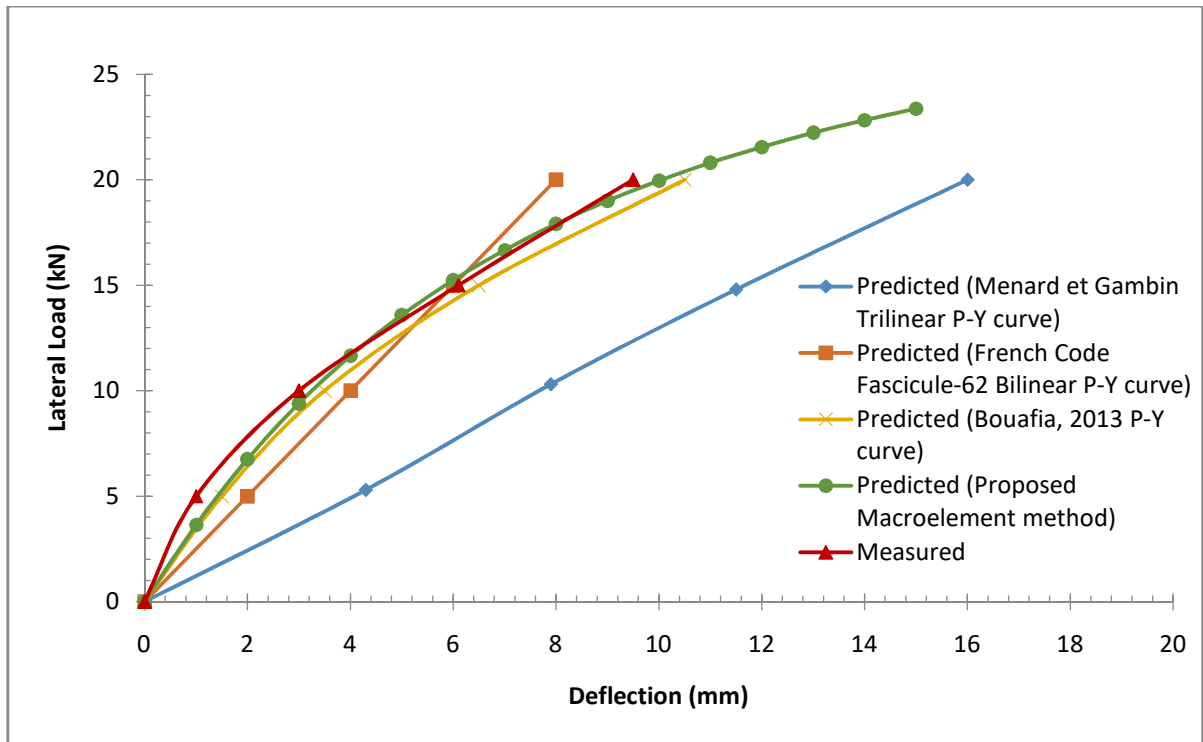


Figure III.7. Comparison of predicted and measured deflection

### III.2 PILE GROUP

The loading-settlement responses in pile group are formed in four-pile group (formation 2x2) and nine-pile group (formation 3x3). The validation on pile group is done to the reaction at every position of pile (centre, edge and corner) either for rigid pile-cap or/and flexible pile-cap (modelled without pile-cap) and compared with loading test result. The defined macroelement parameter for single pile can be applied directly into pile-group as the presentation of single pile properties which is connected by rigid or flexible pile-cap. In these validations with loading test is done with two types of pile group (four-pile group and nine-pile group).

Regarding the loading tests that was reported by *O'Neil et al. (1983)* for the four-pile group and nine group pile with closed-ended steel pipe pile in stiff over-consolidated clays. The piles had external diameter 0,274 m and driven into 13,1 m depth. The configuration of pile groups described as Figure III.6 and III.7 with the configuration 3x3 and the centre to centre spacing is  $3d$ .

From these loading test, *Castely and Maugeri (2002)* evaluated the properties of soil by back analysis. The unit shaft resistance was assumed from 19 kPa in the surface than increased linearly to 93 kPa at the pile base (Figure III.8) and the ultimate end-bearing capacity was 130 kN. *Zhang et al. (2013)* divided the pile into 13 segments to analyse the pile response using hyperbolic model. And the assumption of the value of  $E_m$  (Menard modulus) to divide

the value of  $k_v$  for Macro-element is assumed from 0.07 MPa at the middle of the first segment to 1.64 MPa at the pile base (Figure III.9). From data above defines the value of  $R_c$  is  $7.54 \cdot 10^5$  N for every single pile and the value of  $K_v$  is  $4,0 \cdot 10^7$  N/m. The value of  $f_y$  and  $a$  are defined half of  $R_c$ . As explained above that for the vertical load the value of  $c_s$  is adopted as 4 and to avoid divergence in Flac3D  $\alpha_b$  is adopted 1.01.

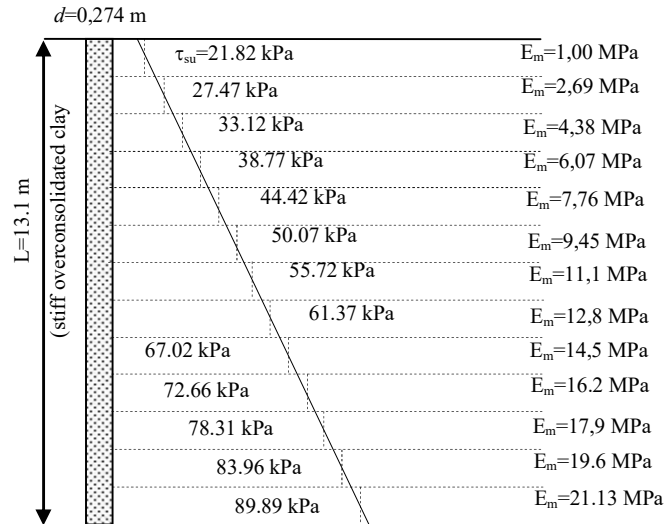


Figure III.8 Calculation Value of limiting unit skin friction of soil at each segment (Zhang et al. (2013)) and the assumption value of  $E_m$  (Menard modulus)

Table III.5 Macro-element Parameters

Parameter	Unit	Value
$k_v$	Kg/m	4.00 E+7
$R_c$	Kg	7.54 E+5
$f_y$	Kg	3.77 E+5
$a$	Kg	3.77 E+5
$b$	m	9.52 E-3
$c_s$		4
$\alpha$		1.01

The first case is in the four-pile group that performs as Figure III.9 with the centre-to-centre spacing  $r=3D$  or equal to the distance between grid pint in Flac3D model where the macro-element attached.

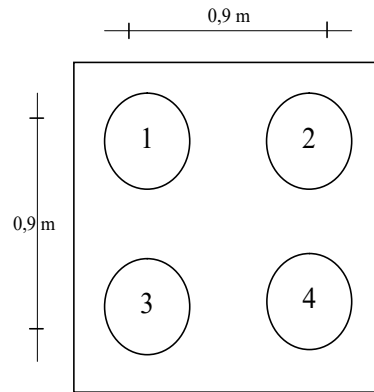


Figure III.9. The configuration of Four-pile group

Table III.6 presents the result of calculation from the macro-element on flac3D where the load are distributed evenly to the piles. Figure III.10 compares the measured of the macro-element method with other calculation method result and measures value that indicates the satisfying result in low loading level.

Table III.6 Predicted pile head load for four pile-group connected by rigid pile-cap.

Displ (mm)	Corner Load (MN)				Total Applied (kN)
	1	2	3	4	
1.0E+00	1.7E-01	1.7E-01	1.7E-01	1.7E-01	6.8E-01
2.0E+00	3.5E-01	3.5E-01	3.5E-01	3.5E-01	1.4E+00
3.0E+00	4.4E-01	4.4E-01	4.4E-01	4.4E-01	1.8E+00
4.0E+00	5.0E-01	5.0E-01	5.0E-01	5.0E-01	2.0E+00
5.0E+00	5.5E-01	5.5E-01	5.5E-01	5.5E-01	2.2E+00
6.0E+00	5.8E-01	5.8E-01	5.8E-01	5.8E-01	2.3E+00
7.0E+00	6.1E-01	6.1E-01	6.1E-01	6.1E-01	2.4E+00
8.0E+00	6.3E-01	6.3E-01	6.3E-01	6.3E-01	2.5E+00

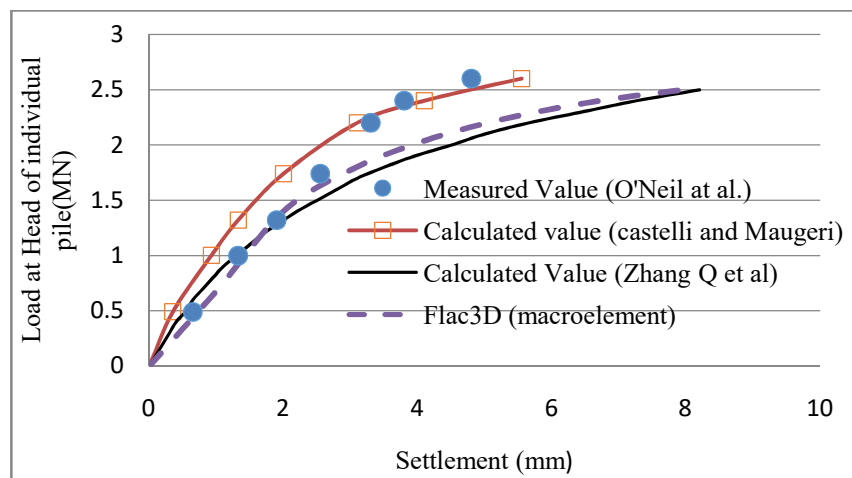


Figure III.10 Measured and calculated load-settlement curve at the pile head of Four- pile group

The second case is in nine-pile group that performs as Figure III.11 with the centre-to-centre spacing  $r=3D$  or equal to the distance between grid point in Flac3D model where the macro-element is attached. The constructed flac3D model presents in Figure III.12, where for the pile group which is connected by rigid pile-cap modelled as Figure III.12.a. And Figure III.12.b is for flexible pile-cap. In modelling of rigid pile-cap, the mesh on flac3d is constructed by soil and properties of pile-cap. The pile-cap properties are the concrete with modulus young 20 GPa, the poisson's ration 0.2 and density  $2.5 \text{ t/m}^3$ .

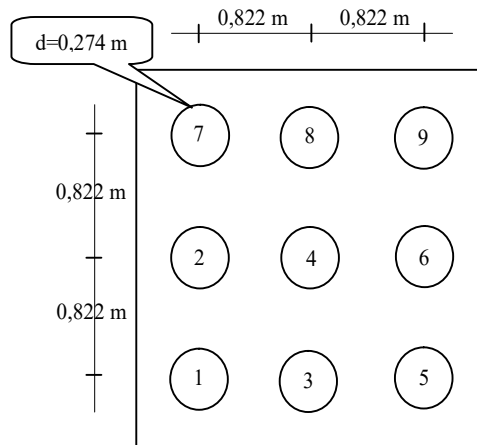


Figure III.11 The configuration of nine-pile

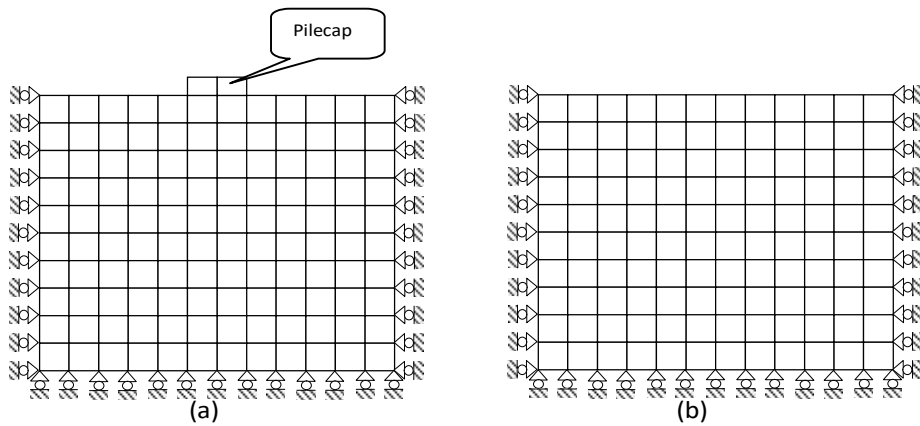


Figure III.12 Sketch of Flac3D mesh and boundary condition (a) with pile-cap and (b) without pile-cap

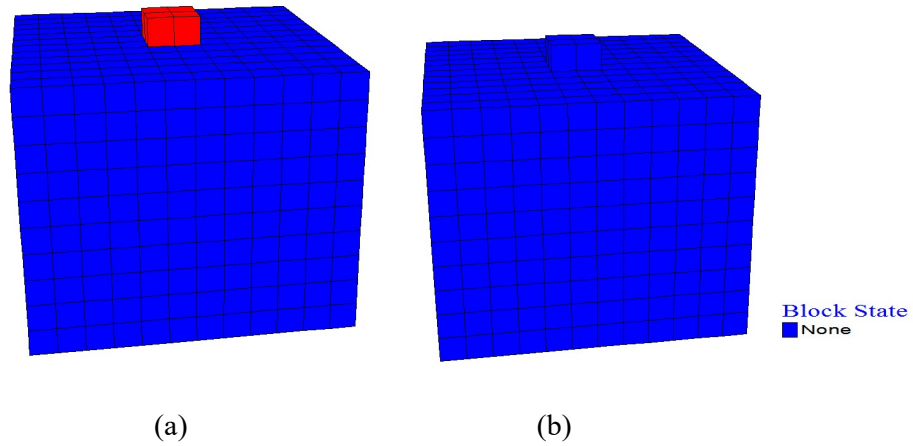


Figure III.13. (a) model (b) plasticity flow

Figure III.13 show that the result of the plasticity flow doesn't exist when the macro-element works in elastic-perfectly plastic under Mohr-Coulomb criterion for the same reason as explained above.

Table III.7. Predicted pile head load at different location connected by rigid pile-cap

Displ (mm)	Corner Load (kN)				Edge Load (kN)				Center Load (kN)	Total Applied (kN)
	1	5	7	9	2	3	6	8	4	
1.94	307.72	307.72	307.72	307.72	304.56	304.56	304.56	304.56	288.63	2737.76
2.90	419.46	419.46	419.46	419.46	420.39	420.39	420.39	420.39	414.38	3775.77
3.84	482.57	482.24	482.52	482.07	481.71	481.79	481.72	481.72	473.77	4330.10
4.79	527.36	527.36	527.36	527.36	527.44	527.44	527.44	527.44	518.88	4738.05
5.74	562.48	562.48	562.48	562.48	562.54	562.54	562.54	562.54	554.34	5054.45
6.71	589.67	589.67	589.67	589.67	589.71	589.71	589.71	589.71	582.61	5300.12
7.70	610.94	610.94	610.94	610.94	610.98	610.98	610.98	610.98	605.18	5492.85
8.71	627.84	627.84	627.84	627.84	627.87	627.87	627.87	627.87	623.35	5646.22
9.73	641.48	641.48	641.48	641.48	641.51	641.51	641.51	641.51	638.12	5770.08
10.76	652.66	652.66	652.66	652.66	652.68	652.68	652.68	652.68	650.31	5871.67
11.82	661.95	661.95	661.95	661.95	661.97	661.97	661.97	661.97	660.48	5956.15

Table III.7. shows the distribution of pile loads. It is predicted by macro-element method at the center, edge and corner at the different loading levels for the nine piles group that is connected by rigid reinforced concrete piles cap. And the piles load are observed the largest at corner (piles number 1, 5, 7 and 9), the second largest at edge (piles number 2, 3, 6 and 8) and the smallest at the center (piles number 4). Table II.8 is prediction result from Zhang *et al*,

2013 that shows the distribution load on rigid pile. The result of macro-element is consistent with the distribution load of previous study also consistent with the field measured results and model test result that reported by *Whitaker (1957); Koizumi and Ito, 1967; Poulos (1980); Comoros et al.,2009; Chow H and Poulos HG, 2015.*

Table III.8. Predicted pile head load at different location connected by Rigid pile-cap (*Zhang et al, 2013*).

Total applied load (kN)	Center load (kN)	Edge load (kN)	Corner load (kN)	Settlement of nine-pile group (mm)
0	0	0	0	0
851.87	88.12	93.37	97.57	0.6
1327.59	138.21	145.73	151.61	1
2231.64	235.74	245.13	253.84	2
2865.43	305.56	314.37	325.59	3
3366.64	359.21	370.45	381.4	4
3793.04	404.79	416.46	428.1	5
4117.53	441.8	453.52	465.41	6
4397.42	472.53	484.13	497.09	7
4634.24	499.29	510.13	523.61	8
4847.65	523.1	534.01	547.13	9
5035.99	542.75	553.97	569.34	10
5192.12	561.1	571.02	586.72	11
5343.23	577.31	588.04	603.44	12

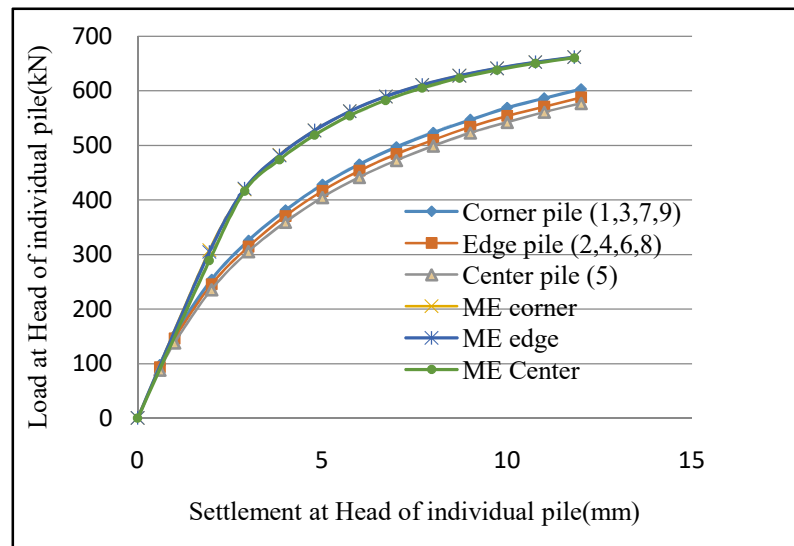


Figure III.14. Load-settlement response of pile at different location of Macro-element result and *Zhang et al* result.



The total load-displacement is shown in Figure III.15. A very good agreement is noticed between the measured displacement-load curve and propose macro-element method.

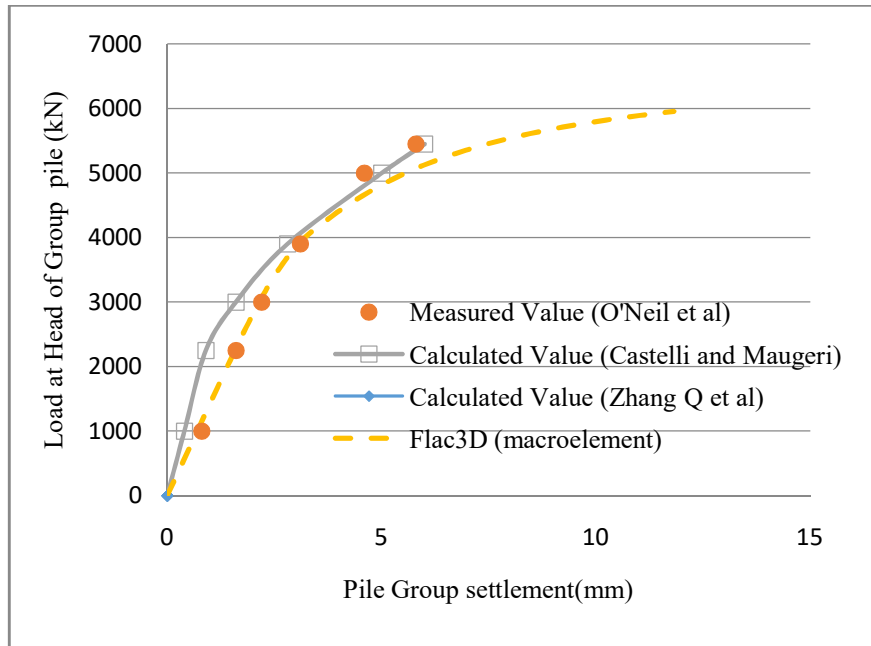


Figure III.15. Measured and calculated load-settlement curve at the rigid pile head of nine-pile group

Table III.9. and Figure III. 16 show the predicted pile head load at a different location which is connected by flexible pile-cap. In term of pile group settlement with respect to the distribution load to single pile, the load is distributed to each pile evenly. These results are in accordance with the theory that the load, in the flexible pile-cap, will be distributed evenly to each pile or often at the cost of higher settlements at the centre caused by a dishing effect of the pile-cap (Rose, 2012).

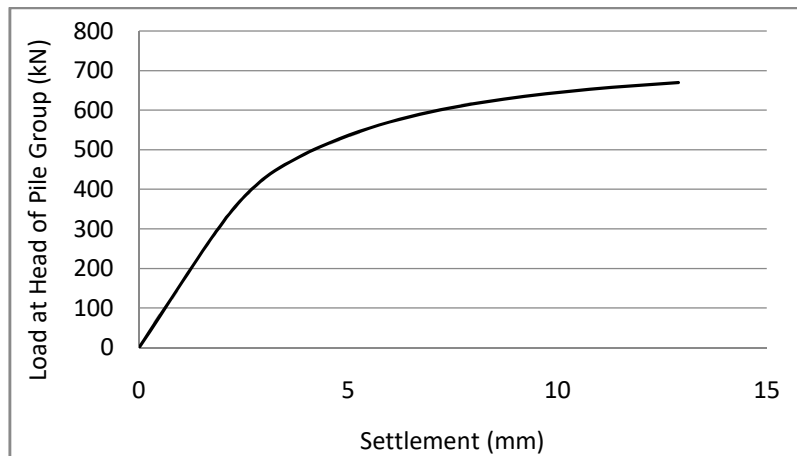


Figure III.16. Load distribution vs -settlement response of pile group

Table III.9. Predicted pile head load by Macro-element at different location connected by flexible pile-cap.

Displ (mm)	Corner Load (kN)				Edge Load (kN)				Center Load (kN)	Total Applied (kN)
	1	5	7	9	2	3	6	8	4	
1.70	2.29E+01	2.29E+01	2.29E+01	2.29E+01	2.29E+01	2.29E+01	2.29E+01	2.29E+01	2.29E+01	2.06E+02
1.90	5.49E+01	5.49E+01	5.49E+01	5.49E+01	5.49E+01	5.49E+01	5.49E+01	5.49E+01	5.49E+01	4.94E+02
2.10	8.69E+01	8.69E+01	8.69E+01	8.69E+01	8.69E+01	8.69E+01	8.69E+01	8.69E+01	8.69E+01	7.82E+02
2.50	1.51E+02	1.51E+02	1.51E+02	1.51E+02	1.51E+02	1.51E+02	1.51E+02	1.51E+02	1.51E+02	1.36E+03
2.70	1.83E+02	1.83E+02	1.83E+02	1.83E+02	1.83E+02	1.83E+02	1.83E+02	1.83E+02	1.83E+02	1.65E+03
2.90	2.15E+02	2.15E+02	2.15E+02	2.15E+02	2.15E+02	2.15E+02	2.15E+02	2.15E+02	2.15E+02	1.93E+03
3.50	3.11E+02	3.11E+02	3.11E+02	3.11E+02	3.11E+02	3.11E+02	3.11E+02	3.11E+02	3.11E+02	2.80E+03
3.70	3.43E+02	3.43E+02	3.43E+02	3.43E+02	3.43E+02	3.43E+02	3.43E+02	3.43E+02	3.43E+02	3.09E+03
3.90	3.75E+02	3.75E+02	3.75E+02	3.75E+02	3.75E+02	3.75E+02	3.75E+02	3.75E+02	3.75E+02	3.37E+03
4.50	4.23E+02	4.23E+02	4.23E+02	4.23E+02	4.23E+02	4.22E+02	4.23E+02	4.23E+02	4.23E+02	3.81E+03
4.70	4.36E+02	4.35E+02	4.36E+02	4.36E+02	4.36E+02	4.36E+02	4.36E+02	4.36E+02	4.36E+02	3.92E+03
4.90	4.48E+02	4.48E+02	4.48E+02	4.48E+02	4.48E+02	4.48E+02	4.48E+02	4.48E+02	4.48E+02	4.03E+03
5.50	4.82E+02	4.82E+02	4.82E+02	4.82E+02	4.82E+02	4.82E+02	4.82E+02	4.82E+02	4.82E+02	4.33E+03
5.70	4.92E+02	4.92E+02	4.92E+02	4.92E+02	4.92E+02	4.92E+02	4.92E+02	4.92E+02	4.92E+02	4.43E+03
5.90	5.01E+02	5.01E+02	5.01E+02	5.01E+02	5.01E+02	5.01E+02	5.01E+02	5.01E+02	5.01E+02	4.51E+03

### III.3 RESULT

The implementation of Macro-element to Flac3D gives a satisfactory result. For the single vertically loaded pile, the field loading test reported by *Bustamante and Jezequel*, 1989 used as validation control. The result of macro-element to the conventional Flac3D, T-z curve (Frank and Zhao method), and the field loading test shows in a good agreement. The same result is also shown in the Transversally loaded pile. It is compared to the field test located in Plancoet (cote du nord, France) in 1984 (*O'Neil et al*), and to others predicted calculation values.

For the Pile group, the macro-element is implemented to two formations (four and nine pile group) and two conditions of pile cap (rigid and flexible pile-cap). The result of load - settlement curve is validated to site load test that reported by *O'Neil et al*, 1983 and compared to predicted calculation value of *Castelli et al*, 2002 and *Zhang et al*, 2013. The distribution load that is applied to pile groups, using macro-element model, are in accordance to the theory of pile groups and the previous research. The result shows that the macro-element can mimic the behaviour of soil-structure interaction of deep foundation.

## CONCLUSION AND PERSPECTIVE

This research work aimed to develop a user-friendly numerical tool to assess the piles foundation response under monotonic axial or lateral load. A model based on macro-element concept has been built to study the Soil-Structure Interaction problem taking into account the different nonlinearities. Its formulation is based on the theory of elastoplasticity and is inspired by European standards (Eurocodes 7 and 8). Wherein, the four parameters describing the pile macro-element are defined from laboratory or in situ tests, or from numerical simulations under static conditions. This model reduces computational costs because the nonlinearities related to the SSI are concentrated in particular points of the computation model. The advantage of macroelement lies in its formulation in forces and displacements, which facilitates its use for the justification of the foundations (bearing capacity, sliding, detachment, settlements, translations, distortions and rotations). Furthermore, this macroelement is implemented in a Finite Element Method framework as a fish function in Flac3D. This tool is capable of simulating the SSI in the monotonic loaded pile.

The preliminary calibration step is required as the first step to simulate the behaviour of deep foundation that corresponds to the defined parameters of the law of movement. The calibration process is improved by defining these parameters that give the physical sense and explaining the method to determine its values.

The Comparison is done with the result of load transfer methods (T-z and P-y method). The validation of Macro-element result is performed with three case histories. The embedded macro-element in Flac3D, as a tool, is used to develop a model. The developed model is intended to account the soil-structure interaction of deep foundation either single pile or pile group.

For the vertically loaded single pile, the field loading test that is reported by *Bustamante and Jezequel*, 1989 used as validation control result, with good agreement. The same result is also shown in transversally loaded pile. It has been compared to field tests located in Plancoet (Côte du Nord, France) in 1982 (*O'Neil et al.*, 1992), and to others predicted calculation values. The macro-element has also been tested in pile group configuration. Its main advantages have been highly demonstrated, as time computation is hugely reduced, and also results are in good agreement with field test results. The distribution load that is applied to pile groups, using macro-element model, are in accordance with the theory of pile groups and the result in previous research. The results show that the macro-element can mimic the behaviour of soil-

structure interaction of deep foundation in simple mathematical model and reduce the calculation time.

Finally, it should be emphasized that the proposed macro-element could be used to build some interaction diagram for pile under monotonic/dynamic combined (vertical and lateral) loading, either in isolated or pile group configuration. Another component of load should also be taken into account, that is pile head moment. Further development of this macro-element is expected for taking into account the pile inclination.

## BIBLIOGRAPHY

- American Petroleum Institute (API). (1993). *Recommended Practice For Planning, Designing, And Constructing Fixed Offshore Platforms— Working Stress Design*, API RP2A-WSD, 20th Ed., Washington, D.C.
- AFNOR (2012). *Calcul Des Fondations Profondes – NF P 94 282*, Norme française. Saint-Denis, France: AFNOR Groupe.
- Boulangier, R. W., Curras, C. J., Kutter, B. L., Wilson, D. W., and Abghari, A. (1999). “*Seismic Soil–Pile–Structure Interaction Experiments And Analyses.*” *J. Geotech. Geoenviron. Eng.*, 125(9), 750–759.
- Bouafia A (2013), *P-Y curves from the prebored Pressure-meter test for laterally loaded single piles*, Proceedings of the 18th International Conference on Soil Mechanics and Geotechnical Engineering, Paris 2013
- Bouafia A (2017), *Laterally loaded single piles - Construction of P-Y curves from the cone penetration tes*, Proceedings of the 19th International Conference on Soil Mechanics and Geotechnical Engineering, Seoul 2017.
- Bustamante M., Jézéquel J.-F. (1989). *Essai statique de pieu isolé sous charge axiale*, Méthode d’essai LPC n°31, LCPC Paris, 12 p.
- Castelli F, Maugeri M. *Simplified Nonlinear Analysis For Settlement Prediction Of Pile Groups*, *Journal of Geotechnical and Geo-environmental Engineering*, 2002, Vol. 128, pp. 76-84.
- Charisis T. Chatzigogos Et Al, (2007). "A Macro-Element For Dynamic Soil-Structure Interaction Analyses Of Shallow Foundations ", 4th International Conference On Earthquake Geotechnical Engineering June 25-28, 2007 Paper No. 1387
- Chen, CF. (1985) “*Mechanics of Geomaterials*”, In: Z. Bazant; editor. John Wiley & Sons Ltd. pg 65-86.
- Chow H and Poulos HG, (2015). *The significance of raft flexibility in pile group and piled raft design*. Researchgate, Articiel: December 2015.
- Coduto, P.D.(1994), *Foundation Design Principles And Practices*, Prentice-Hall Inc., New Jersey.
- Cooke, R. W. 1974. *The settlement of friction pile foundation*. Proc conf on tall building, Kuala Lumpur , Malaysia

- Comodromos E.M, Papadopoulou M.C, Rentzeperis I.K. (2009). *Pile foundation analysis and design using experimental data and 3-D numerical analysis*. ELSIVIER. Computers and Geotechnics Volume 36, Issue 5, June 2009, Pages 819-836
- FHWA (2006), *Soil and Foundation - References manual - Volume II*, FHWA NHI-06-089, U.S. Dep. Of Transportation, Washington, DC
- Fleming, W.G.K., Weltman, A.J., Randolph, M.F., and Elson, W.K., (2009), *Piling Engineering*, John Willey and Sons, New York.
- Frank, R., Zhao, S. R. (1982). *Estimation Par Les Paramètres Pressiométriques De L'enfoncement Sous Charge Axiale De Pieux Forés Dans Les Sols Fins*. Bulletin de Liaison du Laboratoire des Ponts et Chaussées, 119 : 17-24.
- Frank, R. (1999). *Design of Shallow and Deep Foundations*. Paris, Presses de l'Ecole Nationale des Ponts et Chaussées et Techniques de l'Ingénieur, ENPC (in French)
- Frank R, Romagny JC (1990). *Programme De Calcul D'un Pieu Isole Soumis A Des Efforts De Flexion En Tete Et A Des Poussees Laterales De Sol*. LCPC (laboratoire central des pont et chaussees) PILATE-LPCP Version 10.4.
- Hadjadji T., Frank R. and Degny E. 2002. *Analyse du comportement expérimental de pieux sous chargements horizontaux (in French)*, Rapport de recherche série Géotechnique et Risques Naturels no. GT-74, mai 2002, 303 p.
- Itasca, 2009. *FLAC3D: Fast Lagrangian Analysis Of Continua In 3-Dimensions 4.1, Manual*. Itasca, Minneapolis/USA.
- Kareem. A.H.A., Helal A. (2007). "*Estimation Of Hyperbolic Stress-Strain Parameters For Gypseous Soils*". IJCE-7<sup>th</sup> ISSUE.
- Kelly. P.A (2008), "*Solid Mechanic II*" section 8.1. Aucland. New Zealand
- Kondner, R. (1963): "*Hyperbolic Stress-Strain Response of Cohesive Soils*", J. S. M. F. D. ASCE, Vol.89, SM1
- Murff, J. D. (1980), *Pile-capacity In A Softening Soil*. Int I. J. Numerical and analytical methods in geomechanics, 4, No.2 April-June, 1980, pp. 185-189.
- Ménard, L. (1963). *Estimation Of Load Bearing Capacity Of Foundations From Pressure-meter Test Results*. Sols Soils 5, 9–32 (in French).
- Nogami, T., Otani, J., Konagai, K., and Chen, H. L. (1992). "*Nonlinear Soil–Pile Interaction Model For Dynamic Lateral Motion*." J. Geotech. Eng., 118(1), 89–106.

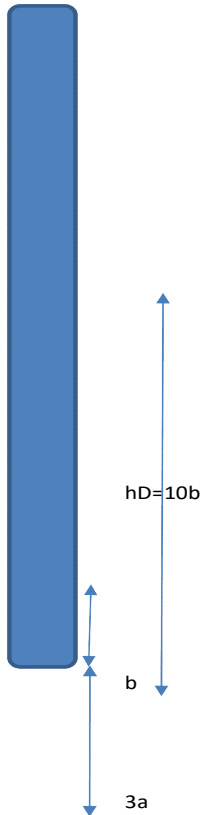
- Nova, R., & Montrasio, L. (1991). Settlements of shallow foundations on sand. *Géotechnique* 41(2), 243–256.
- O'Neill M.W, Hawkins R.A, Mahar L.J. *Load Transfer Mechanisms In Piles And Pile Groups*, Journal of the Geotechnical Engineering Division, 1982, Vol. 108, pp. 1605-1623.
- Osterberg, J. (1989) *New Device For Load Testing Driven Piles And Drilled Shafts Separates Friction And End-Bearing*, Proc. Int. Conf. On Piling an Deep Found., London, Vol. 1, pp. 421–427.
- Poulos H.G. , E.H. Davis (1980). *Pile foundation analysis and design*. John Wiley & Sons Ltd.
- Poulos, H.G. (1994), “*Settlement Prediction For Driven Piles And Pile Groups*”, Proceedings, Vertical and Horizontal Deformations of Foundations and Embankments, Geotechnical Special Publication No. 40, College Station, Texas, Vol. 2, 1629-1649.
- Reiffsteck P. (2009), " *ISP5 Pile Prediction Revisited*". International Foundation Congress and Equipment Expo '09 (IFCEE'09). ASCE Geotechnical Special Publication no. 186
- Rha C and Taciroglu E, *Coupled Macro-element Model of Soil-Structure Interaction in Deep Foundations*, JOURNAL OF ENGINEERING MECHANICS © ASCE / DECEMBER 2007
- Randolph, M. F. (1983), *Design Considerations For Offshore Piles*. Proceedings of the conference on geotechnical practice in offshore engineering, Austin, pp. 422-439.
- Rose A.V. (2012). *Behaviour And Efficiency Of Perimeter Pile Groups*. A dissertation submitted for the Degree of Doctor of Philosophy. City University London Geotechnical Engineering Research Group School of Engineering and Mathematical Sciences.
- Stéphane Grange, P. Kotronis, and J. Mazars (2008), *A macro-element for a circular foundation to simulate 3d soil,structure interaction*, Int. J. Num. Anal. Meth. Geomech.32
- Stéphane Grange et al (2009), *A Macro-Element To Simulate 3D Soil–Structure Interaction Considering Plasticity And Uplift*, International Journal of Solids and Structures Volume 46, Issue 20, 1 October 2009, Pages 3651-3663

- Taciroglu E, Rha C, and Wallace JW. *A Robust Macro-element Model for Soil–Pile Interaction under Cyclic Loads*, JOURNAL OF GEOTECHNICAL AND GEOENVIRONMENTAL ENGINEERING © ASCE / OCTOBER 2006
- Tuna, C., Viana da Fonseca, A. & Santos, J.A. (2008). *Data Interpretation And Analysis Of The Behavior Of Laterally Loaded Piles In ISC'2 Experimental Site By Recourse Of PMT And DMT Based Methods*. In: Huang, A-B.&Mayne, P., (eds) Proceedings of the 3rd International Conference on Site Characterization (ISC'3), 1–4 April 2008, Taiwan. London, Taylor&Francis.
- Viana da F, Butling S, Coutinho R.Q. (2012). In book: *A Handbook of Tropical Residual Soil Engineering*, Chapter: Chap. 6: *Foundations: Shallow and deep foundations, unsaturated conditions, heave and collapse, monitoring and proof testing*, Publisher: A.A. Balkema book, CRC Press, Taylor & Francis Group, Editors: Bujang B. K. Huat, David G. Toll & Arun Prasad, pp.283-412
- Wu.H., Shu.Y. and Zhu.J., 2011. *Implementation And Verification Of Interface Constitutive Model In FLAC3D*. Water Science and Engineering, 2011, 4(3): 305-316
- Z. Li1, P. Kotronis et al ,(2015). "*Macro-element Modeling for Single Vertical Piles*". 6th International Conference on Earthquake Geotechnical Engineering Christchurch, New Zealand 1-4 November 2015
- Zhang Q, et al, (2013)."*Simplified Method For Settlement Prediction Of Single Pile And Pile Group Using A Hyperbolic Model*", international journal of civil engineering November 2013
- Zienkiewicz, OC. (1985) "*Mechanics of Geomaterials*". In: Z. Bazant; editor. John Wiley & Sons Ltd.



# **Annexes**

Annex 1. Defining Macro-element parameters for vertically loaded pile (example)



D =	1.0000 m	(diameter of pile)
A =	0.7854 m <sup>2</sup>	
S =	3.1416 m <sup>2</sup>	
a =	0.5 max(d/2;0,5)	
b =	0.5 min(a,h)	
Em=	64.6 Mpa	
h	10 m	
	2.12	
3	2.12	6.36
0	2.12	0
1	1.73	1.925
		8.285
<b>P*le=</b>	<b>4.1425</b>	
	$p_{le}^* = \frac{1}{b+3a} \int_{D-b}^{D+2a} p_i^*(z) dz$	
	$D_{ef} = \frac{1}{P_{le}} \int_{D-b}^D p_i^*(z) dz$	
10	1.2	6
0	1.2	0
		17
D <sub>ef</sub> =	4.098974049	
D <sub>ef</sub> /D =	4.098974049	If < 5 Def max from tabel
Kpmax =	3.1	driven spun pile on sand Tabel I.4)
qp =	12.84175 Mpa	

Depth	Em mPa	type of soil	pl mPa	qs mPa
10	64.6	Q2	2.12	0.093810822
9	53.7	Q2	1.73	0.086173039
8	54.7	Q2	1.76	0.086831558
7	66.8	Q2	1.55	0.081916641
6	28.4	Q2	1.37	0.077055313
5	34.7	Q2	1.94	0.090518089
4	50.7	Q2	2.29	0.096623131
3	50	Q2	2.86	0.104532423
2	13.1	Q2	1.08	0.067605257
1	3.2	Q2	0.28	0.024642866
<b>Σ</b>	<b>419.9</b>		<b>16.98</b>	<b>0.80970914</b>
<b>Rb</b>	<b>1.01E+07 N</b>			
<b>Rs</b>	<b>2.54E+06 N</b>			
<b>Rb</b>	<b>1.26E+07 N</b>			
<b>Macro-element parameters</b>				
<b>k</b>	<b>4.20E+08 N/m</b>			
<b>Cs</b>	<b>1</b>			
<b>kv</b>	<b>4.20E+08 N/m</b>			
<b>fy= 0,5 Rc</b>	<b>6.31E+06</b>			
<b>a = Rc-fy</b>	<b>6.31E+06</b>			
<b>b = (a/kv)αb</b>	<b>1.50E-02</b>			

	Q1	Q2	Q3	Q4
a =	0.0015	0.006	0.007	0.008
b =	0.042	0.06	0.07	0.08
c =	1.25	1.2	1.3	3

α ==> tabel I.4  
1.4 precat or prestressed pile on sand

**Annex 2. Defining Macro-element parameters for Laterally loaded pile (continued)**

D = 0.5 m  
 Ip = 3.07E-03 m<sup>4</sup>  
 Ep = 3.98E+07 kPa  
 Ip.Ep = 1.22E+08 kN.m<sup>2</sup>

Depth	Em	pl	layer	Emi	De(assume)	Ec	Kr	Ke	Eti	Etic	Lo	De	Eccor	Kr new	Ke	Eti	Kp	pu	
m	mPa	mPa		Kpa	m											kh (kN/m2)		kN (kN/m)	
0	0	0																	
1	15	1.2	1	1.50E+07	10	1.50E+07	8.13E-04	7.675	1.15E+08	1.15E+08	1.014539	3.187267	1.50E+07	7.88E-02	3.08E+00	4.61E+07	3.79E-01	2.27E+05	
2	15	1.2	2	1.50E+07				7.675	1.15E+08						3.08E+00	4.61E+07	3.79E-01	2.27E+05	
3	15	1.2	3	1.50E+07				7.675	1.15E+08						3.08E+00	4.61E+07	3.79E-01	2.27E+05	
4	15	1.2	4	1.50E+07				7.675	1.15E+08										
5	15	1.2	5	1.50E+07				7.675	1.15E+08										
6	15	1.2	6	1.50E+07				7.675	1.15E+08										
7	15	1.2	7	1.50E+07				7.675	1.15E+08										
8	15	1.2	8	1.50E+07				7.675	1.15E+08										
9	15	1.2	9	1.50E+07				7.675	1.15E+08										
10	15	1.2	10	1.50E+07				7.675	1.15E+08										
11	15	1.2																	
12	15	1.2																	

Σ Eti (N/m2)    4.61E+07    Pu(N/m)    6.82E+05

Diameter (m)	0.5
Eti (N/m2)	4.61E+07
Pu(N/m)	6.82E+05
Macro-lement parameter	
Dem	3
Dem/2	1.50
Cs	1
kh (N/m)	6.92E+07
a (N)	2.05E+06
α <sub>b</sub>	2
b (m)	5.91E-02

**Annex 2. Defining Macro-element parameters for Laterally loaded pile**

D = 1 m  
 Ip = 4.91E-02 m<sup>4</sup>  
 Ep = 3.98E+07 kPa  
 Ip.Ep = 1.95E+09 kN.m<sup>2</sup>

Depth	Em	pl	layer	E <sub>mi</sub>	D <sub>e(assume)</sub>	Ec	Kr	Ke	E <sub>ti</sub>	E <sub>tic</sub>	Lo	De	Eccor	Kr new	Ke	E <sub>ti</sub>	Kp	pu	
m	mPa	mPa		Kpa	m				Kpa	Kpa	m	m				kh (kN/m <sup>2</sup> )		kN (kN/m)	
0	0	0																	
1	15	1.2	1	1.50E+07	10	1.50E+07	1.30E-02	4.41E+0	6.61E+07	6.61E+07	2.330798	7.322417	1.50E+07	4.53E-02	3.44E+00	5.15E+07	3.45E-01	4.14E+05	
2	15	1.2	2	1.50E+07				4.41E+0	6.61E+07						3.44E+00	5.15E+07	3.45E-01	4.14E+05	
3	15	1.2	3	1.50E+07				4.41E+0	6.61E+07						3.44E+00	5.15E+07	3.45E-01	4.14E+05	
4	15	1.2	4	1.50E+07				4.41E+0	6.61E+07						3.44E+00	5.15E+07	3.45E-01	4.14E+05	
5	15	1.2	5	1.50E+07				4.41E+0	6.61E+07						3.44E+00	5.15E+07	3.45E-01	4.14E+05	
6	15	1.2	6	1.50E+07				4.41E+0	6.61E+07						3.44E+00	5.15E+07	3.45E-01	4.14E+05	
7	15	1.2	7	1.50E+07				4.41E+0	6.61E+07										
8	15	1.2	8	1.50E+07				4.41E+0	6.61E+07										
9	15	1.2	9	1.50E+07				4.41E+0	6.61E+07										
10	15	1.2	10	1.50E+07				4.41E+0	6.61E+07										
11	15	1.2																	
12	15	1.2																	

Σ E<sub>ti</sub> (N/m<sup>2</sup>) 5.15E+07 Σ Pu(N/m) 2.49E+06

Diameter (m)	1
E <sub>ti</sub> (N/m <sup>2</sup> )	5.15E+07
Pu(N/m)	2.49E+06
Macro-lement parameter	
Dem	6
Dem/2	3.00
C <sub>s</sub>	1
kh (N/m)	1.55E+08
a (N)	1.49E+07
α <sub>b</sub>	2
b (m)	1.93E-01

